Getting there:
Vesicles en route for plant cytokinesis

Agnieszka Esseling-Ozdoba

Promotor: Prof.dr. Anne Mie C. Emons
Hoogleraar in de Plantencelbiologie
Wageningen Universiteit

Co-promotor: Dr. André A.M. van Lammeren
Universitair hoofddocent bij de leerstoelgroep Plantencelbiologie

Samenstelling promotiecommissie:

Prof. Dr. Ir. Frans Leermakers
Wageningen Universiteit

Dr. A. Lacey Samuels
University of British Columbia (Canada)

Dr. Béatrice Satiat-Jeunemaitre
Institut des Sciences du Végétal CNRS
Gif-sur-Yvette (France)

Prof. Dr. Theodorus W. J. Gadella Jr.
SILS, Universiteit van Amsterdam

Dit onderzoek is uitgevoerd binnen de onderzoeksschool Experimentele Plantenwetenschappen.

Agnieszka Esseling-Ozdoba

Getting there:
Vesicles en route for plant cytokinesis

Proefschrift
ter verkrijging van de graad van doctor
op gezag van de rector magnificus
van Wageningen Universiteit
Prof. Dr. M.J. Kropff
in het openbaar te verdedigen
op dinsdag 9 oktober 2007
des namiddags te 13:30 uur in de Aula.

Getting there: Vesicles en route for plant cytokinesis / Esseling-Ozdoba, Agnieszka

Thesis Wageningen Universiteit, The Netherlands.

With references – with summary in Dutch.

ISBN 978-90-8504-746-9

Contents

Chapter 1 General introduction and outline of the thesis 1

Chapter 2 Synthetic lipid (DOPG) vesicles accumulate in the cell plate region but do not fuse 9

Chapter 3 Flexibility contra stiffness: the phragmoplast exit as a physical barrier for polystyrene beads but not for synthetic membranous vesicles 31

Chapter 4 Hydrodynamic flow caused by active transport along cytoskeletal elements 55

Chapter 5 Hydrodynamic flow in the cytoplasm of plant cells 67

Chapter 6 General discussion 84

Samenvatting 91

Summary 93

Dankwoord 95

Curriculum vitae 96

List of publications 98

Chapter 1

General Introduction and Outline of the Thesis

INTRODUCTION AND OUTLINE OF THE THESIS

Cells are structured: they are not mere bags containing enzymes. Cells are dynamic: they do not compare with stapled organized Lego blocks. Cells have a well-regulated infrastructure, allowing their components, such as organelles and chromosomes, to be present at the right site at the right moment. This infrastructure of all eukaryotes is the cytoskeleton consisting of microtubules and actin filaments with their associated and binding proteins and regulators. This infrastructure localizes cell structures and moves them around. In plant cells we observe two types of movements that can in brief be described as "getting there" and "getting around".

"Getting there" concerns specific place/time-resolved 4D action. In this category falls for instance the precisely orchestrated separation of daughter chromosomes to become contained in daughter nuclei of two new cells after cell division. Pushing and pulling forces, manipulated by the cell through the cytoskeleton, make this possible (Dogterom et al., 2005). Another example of "getting there" is the process of precise delivery of cell wall production cargo and machinery to sites of cell elongation, of which process tip growth is the best example, because in this cell type the growth process localizes abundantly at one small site of the cell (Ketelaar et al., 2001). A specific cytoskeleton configuration is required for the deposition of that polysaccharide cargo and exocytosis and cellulose polymer production machinery at the cell tip.

Another example of "getting there" is the preparation for the production of the cell plate, the division wall *in statu nascendi* between the dividing cells, typical for plant cells, which have to produce a cell wall between the daughter cells that links up to the mother wall (Staehelin and Hepler, 1996). If this would not occur, two membrane enveloped cells would be encased into one cell wall. First, the location of the division wall has to be determined and the cargo and production machinery has to be produced. Then, this cell wall cargo and production machinery has to be targeted to that specified location. The cargo again is enclosed in vesicles, and the machinery is the fusion machinery, all of the molecules involved in exocytosis, partly recruited from the cytoplasm and partly present inside the vesicle membrane itself.

My research question was about the physical parameters size and stiffness that vesicles require to reach this forming cell plate: the "getting there" question. To answer this question, I injected synthetic lipid vesicles and polystyrene beads into cell plate forming cells that have a specific structure, the phragmoplast, designed with a specific cytoskeletal configuration for this process. However, first these vesicles have to reach, as vesicles themselves or as Golgi bodies producing them, that discriminating cell area where they are sorted. In other words, they have to "get around" in the streaming cytoplasm. Therefore, apart from focusing on "getting there", I had to pay attention to "getting around".

Cell plate formation

In dividing plant cells, membranous vesicles (60-80 nm) are transported to the area in the cell where the division plane is formed and they fuse with each other to build a new plasma membrane bound cell wall that separates the daughter cells (Fig. 1).

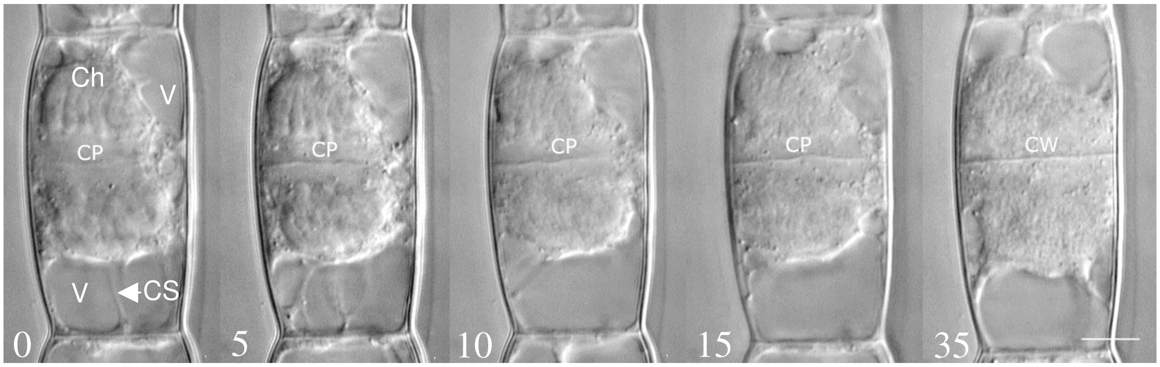

Figure 1. Differential interference contrast microscope (DIC) images of an emerging and growing cell plate in a *Tradescantia virginiana* stamen hair cell. Numbers indicate time in minutes; Ch – Chromosomes, CP - cell plate, CS – cytoplasmic strand, CW - cell wall, V – Vacuole, bar = 10 µm.

The developing cell plate is bordered by a special structure named the phragmoplast. This cytoplasmic dense area is a plant specific structure that contains endoplasmic reticulum, vesicles and a cytoskeleton of microtubules and actin filaments arranged in two opposing, antiparallel cylinders (Staehelin and Hepler, 1996). During growth and expansion of the cell plate, microtubules are present at its edges and disappear from the middle of the phragmoplast when the cell plate matures (Zhang et al, 1990), whereas actin filaments become shorter but remain present in the whole area throughout cell plate formation (Hepler et al., 1993). The vesicles that will produce the cell plate, move through the phragmoplast to its center between the widening cylinders of microtubules and actin filaments, and fuse with each other. The fusion of the vesicles leads to the formation of a cell plate consisting of vesicle-derived membrane at the outside, and vesicle content, cell wall material, at the inside. A complex maturation process that is illustrated in figure 2 yields a fully functional and integrated cell wall. Cell plate forming vesicles are Golgi-derived vesicles (Staehelin and Hepler, 1996) and possibly endosomal vesicles (Dhonukshe et al., 2006). The fusion of cell plate forming vesicles first leads to hourglass-shaped vesicular structures. The neck region of these vesicular structures is stretched and dumbbell-shaped intermediates are produced. During the stretching of the dumbbell necks, the diameter and the surface area of the bulbous ends get smaller. This stretching appears to involve the expansion of dynamin-like springs (asterisk* in Fig. 2; Gu and Verma, 1996; Verma, 2001) and reduces vesicle volume by ~50% (Seguí-Simarro et al., 2004). Later arriving vesicles fuse to the bulbous ends of the dumbbells, giving rise to the tubulo-vesicular network. The tubulo-vesicular network matures into a tubular network and fenestrated sheet. The cell plate expands centrifugally by the fusion of newly arriving vesicles with its margin and undergoes a complex process of maturation, which involves secretion of cell wall material and removal of excess membrane material, resulting in a planar structure. Finally, the cell plate membrane fuses with the parental plasma membrane forming membranes of the two daughter cells with cell wall, the content of the original vesicles between them. By this process the two daughter cells are being formed.

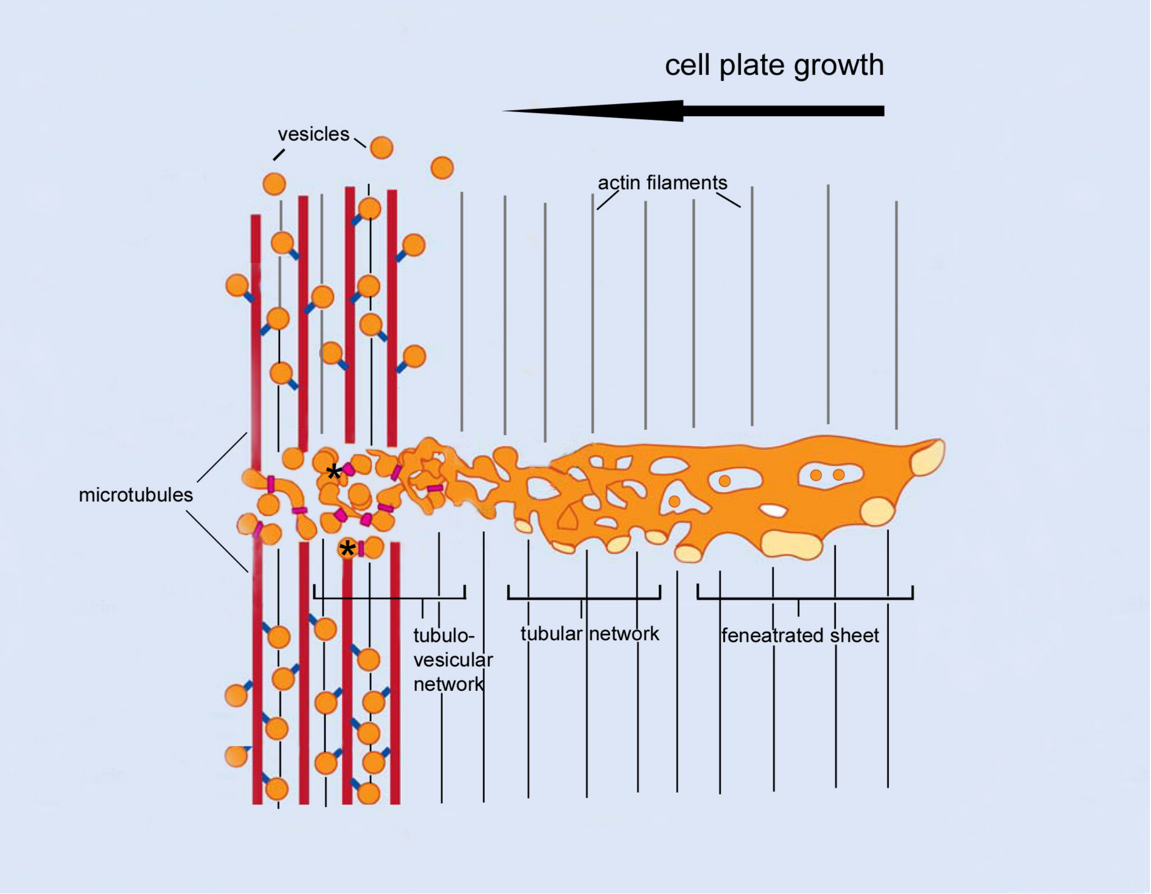

Figure 2. Stages of cell plate formation. Shown is half of a developing cell plate; the right side of the drawing being the middle of the cell plate.

In this thesis I describe results obtained using microinjection of synthetic phospholipid vesicles into plant cells to determine the physical parameters, vesicles size and vesicle stiffness for their transport towards the cell plate and possible fusion with each other (and the existing cell plate).

In chapter 2, I describe the results obtained after microinjection of fluorescent synthetic lipid vesicles made of 1,2-Dioleoyl-*sn*-Glycero-3-[Phospho-*rac*-(1-glycerol)] (DOPG) into interphase and dividing *Tradescantia virginiana* stamen hair cells. In interphase cells, synthetic DOPG vesicles of 60 nm moved through the cytoplasm, similarly to endogenous organelles, albeit a bit slower. In cells at cytokinesis, DOPG vesicles moved to and through the whole phragmoplast and accumulated in the cell plate region together with endogenous vesicles, but did not fuse with the developing cell plate.

From experiments described in chapter 3 we conclude that the size of vesicles is not important for their transport through the phragmoplast towards the cell plate but that stiffness is a limiting parameter. Stiff polystyrene beads were transported into the phragmoplast area but did not reach the cell plate.

Since the synthetic vesicles and beads without motor proteins have to travel from the injection site to the phragmoplast through the cytoplasm, I studied if hydrodynamic flow could be part of the cytoplasmic streaming phenomenon, theoretically (chapter 4) and experimentally (chapter 5).

Cytoplasmic streaming

Plant cells exhibit fast movement of organelles, called cytoplasmic streaming. Cytoplasmic streaming is an important feature of plant cells. Because of their large size, only diffusion would not be efficient enough to distribute organelles throughout the cell. Cytoplasmic streaming is caused by motor proteins, myosins, associated with organelles actively moving along bundles of actin filaments (Shimmen and Yokota, 1994). Myosin steps along actin filaments using the energy that is generated by hydrolysis of ATP. Plant myosin was first isolated from lily pollen tubes (Yokota and Shimmen, 1994). The velocities of the movement of myosins observed in *in vitro* motility assays were consistent with those of cytoplasmic streaming in cells of plant species from which myosins had been isolated (Shimmen and Yokota, 2004). Immunostaining studies have shown co-localization of myosin with organelles (Yokota et al., 1995; Miller et al., 1995), indicating that these myosins are indeed involved in cytoplasmic streaming. Three subfamilies of myosin have been reported in higher plants, myosins VIII, XI and XIII (Reichelt and Kendrick-Jones, 2000; Lee and Liu, 2004). In tobacco (BY-2 suspension cells), two myosin XIs have been isolated - a 170 kDa myosin and a 175 kDa myosin (Yokota et al., 1999). Single myosin XI molecules move processively along actin with 35 nm steps at 7 µm/s, the fastest known processive motion (Tominaga et al., 2003). This processivity enables a small number of higher plant myosin XIs to transport organelles along actin filaments over long distances (Shimmen and Yokota, 2004).

It is not known whether the movement of these myosin-steerd organelles causes movement of molecules/vesicles/other organelles that are not attached to the cytoskeleton. Could it be that when organelles are moving in the cytosol they influence the surrounding fluid and molecules within this fluid, like in the cartoon shown in Fig. 3?

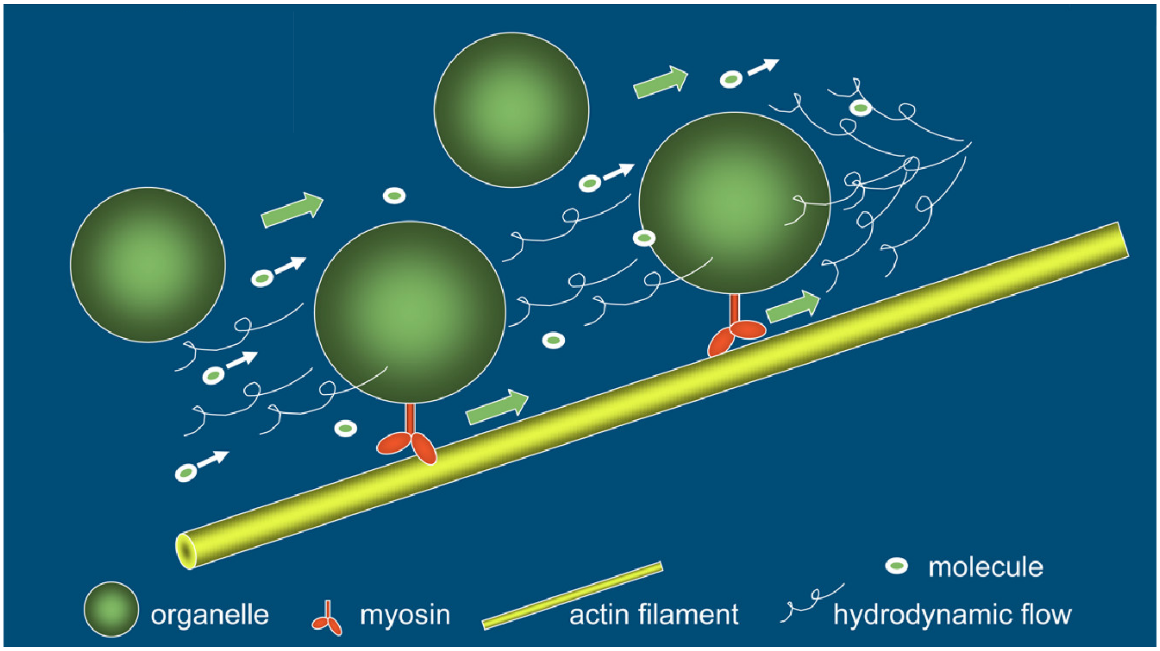

Figure 3. Cartoon showing a possible hydrodynamic flow in the cytoplasm of plant cells. Active movement of organelles (with myosin) along actin filaments are shown to cause hydrodynamic flow that drags the molecules and possibly also vesicles and organelles that are not coated with motor proteins in the same direction.

In chapter 4 and 5 of this thesis we study this phenomenon. In chapter 4 I collaborated with physicists for a theoretical study the hydrodynamic flow. We developed a simple lattice model to describe the hydrodynamic influence of active mass transport (i.e. organelle transport) along bio-filaments (the cytoskeleton) on a freely diffusing mass, the molecules of the cytosol in the cell. In this paper we show that, theoretically, the hydrodynamic forces induced by the movement of molecular motor-organelle complexes attached to the filaments give rise to a non-negligible flux close to the filament. This flux appears to have two effects. Depending on the degree of filament occupation it can exert a sufficiently large influence on unbound molecular motor-organelle complexes to modify their transport and also regulate the flux of motor-organelle complexes bound to the filament.

In chapter 5 we show experimentally that moving organelles indeed produce a drag, a hydrodynamic flow, which is contributing to the movement of molecules in the cytosol. As tools to study this phenomenon we used Green Fluorescent Protein (GFP), introduced in the cells via genetic transformation such that it is expressed in the cytosol, and Fluorescence Recovery After Photobleaching (FRAP), to follow the movement of GFP. We show that GFP molecules move faster in cells with active transport of organelles than in cells where this transport has been inhibited. We show that the direction of GFP movement is the same as that of organelle movement and that the speed of organelle movement influences the speed of GFP movement.

Chapter 6 is a general discussion of the results obtained and gives an outlook of the possibilities and insights to be obtained with microinjection of a variety of synthetic vesicles and beads.

REFERENCES

Dhonukshe, P., Baluška, F., Schlicht, M., Hlavacka, A., Šamaj, J., Friml, J. and Gadella, Jr., W.J. (2006). Endocytosis of cell surface material mediates cell plate formation during plant cytokinesis. Dev. Cell **10**, 137-150.

Dogterom, M., Kerssemakers, J.W., Romet-Lemonne, G., and Janson, M.E. (2005). Force generation by dynamic microtubules. Curr. Opin. Cell Biol. **17,** 67-74.

Gu, X., and Verma, D.P.S. (1996). Phragmoplastin, a dynamin-like protein associated with cell plate formation in plants. EMBO J. **15**, 695-704.

Hepler, P.K., Cleary, A.L., Gunning, B.E.S., Wadsworth, P., Wasteneys, G.O. and Zhang, D.H. (1993). Cytoskeletal dynamics in living plant cells. Cell Biol. Int. **17**, 127-142.

Ketelaar, T. and Emons, A.M.C. (2001). The cytoskeleton in plant cell growth: Lessons from root hairs. The New Phytologist **152,** 409-418.

Lee, Y.-R.J., and Liu, B. (2004). Cytoskeletal motors in Arabidopsis. Sixty-one kinesisns and seventeen myosins. Plant Physiol. **136**, 3877-3883.

Miller, D.D., Scordilis, S.P., and Hepler, P.K. (1995). Identification and localization of three classes of myosins in pollen tubes of *Lilium longiflorum* and *Nicotiana alata*. J. Cell Sci. **108**, 25-49-2653.

Reichelt, S., and Kendrick-Jones, J. (2000). Myosins. In Actin: a dynamic framework for multiple plant cell functions. Edited by Staiger CJ, Balus¡ka F, Volkman D, Barlow PW. Dordrecht/Boston/London: Kluwer Academic Publishers, 29-44.

Seguí-Simarro, J.M., Austin, J.R. II, White, E.A., and Staehelin, L.A. (2004). Electron tomographic analysis of somatic cell plate formation in meristematic cells of Arabidopsis preserved by high-pressure freezing. Plant Cell **16**, 836-856.

Shimmen, T., and Yokota, E. (1994). Physiological and biochemical aspects of cytoplasmic streaming. Int. Rev. Cytol. **155**, 97-139.

Shimmen, T. & Yokota, E. (2004) Cytoplasmic streaming in plants. *Curr Opin. Cell Biol* **16**, 68–72.

Staehelin, A. L. and Hepler, P.K. (1996). Cytokinesis in higher plants. Cell **84**, 821-824.

Tominaga, M., Kojima, H., Yokota, E., Orii, H., Nakamori, R., Katayama, E., Anson, M., Shimmen, T., and Oiwa, K. (2003). Higher plant myosin XI moves processively on actin with 35 nm steps at high velocity. EMBO J. **22**, 1263-1272.

Verma, D.P.S. (2001). Cytokinesis and building of the cell plate in plants. Annu. Rev. Plant Physiol. Plant Mol. Biol. **52**, 751-784.

Yokota, E., and Shimmen, T. (1994). Isolation and characterization of plant myosin from pollen tubes of lily. Protoplasma **177**, 153-162.

Yokota, E., McDonald, A.R., Liu, B., Shimmen, T., and Palevitz, B.A. (1995). Localization of a 170 kDa myosin heavy chain in plant cells. Protoplasma **185**, 178-187.

Yokota, E., Yukawa, C., Muto, S., Sonobe, S., and Shimmen, T. (1999). Biochemical and immunocytochemical characterization of two types of myosins in cultured tobacco bright yellow-2 cells. Plant Physiol. **121**, 525-534.

Zhang, D., Wadsworth, P. and Hepler, P.K. (1990). Microtubule dynamics in living dividing cells: confocal imaging of microinjected fluorescent brain tubulin. Proc. Natl. Acad. Sci. USA **87**, 8820-8824.

Chapter 2

Synthetic (DOPG) Lipid Vesicles Accumulate in the Cell Plate Region but do Not Fuse

Agnieszka Esseling-Ozdoba, Jan W. Vos, André A.M. van Lammeren and Anne Mie C. Emons.

Laboratory of Plant Cell Biology, Department of Plant Sciences, Wageningen University, Arboretumlaan 4, 6703 BD Wageningen, The Netherlands

Submitted to The Plant Cell

Abstract

The cell plate is the new cell wall that is formed between two daughter cells in plants, and it is formed by fusion of membrane vesicles (~60 nm). To study cell plate formation, we microinjected fluorescent synthetic lipid vesicles that were made of 1,2-Dioleoyl-*sn*-Glycero-3-[Phospho-*rac*-(1-glycerol)] (DOPG) and that could partly mimic the endogenous cell plate forming vesicles into *Tradescantia virginiana* stamen hair cells. During cytokinesis, these 60 nm DOPG vesicles were transported through the phragmoplast and accumulated in the cell plate region together with the endogenous vesicles. The synthetic vesicles even accumulated in the central cell plate region when injected into cells at late telophase. At this stage, the microtubules appeared as a torus-shaped array (virtually absent from the central region), but the actin filaments were still present throughout the entire phragmoplast. With this result we suggest a role of phragmoplast actin filaments in the transport of vesicles towards the cell plate. Unlike the endogenous vesicles, the synthetic DOPG vesicles did not fuse with the developing cell plate. Instead, they redistributed into the cytoplasm of the daughter cells upon completion of cytokinesis. Because the redistribution of the vesicles corresponds to the disappearance of actin filaments in the phragmoplast, we suggest that these actin filaments are involved in keeping the vesicles inside the developing cell plate region.

INTRODUCTION

In plant cells, the cell plate constitutes the new cell wall that separates the nuclei and the cytoplasm between the two daughter cells. The cell plate is formed during cytokinesis by the fusion of membrane vesicles of approximately 60 nm that contain a variety of hemicelluloses and pectins, and have callose and cellulose synthesizing enzyme complexes in their membrane (Zuo et al., 2000; Yokoyama and Nishitani, 2001; Verma, 2001).

The cell plate is built up in the middle of a structure called the phragmoplast, often at an equatorial plane in the cell. The phragmoplast is a cytoplasmic dense area containing microtubules, actin filaments, endoplasmic reticulum (ER) and cell plate forming vesicles (Schopfer and Hepler, 1991; Samuels et al., 1995; Staehelin and Hepler, 1996; Seguí-Simarro et al. 2004, Jürgens, 2005). Other organelles, such as the Golgi bodies, mitochondria and the vacuole stay outside the phragmoplast. The phragmoplast is initiated at late anaphase from the antiparallel overlapping microtubule arrays at the spindle mid zone, the plus-ends of which face the accumulating vesicles that form the cell plate (Kakimoto and Shibaoka, 1988; Baskin and Cande, 1990; Wick, 1991; Cleary et al., 1992; Zhang et al., 1990, 1993; Hepler et al., 1993; Sano et al., 2005). During expansion of the cell plate, microtubules disappear from the center of the phragmoplast as soon as a cell plate has formed (Zhang et al., 1990, 1993; Cleary et al., 1992; Hepler et al., 1993; Granger and Cyr, 2000; Ueda at al., 2003), whereas actin filaments become shorter but remain present in the whole area throughout cell plate formation (Hepler et al., 1993; Zhang et al., 1993; Fig. 1).

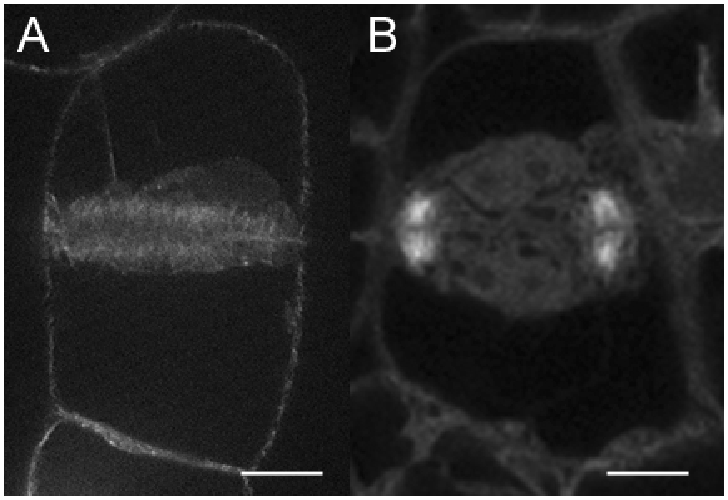

Figure 1. A. Median plane of a Tobacco BY-2 suspension cell at late telophase, transformed with GFP::FABD to visualize the actin cytoskeleton. Actin is present in the whole phragmoplast including the central part. Bar: 10 µm. B. Median plane of Tobacco BY-2 suspension cell at late telophase, transformed with GFP::MBD to visualize the microtubule cytoskeleton. Microtubules are absent from the central part of the phragmoplast. Bar: 10 µm.

The process of cell plate formation with its intermediate stages is well understood (Seguí-Simarro et al., 2004; for reviews see Staehelin and Hepler, 1996; Verma, 2001; Jürgens, 2005). The vesicle fusion in the middle of the phragmoplast is mediated by tethering SNARE complexes (Waizenegger et al., 2000) in a region that has been termed the cell plate assembly matrix in electron tomography studies (CPAM; Otegui et al., 2001; Seguí-Simarro et al., 2004).

With the help of dynamin-like molecules, the fusion of vesicles leads to the formation of membrane fusion tubes with a diameter of 20 nm (Samuels et al. 1995; Gu and Verma, 1996). The fusion tubes fuse with other vesicles and form the tubulo-vesicular network that is transformed into a tubular network and later into a fenestrated membrane sheet. This transformation involves the removal of excess membrane via clathrin coated vesicles and the deposition of callose (Samuels et al., 1995, Otegui et al., 2001, Seguí-Simarro et al., 2004). The cell plate grows centrifugally towards the cell borders due to the fusion processes of later arriving vesicles, until it attaches to the plasma membrane and cell wall of the mother cell (Staehelin and Hepler, 1996).

For years it was believed that cell plate forming vesicles are only Golgi-derived (Whaley and Mollenhauer, 1963). A recent study, however, has attempted to unravel the possible role of endosomes in cell plate formation (Dhonukshe et al., 2006). However, the origin of the cell plate forming vesicles has not yet been characterized as it is difficult to determine the exact membrane composition of isolated vesicles due to contamination from other membrane material (Verma, 2001).

Also, the exact mechanism of vesicle transport through the phragmoplast is not yet known. It has been suggested that phragmoplast microtubules are directly responsible and that actin-myosin plays an important role in the proper attachment of the cell plate to the parental cell wall (Otegui et al., 2001; Molchan et al., 2002). However, injection of the actin-binding protein profilin strongly suggested that actin filaments in the phragmoplast are also crucial for transport of cell plate forming vesicles to the cell plate (Valster et al., 1997). Apart from being transport vehicles, the tight array of microtubules and actin filaments in the phragmoplast might also act as a sieve, allowing only the right sized vesicles to move into the region where fusion occurs, and act as a scaffold for the forming cell plate.

Here, we describe results obtained with the injection of synthetic phospholipid vesicles into plant cells to start to determine possible necessary and sufficient physical properties of cell plate forming vesicles for their transport through the phragmoplast, for their fusion with each other (and the existing cell plate) and the role of the cytoskeleton therein. We used phospholipid vesicles made of 1,2-Dioleoyl-*sn*-Glycero-3-[Phospho-*rac*-(1-glycerol)] (DOPG) that partly mimic the behavior of endogenous vesicles during cell plate formation. We show that upon injection, DOPG vesicles are transported to and through the phragmoplast and accumulate in the region of the existing growing cell plate.

However, unlike endogenous vesicles, synthetic vesicles redistribute into the cytoplasm of the daughter cells upon completion of cytokinesis. This suggests that the phragmoplast is not selective for membrane composition or integral proteins. More important, it shows that the vesicles are kept in the cell plate region during its formation. In this process the CPAM could be involved. Since vesicles keep moving to the centre of the cell plate during late telophase when the microtubules have left that area but actin filaments are still present, we envision a role for the actin cytoskeleton in this process.

RESULTS

Synthetic lipid vesicles (DOPG) distribute throughout the cytoplasm of interphase *Tradescantia virginiana* stamen hair cells

We made synthetic vesicles from negatively charged (anionic) 1,2-Dioleoyl-*sn*-Glycero-3-[Phospho-*rac*-(1-glycerol)] (DOPG), labeled with 2% fluorescent phosphocholine Bodipy FC12-HPC, with a size of 60 nm (± 7 nm) (Fig. 2) to study physical properties of the vesicles that are required for transport through the phragmoplast and the formation of the cell plate. The vesicles did not fuse or aggregate with each other, even after seven days in the buffer used for microinjection (data not shown).

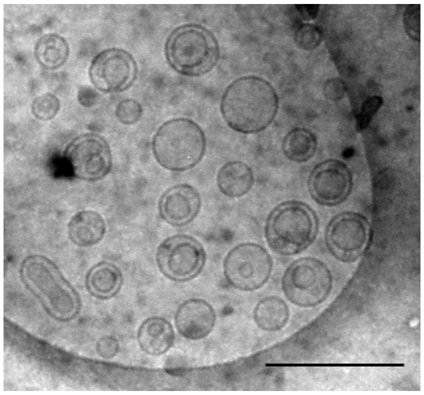

Figure 2. Synthetic lipid vesicles labeled with Bodipy FC12-HPC in microinjection buffer, imaged with cryo-TEM. Bar = 200 nm.

Synthetic lipid (DOPG) vesicles injected into young elongating interphase stamen hair cells of *Tradescantia virginiana* distributed evenly in the cytoplasm within 5-10 min after microinjection and were visible as individual fluorescent speckles (Fig. 3A and B). The injection of these vesicles was not lethal to the cells, nor did it affect cytoplasmic streaming or the cytoarchitecture (Figure 3A: DIC images). Inside the cells, the vesicles also seemed to be stable, since their fluorescence was not incorporated into the plasma membrane, tonoplast, ER or other organelles (mitochondria and plastids) that can be seen with DIC (Differential Interference Contrast) microscopy. In addition, the vesicles did not fuse together in the cytoplasm, as no obvious conglomerates were formed and the number of speckles did not markedly drop over time. Microinjected fluorescent vesicles moved through the cytoplasm for at least 1.5 hours after injection.

The average velocity of vesicles in the cytoplasm was 0.74 ± 0.04 (SE) µm/sec, which is comparable to, but consistently slower than, that of visible organelles with a size of approximately 1-2 µm in these cells (1.12 ± 0.06 (SE) µm/sec) and in cells that were not injected (1.24 ± 0.12 (SE) µm/sec) (Fig. 3C). This suggests that the injected vesicles may be coated with motor proteins and move on cytoskeletal tracks like organelles do, or else, move by hydrodynamic flow produced by the moving organelles.

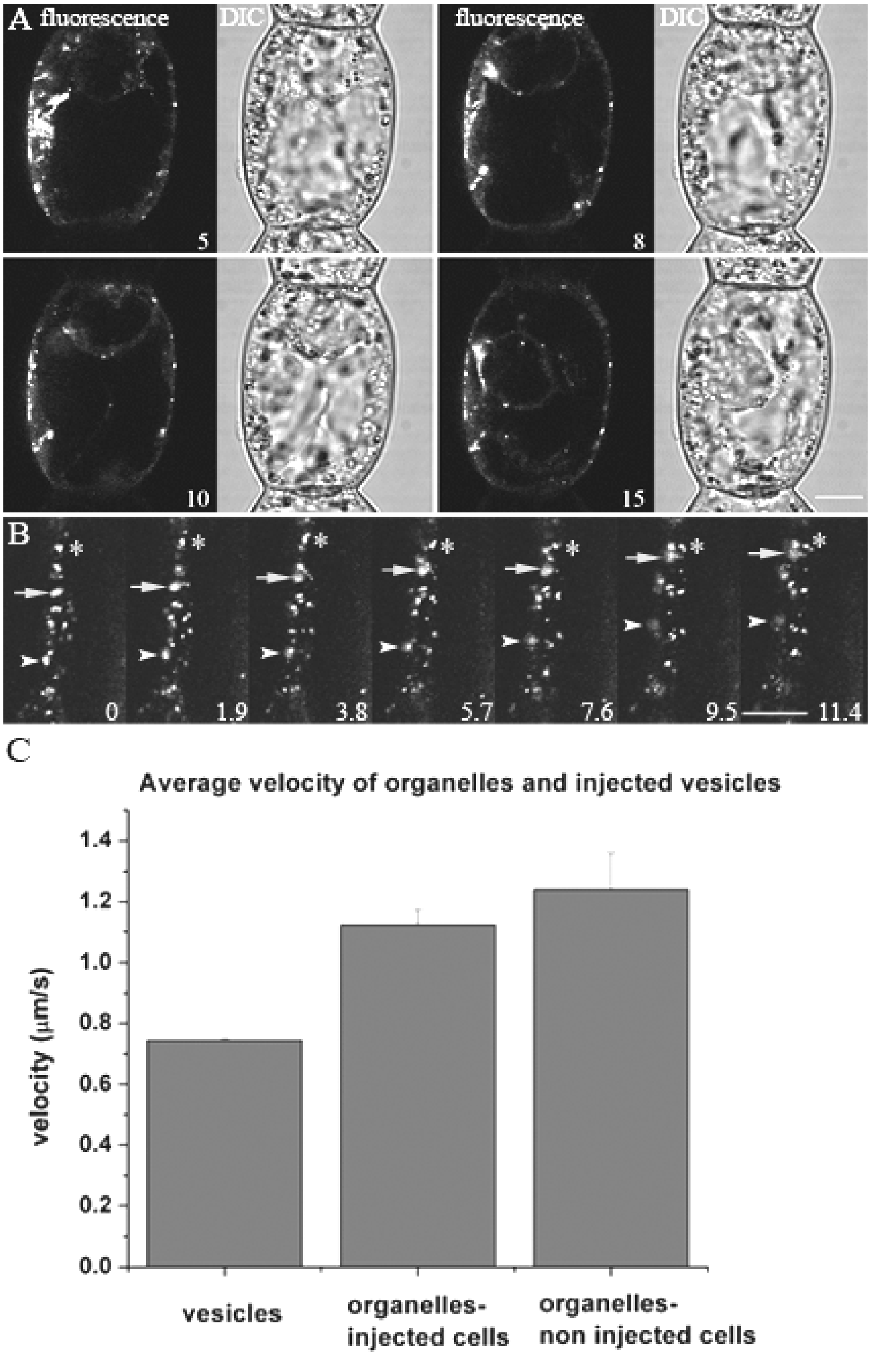

Figure 3 (opposite page). Synthetic lipid vesicles move in the cytoplasm of interphase cells. **(A)** Time series of an interphase stamen hair cell of *T. virginiana* injected with fluorescent lipid (DOPG) vesicles. Time in minutes after injection, bar = 10 µm. **(B)** Time series of moving vesicles in the cytoplasm. Time in sec, bar = 10 µm. Some vesicles move together for a while (asterisk, arrow and arrowhead) and then separate from each other. The fluorescent spot pointed to with an arrow is probably a cluster of three vesicles. **(C)** Graph showing the average velocity (± SE) of injected lipid vesicles (n = 60 in 5 cells) and organelles visible with DIC (n = 61 in 5 cells) in the same cells. The vesicles and organelles were followed for at least 17 sec, with 1.97 sec intervals. The average velocity was calculated from the displacement of vesicles or organelles over the time that they were followed.

Synthetic lipid vesicles accumulate in the cell plate region

Upon microinjection into cells in early to late anaphase, synthetic lipid vesicles moved from the microinjection site and distributed evenly in the cytoplasm. Within 5-10 minutes after injection into anaphase cells, synthetic lipid vesicles spread throughout the cytoplasm and between the chromosomes in the spindle (Fig. 4). When injected cells entered telophase, the vesicles accumulated at the spindle mid zone and were seen as a broad band of fluorescence. In DIC microscopy, a cell plate could not yet be observed at this stage (Fig. 4A, 22 minutes). This band of accumulated synthetic vesicles subsequently narrowed at the same time when the young cell plate became visible with DIC microscopy. This was seen in all injected cells (N = 24 cells). Occasionally, an additional accumulation of lipid vesicles was seen around the edges of the growing cell plate (data not shown).

The accumulation of injected synthetic lipid vesicles in the cell plate region was specific; vesicles did not just fill the accessible volume like co-injected fluorescent dextran did (Fig. 4C).

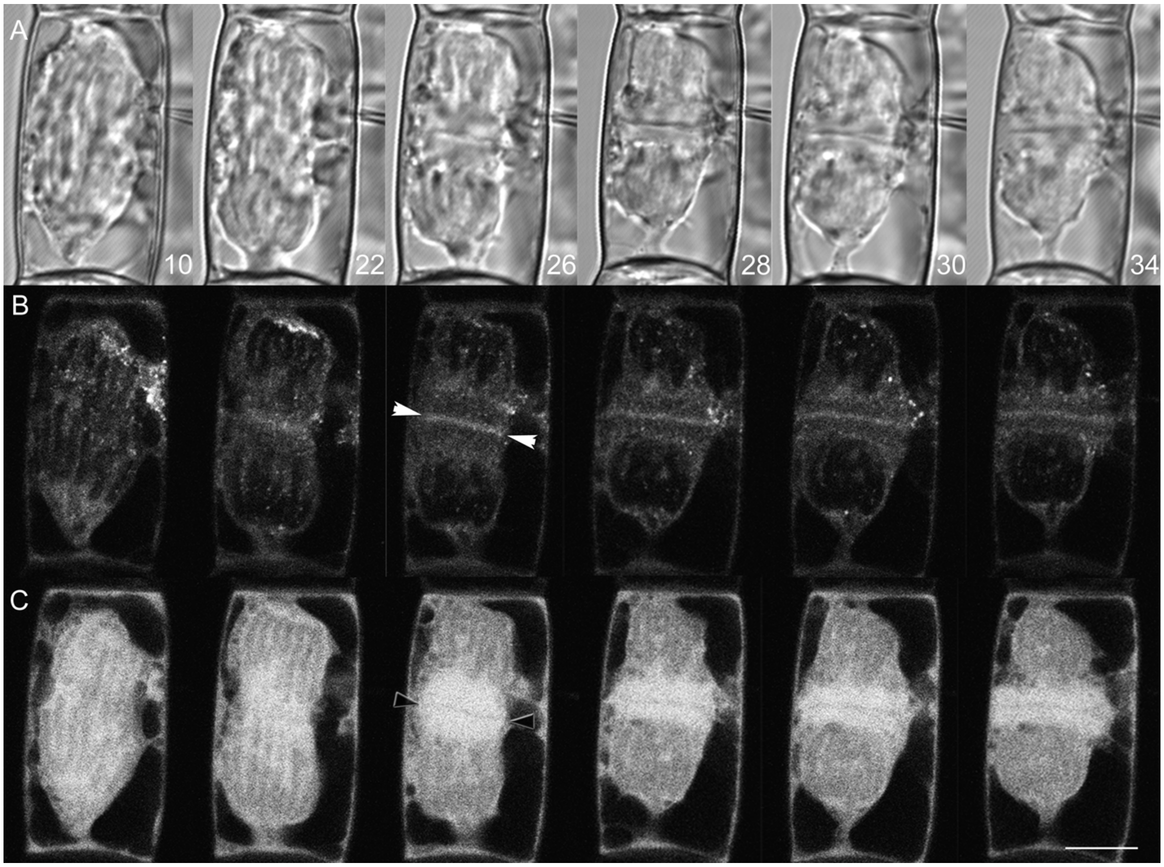

Figure 4. Synthetic vesicles accumulate in the cell plate region. Time series of a *T. virginiana* stamen hair cell, as seen with DIC **(A)**, that was co-injected at anaphase with fluorescently labeled synthetic lipid vesicles **(B)** and 10 kD Alexa-568 dextran **(C)**. Lipid vesicles accumulate in the whole cell plate region while it is being produced (between the white arrowheads). Fluorescently labeled dextran is distributed throughout the accessible cytoplasmic volume, excluding the cell plate (between the black arrowheads). Time in minutes after injection, scale bar = 10 µm.

We observed an uniform distribution of fluorescence throughout the cell plate region, i.e., there was no black line in the middle, which suggests that injected vesicles accumulated not only on the surface of the developing cell plate, but also within the fenestrated cell plate. We compared the width of the vesicle accumulation zone with that of the cell plate itself, as measured with FM4-64 labeling. FM4-64 is a fluorescent lipophilic styryl dye that labels the developing cell plate when applied from the outside of the cell (Bolte et al., 2004). FM4-64 did not label DOPG vesicles in vitro and in vivo (Fig. 5A and B). We followed the behavior of the injected synthetic lipid vesicles during cell plate formation and compared this with the cell plate labeling of externally applied FM4-64 (Fig. 5C). The accumulation of injected lipid vesicles in the cell plate region coincided with FM4-64 labeling of the cell plate. However, the region of synthetic vesicle accumulation was slightly, but consistently thicker than the FM4-64 labeled cell plate (1.5 µm versus 0.8 µm; Fig. 5D). The injection of synthetic lipid vesicles did not hinder or delay cell plate formation. In all vesicle injected cells, cell plate formation took on average 27’ ± 3’, which did not differ from the experimental controls (Fig. 6). Also, the initial appearance, the growth and attachment of the cell plate to the parental cell wall were all normal. Interestingly, the moment of injection did not have any influence on the accumulation of vesicles in the cell plate region. Injected vesicles accumulated in the whole cell plate region when injected at different stages of cell division (Table 1), even in cells in which a cell plate was already visible at the time of injection (Fig. 7A).

Stage of cell division when injected with vesicles	Percentage of cells with vesicle accumulation at the cell plate
Prophase	**100% (n=3)**
Metaphase	**100% (n=9)**
Anaphase	**100% (n=24)**
Telophase	**100% (n=7)**

Table 1. Lipid vesicles accumulate in the cell plate region upon injection at different stages of cell division. The moment of injection does not influence vesicle accumulation. Total cells with vesicle accumulation: 43.

Further, synthetic vesicles are not redistributed as long as the phragmoplast exists. Since microtubules are mostly present at the periphery of the torus shaped phragmoplast, they are not likely to be instrumental in bringing the vesicles to the center or keeping them there (Fig. 7B).

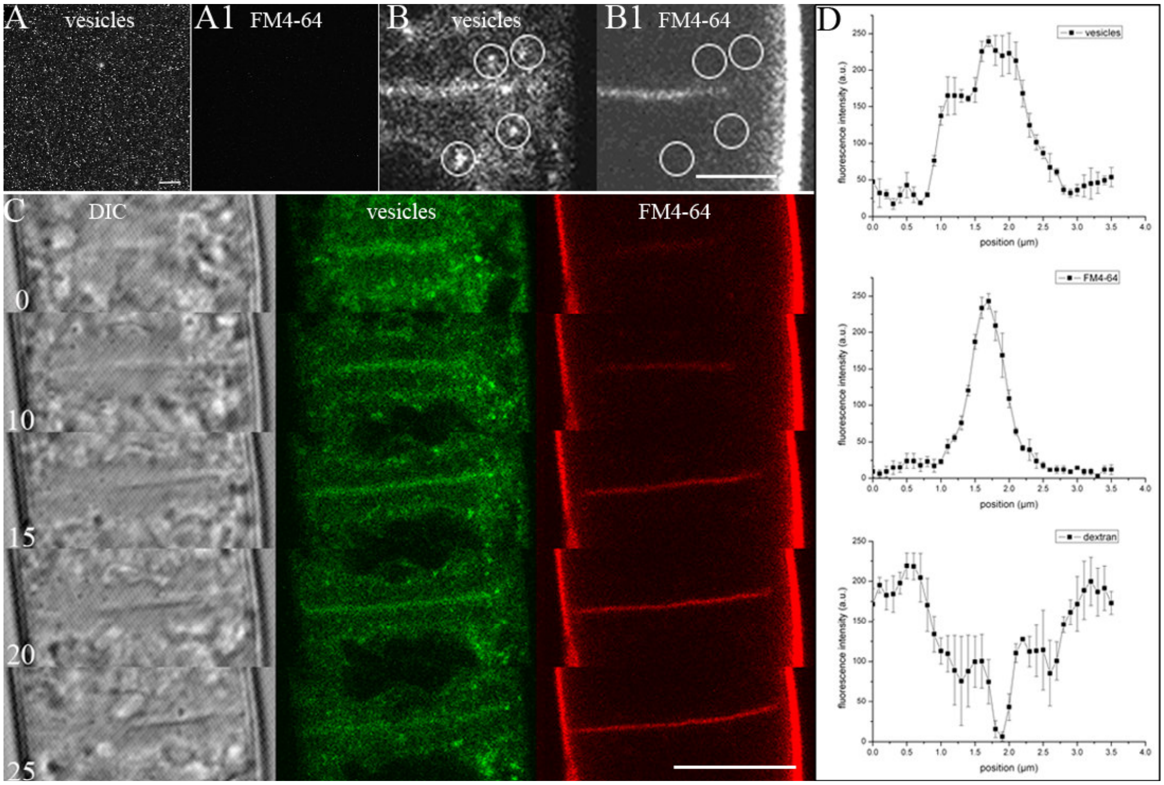

Figure 5. FM4-64 does not label the synthetic lipid vesicles in vitro and in vivo, but the accumulation of injected lipid vesicles in the cell plate region coincides with FM4-64 labeling of the cell plate. Bodipy FC12-HPC labeled DOPG vesicles **(A)** incubated for 1.5 hours with 2 µM FM4-64 in microinjection buffer are not labeled with FM4-64 **(A1)**. Bar = 10 µm. Injected fluorescently labeled DOPG vesicles **(B)** are not labeled with FM4-64 **(B1)** in a cell with a phragmoplast. The vesicles marked with white circles do not co-localize with FM4-64 labeling. The cell plate and plasma membrane however are clearly labeled with FM4-64. Bar = 5 µm. **(C)** The cell plate is labeled by injected lipid vesicles and with FM4-64. The synthetic lipid vesicles accumulate in the region of the cell plate at the same time as the cell plate is labeled with FM4-64, both labels correspond to the cell plate visible in DIC microscopy. Time in minutes, bar = 10 µm, n = 3 cells. FM4-64 concentration is 2 µM (in A1, B1, and C), added to the surrounding medium 15 minutes before injection during anaphase. **D.** Fluorescence intensity profiles of vesicles, FM4-64 and Alexa-568 dextran (10 kD) through the phragmoplast. The line profiles were taken from cells in late telophase, before the cell plate was attached to the parental cell wall. Three regions of 1 x 4 µm perpendicular to the phragmoplast were selected from the images. The average fluorescence intensity of each horizontal row of pixels was plotted versus its vertical position. The accumulation of vesicles in the cell plate region coincides with the FM4-64 labeling. However, the synthetic vesicles in the cell plate show a broader peak of fluorescence than the FM4-64 labeling. The dextran clearly does not enter the cell plate region.

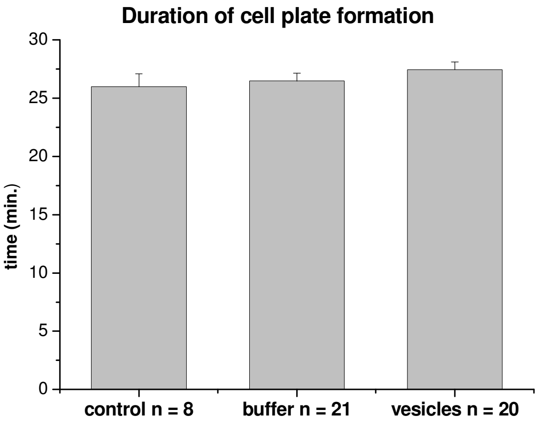

Figure 6. Injected vesicles do not hinder or delay cell plate formation. Duration of cell plate formation in non-injected cells, in cells injected with microinjection buffer, and in cells injected with fluorescent vesicles was measured from the moment of its visible appearance until its attachment to the parental cell wall. The moment of cell plate attachment was chosen as the moment when the cell plate touched the parental cell wall, and appeared straight. Data shown with SE.

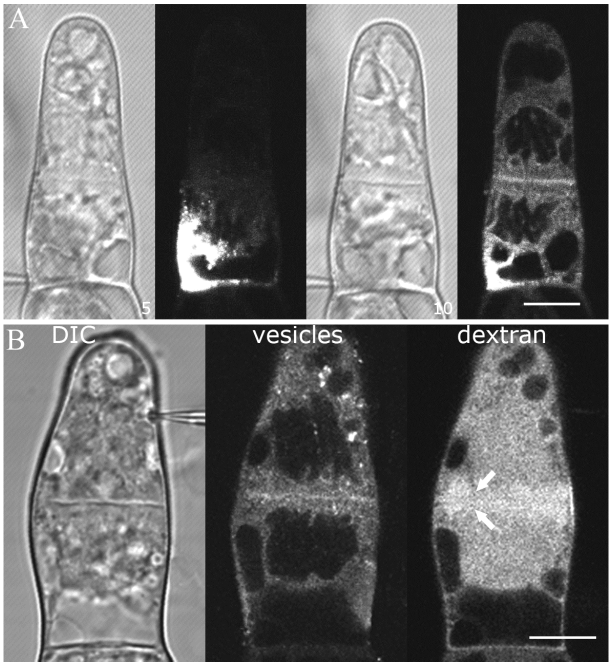

Figure 7. Synthetic vesicles accumulate at the same time in the whole cell plate region when injected at late telophase and are not redistributed from the central region of the torus shaped phragmoplast. **(A)** Vesicle accumulation after injection during late telophase when the cell plate was already partially formed (white arrowheads). Time in minutes after injection, bar = 10 µm. **(B)** Injected synthetic vesicles remain localized to the central cell plate region although the phragmoplast is already torus-shaped (indicated by white arrows). Bar = 10 µm, 46 minutes after injection.

To exclude that fluorescently labeled Bodipy FC12-HPC phosphocholine lipid or free Bodipy dye could label the cell plate without being part of the synthetic vesicles, we injected the vesicles into the interphase cell neighboring a cell in anaphase (Fig. 8). Upon injection, some fluorescence was transferred from the injected cell into the neighboring cells. This could be free Bodipy FC12-HPC, which has a molecular weight of 0.895 kD and is close to the exclusion limit (0.8 kD) of plasmodesmata (Pheasant and Hepler, 1987). In the dividing cell, no labeling of the cell plate occurred, which further underpins that the observed fluorescence in the cell plate region comes from the accumulation of injected fluorescent vesicles, and not from free dye.

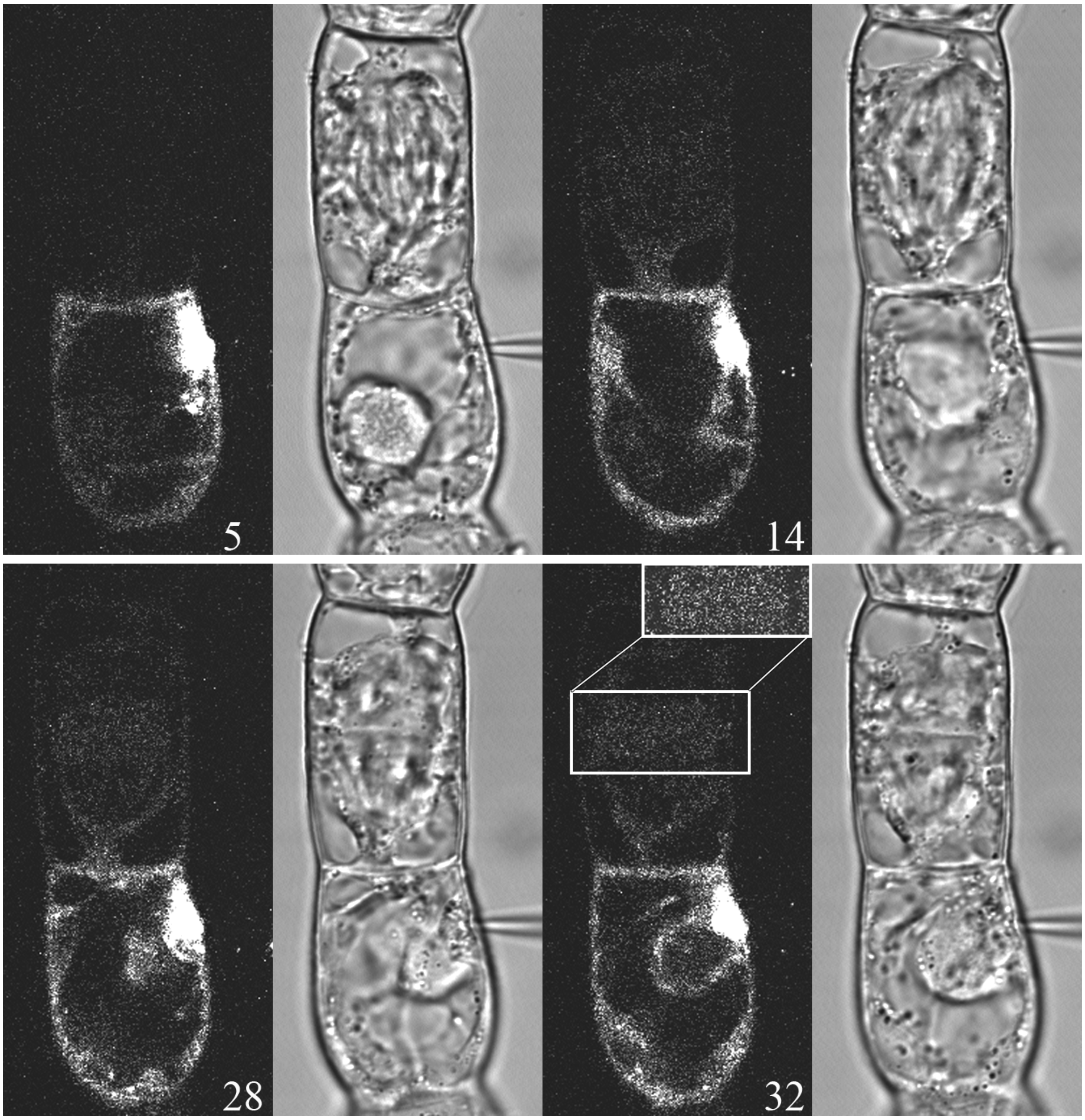

Figure 8. Bodipy FC12-HPC alone does not label the cell plate. A cell below a dividing one was injected with fluorescent synthetic vesicles. No labeling of the cell plate is visible. The probe only accumulates in the cell plate when it is incorporated into vesicles. Insert: zoom in and contrast stretch of the phragmoplast of the cell that neighbors the injected cell shown at 32 minutes to stress that free Bodipy FC12-HPC alone does not label the cell plate. Time in minutes, bar = 20 μm.

Synthetic lipid vesicles redistribute inside the daughter cells after cell plate attachment

At the end of cytokinesis, when the cell plate attached to the parental plasma membrane and cell wall, the lipid vesicles redistributed completely into the cytoplasm, while the FM4-64 labeling remained in the plasma membranes lining the young cell wall (Fig. 9). The fluorescent band of lipid vesicles first broadened (Fig. 9A, 2 minutes), then two clouds of fluorescence were formed on both sides of the cell plate (Fig. 9A, 4-8 minutes), and finally the fluorescence completely redistributed in the cytoplasm of the cells. This shows that synthetic lipid vesicles accumulate in the fenestrated cell plate, but do not fuse together with endogenous vesicles to form the cell plate.

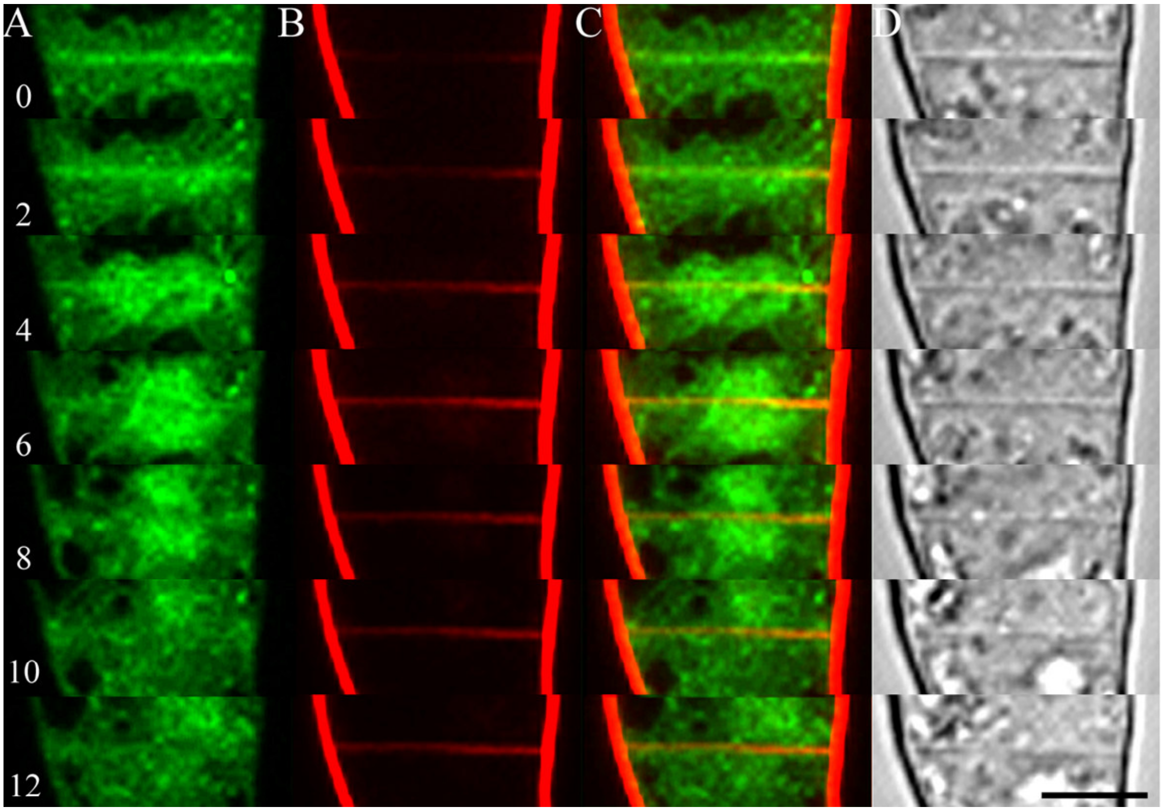

Figure 9. Redistribution of DOPG lipid vesicles after the cell plate is attached to the parental cell wall. The fluorescence of microinjected synthetic vesicles **(A)** is redistributed to the cytoplasm of the daughter cells while the labeling with FM4-64 **(B)** stays in the cell plate region. (**C**) is a merged image of (**A**) and (**B**). The cell plate is visible with DIC microscopy **(D)**. The FM4-64 concentration is 2 µM and was added to the surrounding medium 5 minutes before vesicle injection during telophase. Time in minutes, time 0 is arbitrarily chosen, bar = 10 µm.

We analyzed the fluorescence intensities of a region of 1.5 x 5 µm of the phragmoplast over time, including the cell plate, in cells injected with fluorescent synthetic vesicles and labeled with FM4-64 (Fig. 10). During the initial phase of cell plate growth and expansion, injected DOPG vesicles and FM4-64 labeled membranes showed the same distribution (Fig. 5B). The thickness of the cell plate of synthetic vesicles and FM4-64 labeling, which was measured as the width at half-height of a gauss curve fitted to the fluorescence intensity profile (see also Fig. 5C), stabilized after 10 to 15 minutes at 0.5 to 0.7 µm (Fig. 10A).

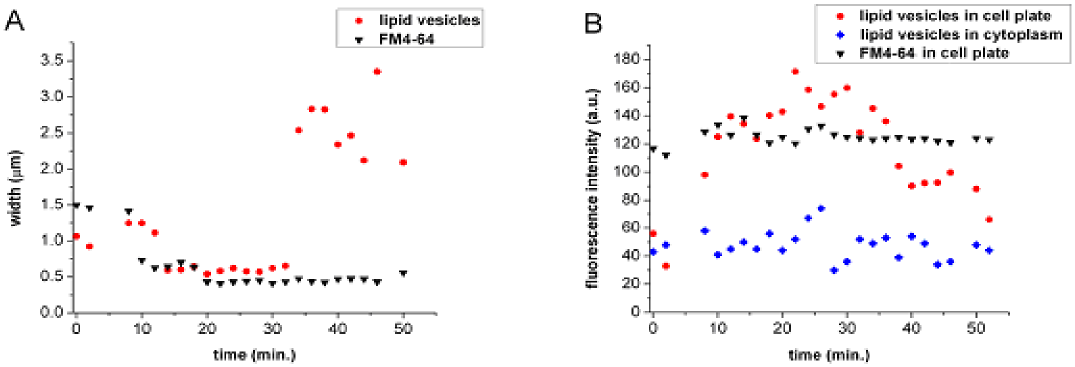

Figure 10. Comparison of vesicle and FM4-64 labeling in a phragmoplast and cell plate region. We measured: **(A)** The width of the maximum fluorescence intensity peak of injected vesicles and FM4-64 in the phragmoplast over time. The width of the peak is the width at the 1/2 maximal height of a gauss curve fitting. **(B)** The peak fluorescence intensity of the gauss curve fitting of injected vesicles and FM4-64 in the phragmoplast and in the cytoplasm over time.

About 30 to 35 minutes after initiation, the cell plate attached to the parental plasma membrane. At this moment the DOPG vesicles lost their confinement to the cell plate region and concomitantly the width of the fluorescence peak broadened. On the other hand, the thickness of cell plate as measured with FM4-64 did not broaden and stayed around 0.5 µm. The disappearance of the synthetic vesicles from the new cell wall between the two daughter cells is also evident from the fluorescence intensity measurements over time (Fig. 10B). Starting at 25 to 30 minutes, the maximum fluorescence intensity at the cell plate decreased steadily to the initial levels, whereas the FM4-64 labeling remained constant during the whole period. The decrease in fluorescence of the synthetic vesicles in the cell plate region was not caused by the bleaching of Bodipy; the fluorescence intensity of synthetic vesicles in the cytoplasm of the same cells did not change over time. This shows that injected vesicles only accumulate in the cell plate region, but do not fuse with each other, with the endogenous cell plate forming vesicles, or with the developing cell plate. They are again redistributed throughout the cytoplasm when the cell plate attaches to the parental plasma membrane and cell wall, and the maturation of the young cell wall begins, at the moment that the typical phragmoplast actin cytoskeleton also disappears.

DISCUSSION

Injected synthetic vesicles move through the cytoplasm

We used synthetic DOPG vesicles to study basic physical properties that vesicles require to enter, move through, and accumulate in the cell plate region. We prepared 60 nm DOPG vesicles with the same size as endogenous Golgi vesicles that are thought to form the cell plate, possibly together with endocytotic vesicles (Dhonukshe et al., 2006). We showed that these synthetic vesicles were stable in vitro and could be successfully microinjected into plant cells. The vesicles were not toxic to the cells and they did not disturb cellular processes.

The injected lipid vesicles did not fuse together or with endogenous membranes, but moved through the cytoplasm of interphase *T. virginiana* stamen hair cells at slightly lower velocities than large endogenous organelles. The presence of the synthetic DOPG membrane did not affect the movement of these endogenous organelles in the cytoplasm (Fig. 2 and 3).

Although we injected uncoated lipid vesicles, these vesicles may be coated in the cells with cytoplasmic proteins. The fast distribution of the vesicles and their movement inside the cytoplasm could be caused by motor protein binding and subsequent transport activity. It is known that myosin-I prefers to bind anionic lipids (Adams and Pollard, 1989), like the DOPG that we used for our vesicles. Pull down assays with DOPG coated magnetic beads in cytoplasmic extracts show the binding of several proteins to the membrane (data not shown). On the other hand, it is unlikely that endo- or trans-membrane proteins, which may be needed for binding of these motor proteins, are inserted into the membranes of injected synthetic vesicles. Furthermore, we cannot exclude the contribution of hydrodynamic flow on vesicle movement. Cytoplasmic movement by hydrodynamic flow is an additional way of transport and may well contribute to transport of large structures like vesicles and even organelles (Houtman et al., 2007; Esseling-Ozdoba et al. submitted).

Synthetic vesicles are transported through the phragmoplast and accumulate in the cell plate region

Although their membrane composition and content are different from endogenous vesicles, microinjected synthetic DOPG vesicles passed through the phragmoplast structure of microtubules, actin filaments and ER and accumulated at the developing cell plate. They did not disturb the transport of endogenous vesicles towards the cell plate since the initiation and the subsequent development of the cell plate was not disturbed in any of the injected cells (as visualized with DIC and FM4-64 and with regard to time) (Fig. 4 to 6 and Table 1).

The specific accumulation of synthetic vesicles in the cell plate region of the phragmoplast, instead of filling the accessible volume, points to a dual process in which there is directional transport of these vesicles in the phragmoplast and inhibition of transport away from the cell plate. Because the vesicles were transported through the cytoplasm after they were injected, it could well be that these vesicles were, as we discussed above, coated with cytoplasmic motor proteins that caused their movement along the phragmoplast microtubule and/or actin cytoskeleton. However, the mode of transport of endogenous vesicles through the phragmoplast is still unclear. With electron microscopy (EM), it has been observed that some vesicles are associated with phragmoplast microtubules, suggesting the microtubules as the cytoskeletal element along which the vesicles are transported, but some other vesicles apparently were not associated with microtubules (Otegui et al., 2001). Actin filaments were not considered in those studies since it was not possible to preserve them for EM observations (Seguí-Simarro et al., 2004). Based on these studies, it is not possible to assess if actin filaments, which are located in arrays parallel with the microtubules in the phragmoplast, are involved in vesicle transport. Synthetic vesicles injected at different stages of cell division, even at late telophase when the cell plate was already partially formed, accumulated at the same time in the whole cell plate region. This means that vesicles at late telophase are transported towards the cell plate along the remaining actin filaments, at least in that part of the phragmoplast from which microtubules have already disappeared (*T. virginiana*: Zhang et al., 1990; Tobacco BY2 cells: Granger and Cyr, 2000). In that middle part, the actin cytoskeleton is still present as shown with microinjections of fluorescent phalloidin (Zhang et al., 1993), which we confirmed in living cells of tobacco BY-2 suspension cells using a GFP::FABD construct for visualization of the actin cytoskeleton, and a spinning disc microscope (Fig. 1). One might also think that in this situation injected vesicles are transported to the cell plate through the margins of the phragmoplast in which there are still microtubules present and subsequently move laterally along the surface of the developing cell plate. However, in those cells that were injected at late telophase, we never observed a flow of fluorescence from the phragmoplast margins towards the microtubule-free middle of the cell plate region, excluding the possibility that synthetic vesicles only "incorporated" at the margins and moved laterally along the cell plate. This demonstrates that it could well be that vesicles use F-actin to be transported through the phragmoplast towards the cell plate. This transport could be also in the form of hydrodynamic flow produced by endogenous vesicles moving along the phragmoplast cytoskeleton towards the cell plate, as our results indicate for vesicle movement in interphase cells and prove for molecules the size of GFP (Esseling-Ozdoba et al. submitted).

Synthetic vesicles do not fuse with the cell plate

Although the injected synthetic vesicles were transported through the phragmoplast and accumulate in the cell plate region, they did not fuse with the developing cell plate, but redistributed again throughout the cytoplasm upon attachment of the cell plate to the parental cell wall (Fig. 8). This redistribution strongly suggests that these vesicles cannot fuse with endogenous vesicles/cell plate or with each other. This is already indicated by the fact that the vesicles did not fuse in vitro, even after 7 days. In injected cells, the DOPG vesicles probably reside in the tubulo-vesicular network, the tubular network and finally in the fenestrae (Samuels et al., 1995; Staehelin and Hepler, 1996; Seguí-Simarro et al., 2004) of the developing cell plate. Whether the region of DOPG vesicle accumulation coincides with the CPAM, which is suggested to be responsible for regulation of the fusion events in the cell plate region, is difficult to determine. The CPAM including the cell plate proper has a total width of 155 nm (Seguí-Simarro et al., 2004), smaller than the resolution of the CLSM

Our observation that injected vesicles cannot fuse with endogenous vesicles in the developing cell plate was to be expected. Firstly, the injected vesicles lack trans-membrane SNARE proteins and are probably not able to acquire them after injection. SNAREs are necessary for the fusion of cell plate forming vesicles, since the Arabidopsis SNARE mutants *knolle* and *keule* have unfused cytokinetic vesicles in the cell plate region (Lukowitz et al., 1996; Assaad et al., 1996; Lauber et al., 1997; Waizenegger et al. 2000). Secondly, only homotypic fusions may occur in the cell plate region, which means that only the similar vesicles are able to fuse as has been observed with electron tomography (Seguí-Simarro et al., 2004) and reviewed by Albertson et al. (2005). Our synthetic vesicles are physically identical to each other and do not fuse with each other or other membranes in medium and cells in interphase. We wondered whether their close proximity and the environment of the phragmoplast would make them fuse to each other in the cell plate region of dividing cells. Based on these observations we conclude that close proximity alone and in combination with the specific environment in the cell plate region is not sufficient for fusion of DOPG vesicles.

F-actin may keep unfused vesicles in the cell plate region

During the centrifugal growth of the cell plate, the centrally located microtubules depolymerize and reassemble at the periphery of the phragmoplast, which then becomes torus-shaped (second phase) (Valster and Hepler, 1997; Kost and Chua, 2002). The microtubules would therefore not be able to keep unbound vesicles from diffusing away from the central region of the cell plate. This suggests that another mechanism is responsible for keeping the synthetic vesicles close to the cell plate region. We hypothesize that actin filaments could play this role to keep the synthetic vesicles in the cell plate region, like they could also act as a scaffold for the fragile developing cell plate (Samuels and Staehelin, 1996).

The breakdown of actin filaments in the phragmoplast occurs uniformly along the whole width at the moment when the cell wall is completed, rather than in a centrifugal pattern (Cleary et al., 1992; Zhang et al., 1993; Hepler et al., 1993). A similar mechanism has been proposed for keeping exocytotic vesicles close to the growing tip of tip growing cells, where F-actin delivers vesicles to the vesicle rich region in pollen tube (Geitmann et al., 2000) and root hair tips (Miller et al., 1999) and keeps them in the tip (Ketelaar et al., 2003). F-actin in the phragmoplast could be involved in delivering vesicles to the cell plate and keeping them there, while at the same time keeping larger organelles away from the developing cell plate, thus acting as a physical sieve for these vesicles and barrier for the larger organelles, that otherwise would obstruct the accumulation processes. These roles of F-actin in the phragmoplast are supported by experiments in which cells during cytokinesis were injected with excess amounts of the G-actin binding protein profilin (Valster et al., 1997). Upon injection, the actin filaments in the phragmoplast depolymerized resulting in a delay in the cell plate formation, or a complete absence of the cell plate.

We have shown that DOPG vesicles are a useful tool to study the processes involved in cell plate formation. Using these synthetic vesicles, we uncovered a possible new role for the phragmoplast actin cytoskeleton in cell plate formation. The next challenge is to elucidate the exact origin(s) and nature of the endogenous vesicles that form the cell plate. As one of the direct experimental approaches, we propose to inject vesicles with experimentally defined surfaces (e.g., specific phospho- and/or glycolipid compositions and embedded and/or (covalently) attached proteins) to analyze the vesicle transport mechanism and requirements for vesicles to fuse and form the cell plate. In addition, injection of biological vesicles from endosomal origin could help elucidate their proposed role in cell plate formation.

MATERIAL AND METHODS

Plant Material

Tradescantia virginiana plants were grown in a growth chamber with a 16-hrs photoperiod at 25°C and 8-hrs dark period at 18°C and 75-80% relative humidity. Stamen hairs with dividing cells in the apical region were dissected from immature flower buds with a length of approximately 5 mm. For microinjection experiments, we immobilized these stamen hairs in a thin layer of 1% low temperature gelling agarose (BDH Laboratory Supplies, UK) in culture medium (5 mM HEPES, 1 mM $MgCl_2$, and 0.1 mM $CaCl_2$, pH 7.0) and 0.025% Triton X-100 (BDH Laboratory Supplies, UK), following the procedure described by Vos et al. (1999). The layer of agarose with stamen hair cells was solidified by cooling at 4°C for 10 to 15 sec and then flooded with culture medium.

Preparation of synthetic vesicles, dextran and FM4-64

Synthetic vesicles consisted for 98% of the anionic non-fluorescent phospholipid 1,2-Dioleoyl-*sn*-Glycero-3-[Phospho-*rac*-(1-glycerol)] (DOPG, Avanti Polar Lipids) and for 2% of the fluorescent phosphocholine Bodipy FC12-HPC (Molecular Probes, excitation maximum at 503 nm, emission maximum at 512 nm). Bodipy FC12-HPC was especially chosen because it labels the acyl chain rather than the hydrophilic head of the phospholipid. It therefore prevents the movement of the fluorescent probe between lipid layers (jumping). DOPG was purchased as a chloroform solution of a sodium salt. Bodipy FC12-HPC was purchased as a powder and was than dissolved in ethanol. Phospholipids were mixed together and dried onto a glass surface under a stream of nitrogen, followed by at least 2 hours under vacuum to remove the last traces of solvent. The dried lipid mixture was hydrated with injection buffer (5 mM HEPES, 0.1 mM KCl, pH 7.0) to a concentration of 0.5 mg/ml; an optimal concentration to observe vesicles in the microscope and to measure them with dynamic light scattering. The lipids were freeze-thawed with liquid nitrogen for five cycles to disperse them and pushed through an extruder with a polycarbonate filter with a 50 nm pore size to yield vesicles with a diameter of ~60 nm. The vesicle diameter was determined using dynamic light scattering and cryo-TEM. For dynamic light scattering, the instrumental setup consisted of an ALV-5000 correlator and a scattering device with an ALV-125 goniometer and a multiline Lexel AR-laser source. Data for monodispersity were collected at scattering angles of 60, 90 and 120 degrees at a wavelength of 513 nm. After preparation, vesicle fluorescence was checked under the CLSM microscope. Vesicles were stored at 4°C and used for microinjection within 4 days, although they were stable in microinjection buffer for more than 7 days as determined with dynamic light scattering.

For co-injection experiments, vesicles were mixed with fluorescent dextran (Alexa-568 dextran, 10 kD, Invitrogen, Eugene, OR). Dextran was dissolved in microinjection buffer as a 5 mg/ml stock and diluted to 0.5 mg/ml before microinjection experiment in the microinjection buffer containing the DOPG vesicles. For labeling of the cell plate with FM4-64 (Invitrogen), the dye was dissolved in DMSO as a stock of 200 µM and further diluted in the preparation medium or water and used at a final concentration of 2 µM.

Visualization of vesicles in cryo-TEM

For observation of synthetic DOPG vesicles in cryo-TEM, 200-mesh copper grids covered with holey carbon film were submerged in the vesicle solution in microinjection buffer. The excess fluid from the film was removed with filter paper. The grids were plunge-frozen in liquid propane and after short storage in liquid nitrogen placed in a cryo-holder (Gatan 626, Abingdon, UK). The vesicles were observed with a transmission electron microscope JEOL 1200 EX II (Tokyo, Japan). Images were made with a KeenView digital camera (SIS, Münster, Germany).

Microinjection

The microinjection experiments were conducted according to Vos et al. (1999). In short, needles were pulled from borosilicate capillaries with filament (World Precision Instruments, Sarasota, FL) by using a vertical pipette puller (model 700C, David Kopf Instruments, Tujunga, California). The opening of these needles was 200-240 nm (measured from scanning electron microscopy images; data not shown). The needles were back-filled with the experimental solution and water and mounted onto a pressure injector consisting of a micro-needle holder (Eppendorf, Madison, Wisconsin) and a 2 ml micrometer syringe (Gilmont Instruments, Barrington, Illinois) connected via a water-filled fine polyethylene tubing. The position of the pressure injector was controlled by a hydraulic micromanipulator (model N0-303, Narashige Scientific Instruments, Tokyo, Japan).

Microscopy, imaging and data analysis

Microinjections were performed on inverted microscopes. Images were collected with a Cell Map IC (BioRad, Hemel Hampstead, UK) confocal laser-scanning microscope, coupled to an Eclipse TE2000-S (Nikon, Tokyo, Japan) or with an LSM 5 Pascal confocal laser-scanning microscope coupled to an Axiovert 200 microscope (Zeiss, Jena, Germany). For Bodipy/Alexa-568 dextran or FM4-64 dual scanning we used the excitation/emission combination of 488/520-540 nm BP and 532/560 nm LP (Cell Map IC) or the combination of 488/BP 505-550 nm BP and 543/560 nm LP (HFT 488/NFT 545/HFT 543; LSM 5 Pascal). Images were obtained with a 1.4 NA 60X or 1.4 NA 63X oil immersion objective, collected by Kalman averaging of 2-3 full scans (Cell Map IC) or with scan speed 7 (LSM 5 Pascal).

Images were taken at 2 or 3 minutes intervals, which allowed observation of developing cell plates for long periods of time without disturbing the cell plate formation process. Images were processed and analyzed with the software programs Confocal Assistant 4.02 (written by Todd Clark Brelje), Adobe Photoshop 5.0 and 8.0 (Adobe Systems, Mountain View, CA), Image J (version 1.32j, National Institute of Health, Bethesda, MD). For fluorescence intensity plots, rectangles (10 x 50 pixels) of images at different time points were cut out and reduced to 1 x 50 pixels in order to average the fluorescence. The resulting pixel intensities were saved as text files with Image J, and plotted and curve-fitted in Origin (version 7.5 SR5, OriginLab Corporation, Northampton, MA) using standard Gauss equations.

Images of actin filaments in phragmoplast of BY-2 cells transformed with GFP::FABD were made with a spinning disk confocal microscope (PerkinElmer) coupled to an Eclipse TE2000-S (Nikon, Tokyo, Japan).

ACKNOWLEDGEMENTS

We gratefully thank Richard Kik, Mieke Kleijn and Frans Leermakers of the Laboratory of Physical Chemistry and Colloid Science, Wageningen University, for help with designing the vesicles and for useful discussions. We thank Magdalena Szechyńska-Hebda for initial help with the vesicle microinjections. She was supported by the 5th Framework Program project CROPSTRESS under contract number QLK5-CT-2002-

30424. We also thank Tijs Ketelaar for providing figure 1A, Adriaan van Aelst for help with cryo-TEM and John Esseling for critical reading of the manuscript. AMCE thanks the FOM Institute for Atomic and Molecular Physics (AMOLF), Amsterdam, for financial support for this project.

REFERENCES

Adams R.J., Pollard T.D (1989). Binding of myosin I to membrane lipids. Nature, **340**, 565-568.

Albertson, R., Riggs, B. and Sullivan, W. (2005). Membrane traffic: a driving force in cytokinesis. Trends Cell Biol. **15**, 92-101.

Assaad, F.F., Mayer, U., Wanner, G. and Jürgens, G. (1996). The *KEULE* gene is involved in cytokinesis in *Arabidopsis*. Mol. Gen. Genet. **253**, 267-277.

Baskin, T.I. and Cande, W.Z. (1990). The structure and function of the mitotic spindle in flowering plants. Annu. Rev. Plant Physiol. Plant Mol. Biol. **41**, 277-315.

Bednarek, S.Y., and Falbel, T.G. (2002). Membrane trafficking during plant cytokinesis. Traffic **3**, 621-629.

Bolte, S., Talbot, C., Boutte, Y., Catrice, O., Read, N.D. and Satiat-Jeunemaitre, B. (2004). FM-dyes as experimental probes for dissecting vesicle trafficking in living plant cells. J. Microsc. **214**, 159-173.

Cleary, A.L., Gunning, B.E.S., Wasteneys, G.O., and Hepler, P.K. (1992). Microtubule and F-actin dynamics at the division site in living *Tradescantia* stamen hair cells. J. Cell Sci. **103**, 977-988.

Dhonukshe, P., Baluška, F., Schlicht, M., Hlavacka, A., Šamaj, J., Friml, J. and Gadella, Jr., W.J. (2006). Endocytosis of cell surface material mediates cell plate formation during plant cytokinesis. Dev. Cell **10**, 137-150.

Esseling-Ozdoba, A., Houtman, D., van Lammeren, A.A.M., Eiser, E., and Emons, A.M.C. (2007). Hydrodynamic flow in the cytoplasm of plant cells. Submitted to Journal of Microscopy.

Geitmann, A., Snowman, B.N., Emons, A.M.C., and Franklin-Tong, V.E. (2000). Alterations in the Actin Cytoskeleton of Pollen Tubes Are Induced by the Self-Incompatibility Reaction in *Papaver rhoeas*. Plant Cell, **12**, 1239-1252.

Gu, X., and Verma, D.P.S. (1996). Phragmoplastin, a dynamin-like protein associated with cell plate formation in plants. EMBO J. **15**, 695-704.

Granger, C.L. and Cyr, R.J. (2000). Expression of GFP-MAP4 reporter gene in a stably transformed tobacco cell line reveals dynamics of microtubule reorganization. Planta **210**: 502-509.

Hepler, P.K. (1982). Endoplasmic reticulum in the formation of the cell plate and plasmodesmata. Protoplasma **111**: 121- 133.

Hepler, P.K., Cleary, A.L., Gunning, B.E.S., Wadsworth, P., Wasteneys, G.O. and Zhang, D.H. (1993). Cytoskeletal dynamics in living plant cells. Cell Biol. Int. **17**, 127-142.

Houtman, D., Pagonabarraga, I., Lowe, C.P., Esseling-Ozdoba, A., Emons A.M.C. and Eiser, E. (2007). Hydrodynamic flow caused by active transport along cytoskeletal elements. *EPL*, **78**, 18001p1-p5.

Jürgens, G. (2005). Cytokinesis in higher plants. Annu. Rev. Plant Biol. **56**, 281-299.

Kakimoto, T. and Shibaoka, H. (1988). Actin filaments and microtubules in the preprophase band and phragmoplast of tobacco cells. Protoplasma **140**,151-156.

Ketelaar, T., de Ruijter, N.C.A., and Emons, A.M.C. (2003). Unstable F-actin specifies the area and microtubule direction of cell expansion in Arabidopsis root hairs. Plant Cell **15**, 285-292.

Kost, B., Chua, N.-H. (2002). The plant cytoskeleton: vacuoles and cell walls make the differences. Cell **108**, 9-12.

Lauber, M.H., Waizenegger, I., Steinmann, T., Schwarz, H., Mayer, U., Hwang, I., Lukowitz, W. and Jürgens, G. (1997). The Arabidopsis KNOLLE protein is a cytokinesis-specific syntaxin. J. Cell Biol. **139**, 1485-1493.

Lukowitz, W., Mayer, U., and Jürgens, G. (1996). Cytokinesis in Arabidopsis embryo involves the syntaxin-related KNOLLE gene product. Cell **84**, 61-71.

Miller, D.D., de Ruijter, N.C.A., Bisseling, T., and Emons, A.M.C. (1999). The role of actin in root hair morphogenesis: studies with lipochito-oligosaccharide as a growth stimulator and cytochalasin as an actin perturbing drug. Plant J. **17**, 141-154.

Molchan, T. M., Valster, A.H. and Hepler, P.K. (2002). Actomyosin promotes cell plate alignment and late lateral expansion in *Tradescantia* stamen hair cells. Planta **214**, 683-693.

Otegui, M.S., Mastronarde, D.N., Kang, B.-H., Bendarek, S.Y., and Staehelin, L.A. (2001). Three-dimensional analysis of syncytial-type cell plates during endosperm cellularization visualized by high resolution electron tomography. Plant Cell **13**, 2033-2051.

Pheasant, D.J., and Hepler, P.K. (1987). Intracellular pH change is not detectable during metaphase/anaphase transition in *Tradescantia* stamen hair cells. European J. Cell Biol. **43**, 10-13.

Samuels, A.L. and Staehelin, L.A. (1996). Caffeine inhibits cell plate formation by disrupting membrane reorganization just after the vesicle fusion step. Protoplasma **195**, 144-155.

Samuels, A.L., Giddings, Jr., T.H., and Staehelin, L.A. (1995). Cytokinesis in tobacco BY-2 and root tip cells: a new model of cell plate formation in higher plants. J. Cell Biol. **130**, 1345-1357.

Sano, T., Higaki, T., Oda, Y., Hayashi, T., and Hasezawa, S. (2005). Appearance of actin microfilament "twin peaks" in mitosis and their function in cell plate formation, as visualized in tobacco BY-2 cells expressing GFP-fimbrin. Plant J. **44**, 595–605.

Schopfer, C. R., and Hepler, P.K. (1991) Distribution of membranes and the cytoskeleton during cell plate formation in pollen mother cells of Tradescantia. J. Cell Sci. **100**: 717-728.

Seguí-Simarro, J.M., Austin, J.R. II, White, E.A., and Staehelin, L.A. (2004). Electron tomographic analysis of somatic cell plate formation in meristematic cells of Arabidopsis preserved by high-pressure freezing. Plant Cell **16**, 836-856.

Staehelin, A. L. and Hepler, P.K. (1996). Cytokinesis in higher plants. Cell **84**, 821-824.

Ueda, K., Sakaguchi, S., Kumagai, F., Hasezawa, S., Quader, H. and Kristen, U. (2003) Development and disintegration of phragmoplasts in living cultured cells of a GFP:TUA6 transgenic Arabidopsis thaliana plant. Protoplasma **220**: 111-118.

Valster, A.H., and Hepler, P.K. (1997). Caffeine inhibition of cytokinesis: effect on phragmoplast cytoskeleton in living *Tradescantia* stamen hair cells. Protoplasma **196**, 155-166.

Valster, A.H., Pierson, E.S., Valenta, R., Hepler, P.K. and Emons, A.M.C. (1997). Probing the plant actin cytoskeleton during cytokinesis and interphase by profilin microinjection. Plant Cell **9**, 1815-1824.

Verma, D.P.S. (2001). Cytokinesis and building of the cell plate in plants. Annu. Rev. Plant Physiol. Plant Mol. Biol. **52**, 751-784.

Vos, J.W, Valster, A.H, and Hepler, P.K. (1999). Methods for studying cell division in higher plants. In Methods in Cell Biology, C.L. Rieder, ed (San Diego, CA: Academic Press) **61**, 413-437.

Waizenegger, I., Lukowitz, W., Assaad, F., Schwarz, H., Jürgens, G., and Mayer, U. (2000). The *Arabidopsis KNOLLE* and *KEULE* genes interact to promote vesicles fusion during cytokinesis. Curr. Biol. **10**, 1371-1374.

Whaley, W.G and Mollenhauer, H.H. (1963). The Golgi apparatus and cell plate formation. A postulate. J. Cell Biol. **17**, 216-221.

Wick, S.M. (1991). Spatial aspects of cytokinesis in plant cells. Curr. Opin. Cell Biol. **3**, 253-260.

Yokoyama, R. and Nishitani, K. (2001). Endoxyloglucan transferase is localized both in the cell plate and in the secretory pathway destined for the apoplast in tobacco cells. Plant Cell Physiol. **42**, 292-300.

Zhang, D., Wadsworth, P. and Hepler, P.K. (1990). Microtubule dynamics in living dividing cells: confocal imaging of microinjected fluorescent brain tubulin. Proc. Natl. Acad. Sci. USA **87**, 8820-8824.

Zhang, D., Wadsworth, P. and Hepler, P.K. (1993). Dynamics of microfilaments are similar, but distinct from microtubules during cytokinesis in living, dividing plant cells. Cell Motil. Cytoskel. **24**, 151-155.

Zuo, J., Niu Q-W., Nishizawa, N., Wu, Y., Kost, B. and Chua, N-H. (2000). KORRIGAN, an Arabidopsis endo-1,4-β glucanase, localized to the cell plate by polarized targeting is essential for cytokinesis. Plant Cell **12**, 1137-1152.

Chapter 3

Flexibility contra Stiffness: the Phragmoplast Exit as a Physical Barrier for Polystyrene Beads but not for Synthetic Membranous Vesicles

Agnieszka Esseling-Ozdoba[1], Richard A. Kik[2], André A.M. van Lammeren[1], Mieke J. Kleijn[2], Anne Mie C. Emons[1]

[1]Laboratory of Plant Cell Biology, Department of Plant Sciences, Wageningen University, Arboretumlaan 4, 6703 BD Wageningen, The Netherlands

[2]Laboratory of Physical Chemistry and Colloid Science, Wageningen University, Dreijenplein 6, 6703 HB Wageningen, The Netherlands

Submitted to Journal of Cell Science

Abstract

During plant cytokinesis, membranous vesicles (60 - 80 nm in diameter) are transported to the cell division location of the cell where they fuse with each other to form a cell plate, the initial cell wall that will separate the daughter cells. These vesicles move through a cytoplasmic dense area, the phragmoplast, consisting of actin filaments and microtubules, endoplasmic reticulum and vesicles. Using microinjection of fluorescent synthetic DOPG vesicles and polystyrene beads into *Tradescantia virginiana* stamen hair cells, we studied the physical parameters size and stiffness that the cell plate forming vesicles need to have to be transported through the phragmoplast towards the forming cell plate. We show that the phragmoplast is non-selective for the size of tested synthetic DOPG vesicles which is up to 150 nm, but that the phragmoplast exit site, or cell plate region entry site, forms a physical barrier for stiff polystyrene beads of 20 and 40 nm also when these are coated with the same DOPG membrane. With this, we show that flexibility is an important parameter for vesicle transport through the whole phragmoplast towards the cell plate.

INTRODUCTION

Cytokinesis in higher plant cells partitions the cytoplasm between two daughter cells by the formation of a cell plate that will become the cell wall between the new cells. This process occurs in telophase with the delivery and fusion of cytokinetic membrane vesicles carrying cell wall material. In the plane of cell division, the local fusion of vesicles produces a transient membrane compartment, the cell plate filled with the content of vesicles, cell wall material, and surrounded by a so-called cell plate assembly matrix (CPAM) of unknown molecular makeup (Seguí-Simarro et al., 2004). The cell plate grows centrifugally until it meets the parental cell wall, where it fuses. During its maturation, the cell plate undergoes complex reorganization, which involves the fusion of new vesicles, secretion of cell wall material into the forming cell wall, and removal of excess membrane from the forming cell plate (Staehelin and Hepler, 1996).

The cytokinesis-specific structure that is crucial for cell plate formation is called the phragmoplast. The phragmoplast consists of endoplasmic reticulum and cell plate forming vesicles and microtubules and actin filaments. The phragmoplast cytoskeleton transports vesicles to the plane where the cell plate is being formed (Staehelin and Hepler, 1996; Valster et al., 1997), keeps them in the cell plate region (Esseling-Ozdoba et al., submitted), where they fuse with each other (Samuels et al., 1995; Otegui et al., 2001; Seguí-Simarro et al., 2004), and assists in the proper attachment of the cell plate to the parental cell wall (Valster and Hepler, 1997; Molchan et al., 2002). Fusion occurs at a place that is, earlier in the cell division process, determined by the preprophase band (PPB) of microtubules and actin filaments (Mineyuki et al., 1999), which disassembles at nuclear envelope breakdown, but is still recognizable during cell plate fusion with the maternal plasma membrane as the actin-depleted zone of the cell cortex (Cleary et al., 1992). The phragmoplast cytoskeleton consists of two opposing cylindrical arrays of parallelly aligned microtubules and actin filaments. The fast growing plus ends of microtubules (Kakimoto and Shibaoka, 1988; Baskin and Cande, 1990; Wick, 1991; Cleary et al., 1992) as well as those of actin filaments (Kakimoto and Shibaoka, 1988; Wick, 1991; Cleary et al., 1992) are perpendicular to the forming cell plate (Baskin and Cande, 1990; Wick, 1991; Cleary et al., 1992; Zhang et al., 1990, 1993; Hepler et al., 1993; Sano et al., 2005). During cell plate formation, the opposing cylinders of microtubules widen and disassemble in a gradient from the center outwards (Hepler et al., 1993), while actin filaments occur uniformly throughout the phragmoplast and remain present perpendicular to the whole cell plate area during its maturation (Hepler et al., 1993, Zhang et al., 1993) also in the center of the cell plate where consolidation of the cell plate starts (Samuels et al., 1995).

During cytokinesis, micron-sized organelles such as Golgi bodies, mitochondria and plastids do not enter the phragmoplast (Nebenführ et al., 2000; Seguí-Simarro et al., 2004), but vesicles of about 60 – 80 nm are transported through it to form the cell plate (Jürgens, 2005). This indicates that the phragmoplast cytoskeleton might act as a transport device but, in addition, excludes organelles from the developing cell plate acting as a sieve. This is a comparable cytoplasmic set up as observed in growing root hairs (Miller et al., 1999; Sieberer et al., 2000) where exocytotic vesicles on their way to fuse with the plasma membrane enter the subapical area with dense cytoskeleton, but organelles do not reach the root hair tip. Earlier transmission electron microscopy - (Hepler and Jackson, 1968), including electron microscopy after high pressure freezing and freeze substitution (Thijssen et al., 1998) and electron tomography studies (Otegui et al., 2001; Segui-Simarro et al., 2004; Austin et al., 2005) show that, in the early stage of cell plate formation in the center and later only at the phragmoplast border, microtubules are aligned parallel to each other at such a close distance that they could form a physical barrier for micron-sized organelles to enter the phragmoplast area. The distances between microtubules seen on these images are often smaller (20 – 30 nm) or just large enough (55 – 100 nm) (Thijssen et al., 1998; Seguí-Simarro et al., 2004; Austin et al., 2005) for cell plate forming vesicles to go through. So it seems that there is not much room for the cell plate forming vesicles during their transport through the phragmoplast, keeping in mind that also actin filaments and ER membranes, aligned in the same orientation, are present in between the microtubules.

Here, we test whether the size and flexibility of the cell plate forming vesicles are factors in their transport through the phragmoplast towards the cell plate and/or entry into the cell plate region. Previously, we have shown that synthetic lipid (DOPG) vesicles of 60 nm are transported through the phragmoplast and accumulate and are being kept in the cell plate region (Esseling-Ozdoba et al., submitted). Now, we study whether similar, flexible, synthetic lipid (DOPG) vesicles of various sizes, smaller and larger than endogenous vesicles, as well as stiff polystyrene beads, are transported through the phragmoplast.

RESULTS

Injected synthetic lipid vesicles and polystyrene beads move in interphase cells of *Tradescantia virginiana* stamen hair cells

Fluorescently labeled synthetic vesicles made of 1,2-Dioleoyl-*sn*-Glycero-3-[Phospho-*rac*-(1-glycerol)] (DOPG) and fluorescent polystyrene beads injected into interphase cells of *T. virginiana* stamen hair cells distributed in the cytoplasm (Fig. 1A, B) and moved comparably to organelles (Fig 1C, D and E). They distributed evenly in the complete cytoplasm within 5-10 min after microinjection and were visible as individual fluorescent speckles (Fig. 1A, B). Injection of these vesicles and polystyrene beads was not lethal to the cells. In addition, proper injection did not affect cytoplasmic streaming or cytoarchitecture of injected cells. Like the microinjected fluorescent vesicles that we described before (Esseling-Ozdoba et al., submitted), polystyrene beads moved through the cytoplasm for at least 1.5 hours after injection. Just as for the vesicles, we observed a range of velocities for the polystyrene beads (Fig. 1C, D). The average velocities of beads and vesicles in the cytoplasm were slower than those of visible organelles with a size of approximately 1-2 µm. Polystyrene beads moved with velocities of 0.64 µm/s (SD = 0.34) and vesicles with 0.75 µm/s (SD = 0.28), whereas the velocity of the organelles mentioned is 0.95 µm/s (SD = 0.20).

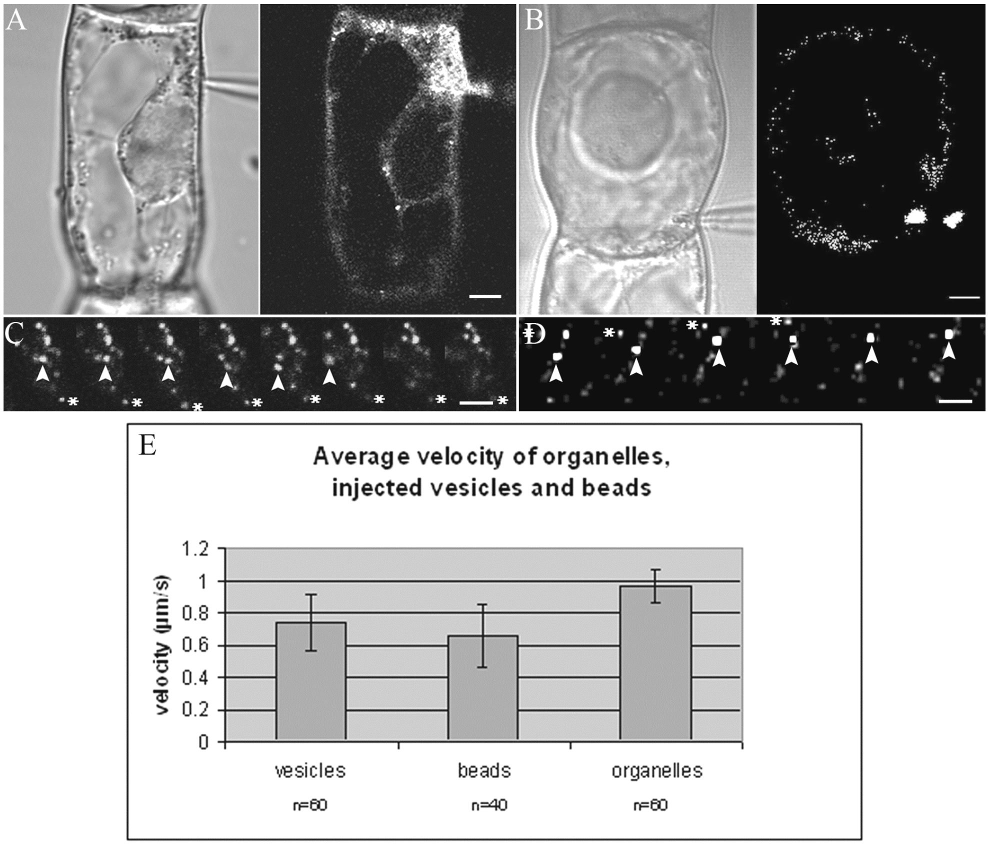

Figure 1. Fluorescently labeled synthetic lipid vesicles of 60 nm (**A**) and polystyrene beads of 40 nm (**B**) distribute in the cytoplasm, i.e. the cytoplasmic strands of interphase stamen hair cells of *T. virginiana* upon injection. Cells in A and B, 10 min. after microinjection, bar = 10 µm in A and 5 µm in B. A and B are DIC images showing undisturbed cyto-architecture; A'and B' corresponding CLSM images. N: nucleus, V: vacuole, CS: cytoplasmic strand. Time series of moving vesicles (**C**) (moving vesicles indicated by white arrowhead or asterisks) and polystyrene beads (**D**) (moving bead indicated by white arrowhead or asterisks) in the cytoplasm, time intervals 1.9 sec, bar = 5 µm. **E**. Average velocity of organelles, injected vesicles, and polystyrene beads in interphase cells of *T. virginiana*. The average velocity was calculated from the displacement of vesicles or organelles over the time that they were followed in the plane of observation (data shown with SD).

Synthetic vesicles of various sizes are transported through the phragmoplast, delivered to the cell plate region, and kept in this region, but redistribute into the cytoplasm after cell plate completion

Previously, we have shown that injected fluorescently labeled synthetic lipid (DOPG) vesicles of 60 nm accumulate in the cell plate region but redistribute again in the cytoplasm of the daughter cells after the cell plate has attached to the parental plasma membrane and cell wall (Esseling-Ozdoba et al., submitted). This shows that synthetic vesicles with the same size as endogenous vesicles are transported through the phragmoplast and accumulate in the cell plate region like endogenous vesicles do, but do not fuse with the developing cell plate. This showed that vesicles were transported through the phragmoplast, released from it into the cell plate region, but could not escape from this region as long as the phragmoplast was present, although they were not fused together or with endogenous vesicles. Here we test if the size of the lipid vesicles is an important physical parameter for their transport through the phragmoplast and accumulation in the cell plate region. Vesicles ranging from 45 nm, which are 0.75 times the diameter of endogenous vesicles, up to vesicles of 150 nm, a diameter of 2.5 times that of endogenous vesicles, all accumulated in the cell plate region (Fig. 2, Table 1), without any delay or disruption of cell plate formation (Fig. 3).

Size of injected vesicles	Percentage of cells with vesicle accumulation
45 nm	**100% (n=3)**
60 nm	**100% (n=29)**
75 nm	**100% (n=8)**
150 nm	**100% (n=3)**

Table 1 Synthetic vesicles of various sizes accumulate in the cell plate region.

Like the vesicles of 60 nm that we injected before (Esseling-Ozdoba et al., submitted), the vesicles of different sizes also only accumulated and did not fuse with the cell plate. At the time point at which the cell plate membrane fuses with the parental plasma membrane when two separate cells have been formed, the injected vesicles redistributed away from the new cell wall into the two daughter cells.

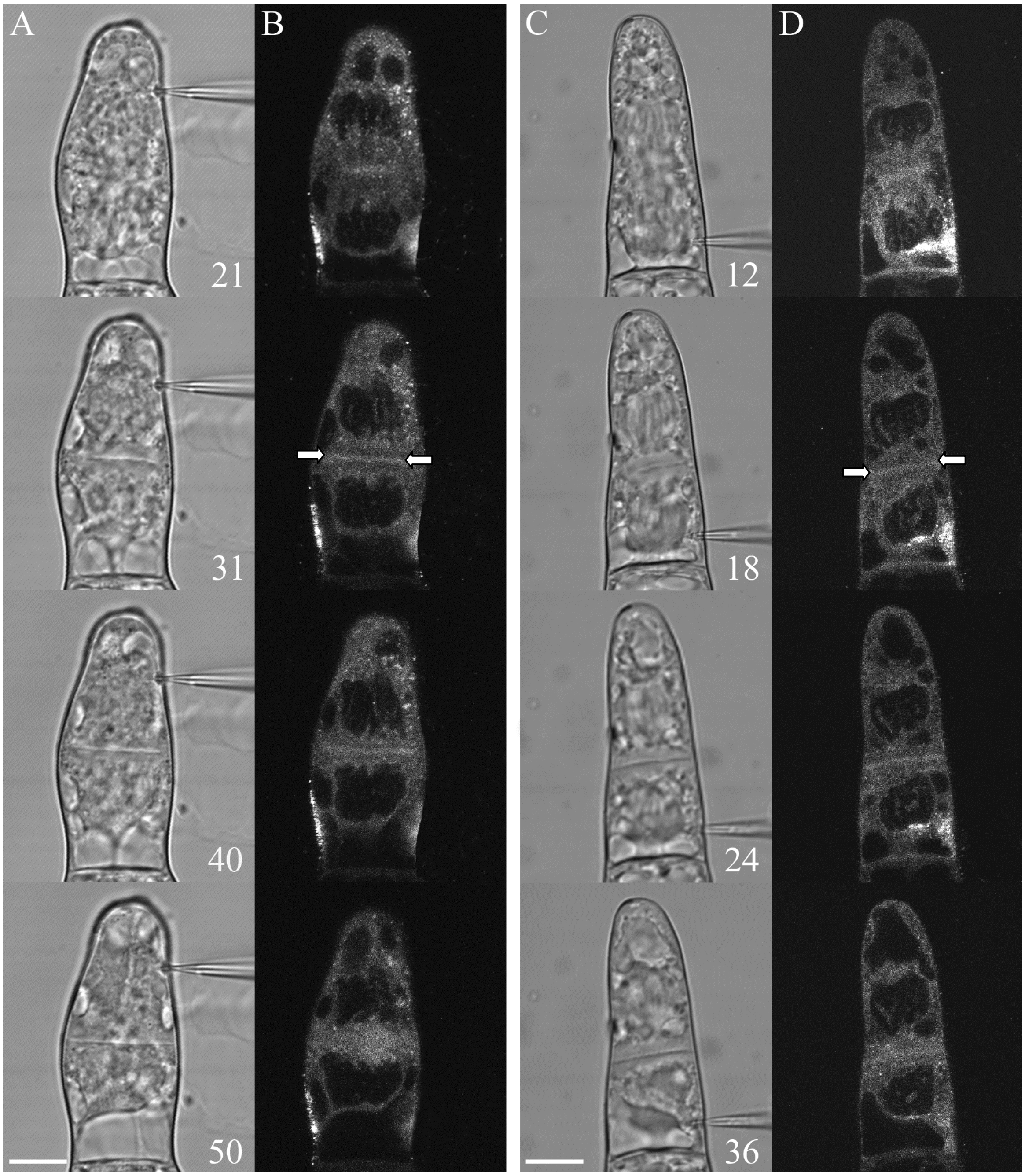

Figure 2. Time course of *T. virginiana* stamen hair cells at anaphase with injected fluorescently labeled synthetic (DOPG) lipid vesicles of 60 nm (column **A** and **B**) and 150 nm (column **C** and **D**). A and C: DIC images; Band D corresponding CLSM images. Synthetic lipid vesicles of 60 and 150 nm accumulate in the cell plate region (white arrows). Both types of injected vesicles redistributed in the cytoplasm of the daughter cells after the cell plate had attached to the parental cell wall (50 min. in column B and 36 min. in column D). Synthetic vesicles in all injected cells show the same behavior. Time in minutes after microinjection, bar = 10 µm.

Polystyrene beads of 20 and 40 nm diameter enter the phragmoplast but are not released from it into the cell plate region

Fluorescent polystyrene beads with sizes of 20 and 40 nm, which are much smaller than endogenous vesicles, and even smaller than the smallest injected DOPG vesicles, entered the phragmoplast but did not accumulate in the developing cell plate region when they were injected into cells at anaphase (Fig. 4, 5A, Table 2). These beads show the same distribution as co-injected dextran: they distribute within the accessible volume of the phragmoplast, but are excluded from the cell plate region (Fig. 4, 5B). They did not exit the phragmoplast towards the cell plate.

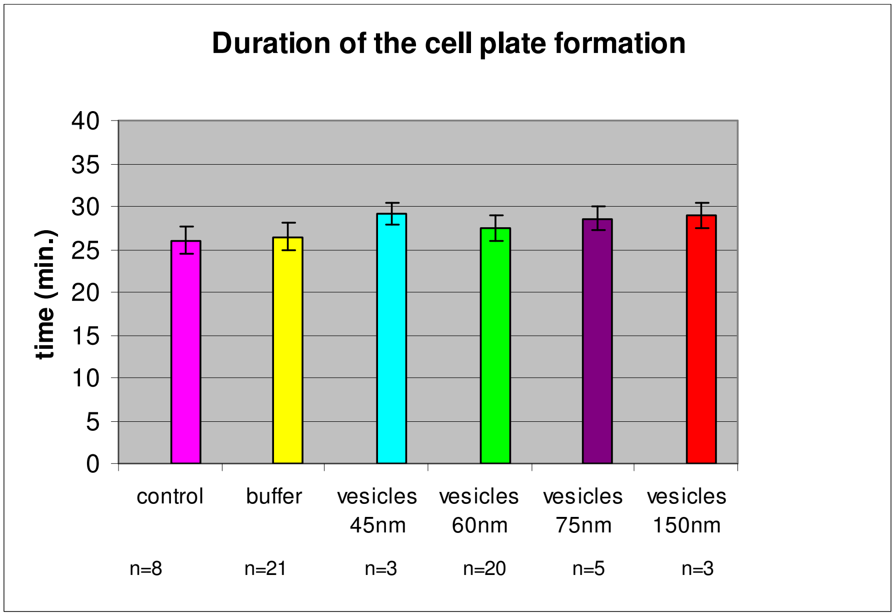

Figure 3. Duration of cell plate formation in control non-injected cells and in cells injected with lipid vesicles of various sizes. Synthetic lipid vesicles of various sizes do not disrupt or delay cell plate formation.

Injected polystyrene beads	Percentage of cells without beads accumulation
20 nm	**100% (n=5)**
40 nm	**100% (n=8)**
beads (40 nm) coated with DOPG	**100% (n=5)**

Table 2. Polystyrene beads (20 and 40 nm) not coated and coated with DOPG do not accumulate in the cell plate region.

Polystyrene beads of 40 nm delayed cell plate formation, while smaller polystyrene beads of 20 nm did not (Fig. 5C), even when the total number of 20 nm beads injected into a cell was twenty times higher than that of the 40 nm beads (see also Material & Methods). Therefore we conclude that polystyrene beads of 40 nm block the transport of endogenous vesicles to the cell plate.

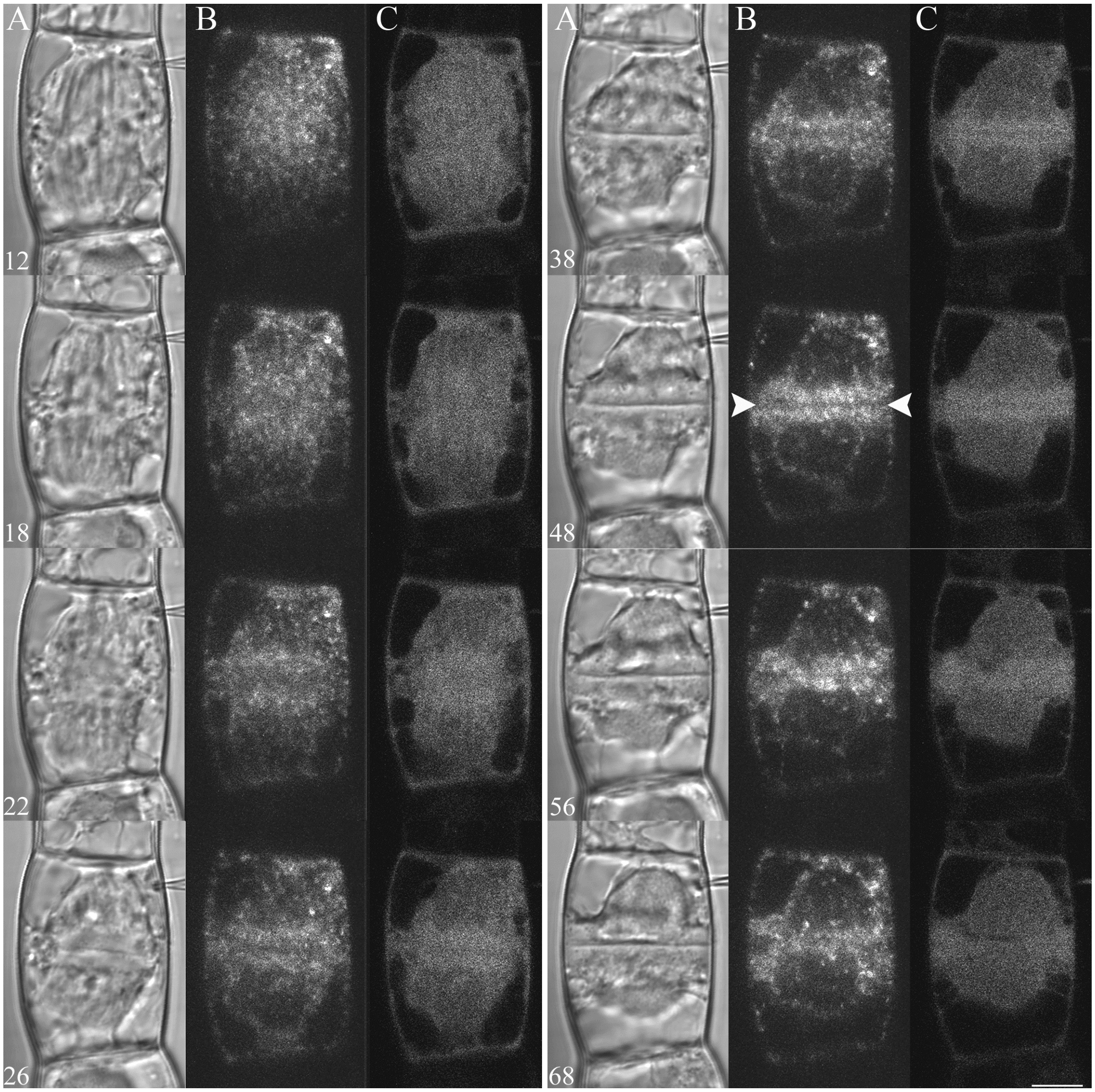

Figure 4. Time course of a *T. virginiana* stamen hair cell (column **A**, DIC images) co-injected at anaphase with fluorescently labelled polystyrene beads of 40 nm (column **B**) and Alexa 568 dextran (10 kD, column **C**). Polystyrene beads do not accumulate in the cell plate region (white arrowheads); polystyrene beads and dextran are distributed within their respective accessible volumes of the phragmoplast. Numbers indicate time in minutes after injection, scale bar = 10 µm.

Polystyrene beads coated with a DOPG membrane do not accumulate in the cell plate region

To test if the reason why DOPG vesicles enter the cell plate region and beads do not is the presence of a lipid surface, we coated 40 nm polystyrene beads with DOPG in such a way that their outside surface was the same as that of the synthetic vesicles. The polystyrene beads that we used for microinjections have negatively charged carboxyl groups on their surface. In order to coat such beads with DOPG that is also negatively charged, beads first were coated with the positively charged surfactant cetyl trimethyl ammonium bromide (CTAB), and then with DOPG. The adsorption of DOPG on CTAB-coated beads is entirely driven by hydrophobic interaction, resulting in the formation of a surfactant/lipid monolayer on the outside of the beads. In this monolayer the tails are oriented toward the bead and the hydrophilic heads are directed outwards, such that the outer monolayer resembles that of a normal DOPG layer. The coating with DOPG did not significantly change the diameter of the beads (Fig. S1, supplemental data) and the layer of DOPG on the surface of beads had the same biophysical properties as the bilayer of DOPG vesicles (Fig. S2, supplemental data).

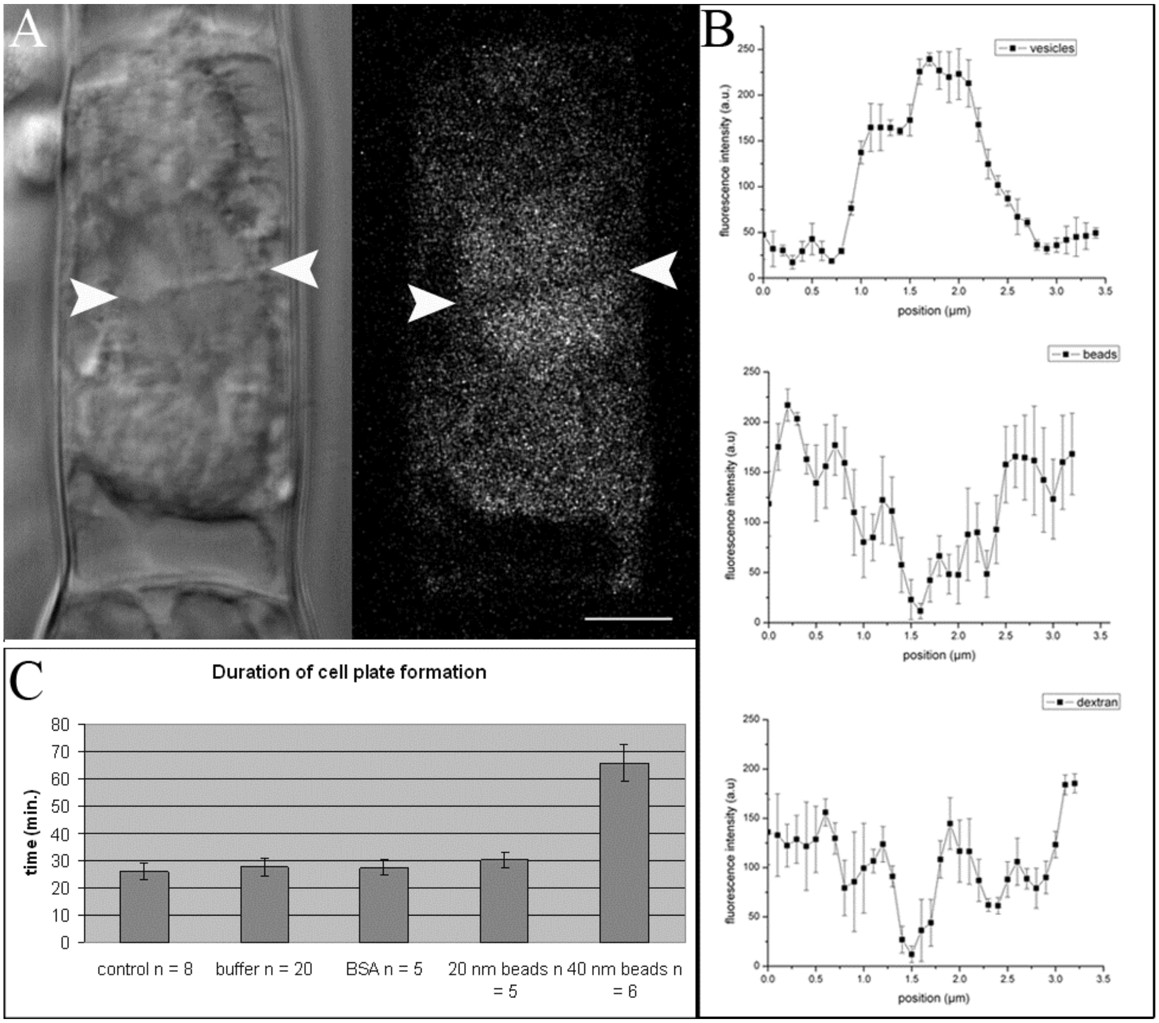

Figure 5. A. *T. virginiana* stamen hair cell injected at anaphase with fluorescent polystyrene beads of 20 nm (left – DIC image, right - fluorescence of beads). Polystyrene beads of 20 nm were observed in the cytoplasm including the phragmoplast but did not accumulate in the cell plate region (white arrowheads); bar = 10 µm. Polystyrene beads were mixed with 1% BSA to prevent their clustering. **B**. Line profiles through the phragmoplast of cells, injected either with vesicles, or polystyrene beads or dextran. Three regions of 1 x 3.5 µm through the phragmoplast were cut from the images. The average fluorescence intensity of each horizontal row of pixels was plotted versus its vertical position. The fluorescence of vesicles is highest in the cell plate region, while fluorescence of beads and dextran is lowest in the cell plate region. This shows that polystyrene beads and dextran do not accumulate in the cell plate region, while vesicles accumulate there specifically. **C**. Duration of cell plate formation in control non-injected cells, and cells injected with 20 or 40 nm polystyrene beads with 1% BSA in microinjection buffer added to prevent the clustering of the beads. Polystyrene beads of 40 nm delay cell plate formation, while those with diameter of 20 nm do not.

Upon injection of these DOPG-coated polystyrene beads into dividing cells at anaphase, they behaved as 40 nm uncoated beads: they entered the phragmoplast but did not accumulate in the cell plate region (Fig. 6, Table 2). These results indicate that it only can be the stiffness of the beads that inhibits their release from the phragmoplast and entry into the cell plate region, rather than the surface properties of the beads.

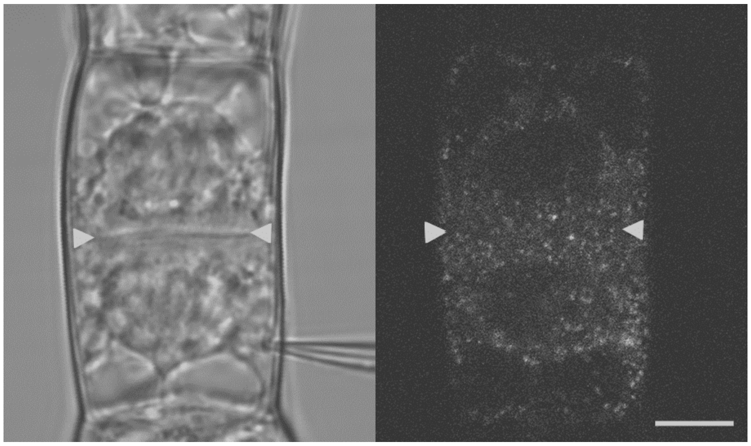

Figure 6. *T. virginiana* stamen hair cell injected at anaphase with fluorescent polystyrene beads of 40 nm coated with DOPG. Polystyrene beads coated with DOPG were observed in the cytoplasm and the phragmoplast but did not accumulate in the cell plate region (white arrowheads); bar = 10 µm, N = 6.

DISCUSSION

During cytokinesis, the phragmoplast inhibits transport of micron-sized organelles (e.g. mitochondria, Golgi bodies and plastids) towards the cell plate region but allows transport of cell plate forming vesicles (approximately 60 - 80 nm in diameter (Jürgens, 2005). Using microinjection of fluorescent synthetic (DOPG) lipid vesicles, fluorescent polystyrene beads, and the same beads coated with DOPG, we show that the phragmoplast is non-selective for the size of the synthetic lipid vesicles, tested up to 150 nm diameter. However, there appears to be a barrier for the stiff polystyrene beads of 20 and 40 nm diameter to exit from the phragmoplast, or entry into the cell plate region. With this we show that flexibility is an important parameter for vesicle exit from the phragmoplast or entry into the cell plate region.

Vesicles and polystyrene beads of different sizes can enter the phragmoplast

Microtubules are thought to be the transport vehicles for motor molecule coated endogenous vesicles during cell plate formation (Otegui et al., 2001; Smith, 2002). The largest injected vesicles (150 nm in diameter) were transported through the phragmoplast similarly to the smallest vesicles (45 nm) when microtubules were present. This is an interesting observation, taking into account the dense arrays of microtubules, actin filaments and ER membranes in the phragmoplast, in which the measured distance between the phragmoplast microtubules (20 - 100 nm) (Thijssen et al., 1998; Seguí-Simarro et al., 2004; Austin et al., 2005) is smaller than the diameter of these vesicles. It seems that these large vesicles are squeezed through the phragmoplast when they are transported to the developing cell plate. The force for pushing/pulling these vesicles through the phragmoplast is possibly created by motor proteins that are attached to the surface of injected vesicles. The motor proteins could pull the vesicular membrane along the phragmoplast cytoskeleton, deforming them to go through the phragmoplast. This would be comparable to the results from in vitro experiments shown by Koster et al.

(2003), where kinesin motor proteins could pull thin tubes from phospholipid (DOPC) vesicles along microtubules.

One should also take into account that individual microtubules (Dogterom et al., 1997, Janson et al., 2004) and actin filaments (Kovar et al., 2004) can buckle, thus making way for bigger vesicles. However, if this would happen with the larger injected vesicles, one would expect to observe a delay in cell plate formation because by the deformation of the cytoskeleton, endogenous vesicles would be inhibited to go through the phragmoplast. Such a delay we only observed when we injected polystyrene beads of 40 nm. These beads, in between the phragmoplast cytoskeleton, appear to partially block the transport of endogenous vesicles towards the cell plate, possibly by occupying the space in between the phragmoplast cytoskeleton polymers/ER membranes. The fact that beads of 20 nm diameter, do not hinder cell plate formation, supports this hypothesis.

Flexibility is a physical parameter for vesicles/material to be released from the phragmoplast into the cell plate region

Injected vesicles of all sizes (45-150 nm) were transported through the phragmoplast into the cell plate region. On the contrary, polystyrene beads of 40 nm and even of 20 nm in diameter were observed inside the phragmoplast, but never reached the cell plate region. Even though beads of both sizes are smaller than the smallest vesicles, they were not released from the phragmoplast to enter the region around the cell plate. It seems that there is a selective barrier for material to exit the phragmoplast or else enter the cell plate region. Recently, it has been shown that the developing cell plate is surrounded by a so-called cell plate assembly matrix (CPAM) (Seguí-Simarro et al., 2004). Possibly, this CPAM can be such a selective barrier. Our work indicates that not the lipid outside is a parameter for keeping the material out of the cell plate region, but that stiffness of the object is a limiting factor for this step to be taken.

Results indicate actin filaments as the primary cytoskeletal agent in the second phase of cell plate formation

The flexible vesicles not only line up in the cell plate area, but are also kept there as long as the phragmoplast is present; they do not go back into the phragmoplast area. They do not fuse with each other, nor with the endogenous vesicles (Esseling-Ozdoba et al., submitted to “The Plant Cell”) and are only released at the moment that the cell plate attaches to the mother cell wall. The question is: What keeps the DOPG vesicles in the cell plate region during cell plate formation? We can only speculate about this. There may be tethering proteins of the CPAM binding or capturing the vesicles as soon as the vesicles reach the cell plate area, what the membrane coated beads do not do. Another reason could be that molecular motors are only supporting movement towards the cell plate, and not back from it. If this is the case, it should be the actin cytoskeleton-based motors, since at the later stages of cell plate formation, microtubules have already disappeared for a great deal from the central part of the phragmoplast. That the actin cytoskeleton plays a role here is also supported by the fact that the vesicles disappear from the cell plate region rapidly at the same time as the disappearance of the actin filaments of the phragmoplast (Esseling-Ozdoba et al., submitted). In addition, vesicles still accumulate in the center of the forming cell plate after the microtubules have already disappeared from that region and are at the border of the forming cell plate only. Although more direct evidence is needed for this hypothesis, our results suggest that actin filaments are transporters for the vesicles, at least during the maturation phase of cell plate formation. Microtubules could be the leader of cell plate growth by transporting vesicles to its edges for their initial fusion to form vesicular tubes, the first stage of cell plate formation (Seguí-Simarro et al., 2004).

Synthetic lipid (DOPG) vesicles and polystyrene beads – Tools to study transport through and properties of cell areas with different cytoskeletal configurations

In interphase cells of *T. virginiana* stamen hair cells, microinjected synthetic lipid vesicles of 60 nm (as shown before) (Esseling-Ozdoba et al., submitted to "The Plant Cell") and polystyrene beads of 40 nm move comparably to organelles (Fig.1), though slower, which makes them excellent tools to study transport processes in these cells. The movement of synthetic lipid vesicles and polystyrene beads might be an active process caused by cytoplasmic motor proteins that possibly attach to their surfaces after injection into the cells. This would be in line with results obtained with uncoated polystyrene beads introduced into internodal cells of the green alga *Chara* (Chaen et al., 1995) and monkey BSC-1 cells (Beckerle, 1984). In these studies it has been shown that polystyrene beads move in the cytoplasm along the cytoskeleton as a result of the attachment of cytoplasmic motor proteins to the bead surface. If motor molecules indeed attach to the beads and vesicles, similar studies in higher plant cells can reveal which motor proteins are involved in organelle movement through cytoplasmic strands and vesicular movement through the phragmoplast. It cannot be excluded at the moment, however, that the injected beads and synthetic vesicles are moved by hydrodynamic flow caused by the active transport of endogenous organelles, which we have shown to be expected theoretically (Houtman et al., 2007) and experimentally to be the case for free GFP in the cytoplasm (Esseling-Ozdoba et al., submitted).

A second type of questions that could be solved using experiments with injected beads and synthetic vesicles of various sizes pertain to the physical properties of cell areas with specific cytoskeleton configurations. It would for instance be interesting to study the behavior of injected beads and synthetic vesicles, -and biological vesicles-, in the subapex of tip growing cells with dense fine F-actin in vetch (Miller et al. 1999) and Arabidopis (Ketelaar et al., 2003), and a similar configuration with in addition a dense network of endoplasmic microtubules in growing *Medicago truncatula* root hairs (Sieberer et al., 2002).

In addition, specific coating of vesicles with a protein prior to injection, or insertion of specific proteins into the vesicle membrane, could help to reveal the function of these proteins in various cell processes, notably cell plate formation.

MATERIAL AND METHODS

Plant Material

Tradescantia virginiana plants were grown in a growth chamber with a 16-hrs photoperiod at 25°C and 8-hrs dark period at 18°C and 75-80% relative humidity. Stamen hair cells with dividing and elongating cells in the apical region were collected from immature, unopened flower buds with a length of approximately 5 mm. For microinjection experiments, we dissected and immobilized stamen hairs in a thin layer of 1% low temperature gelling agarose (BDH Laboratory Supplies, UK) in culture medium (5 mM HEPES, 1 mM $MgCl_2$, and 0.1 mM $CaCl_2$, pH 7.0) and 0.025% Triton X-100 (BDH Laboratory Supplies, UK), following the procedure described by Vos et al. (1999) and Esseling-Ozdoba et al. (submitted).

Preparation of synthetic vesicles, polystyrene beads and dextran

Synthetic vesicles were made from 98% of anionic nonfluorescent phospholipid 1,2-Dioleoyl-*sn*-Glycero-3-[Phospho-*rac*-(1-glycerol)] (DOPG, Avanti Polar Lipids) and 2% of fluorescent phosphocholine BodipyFC12-HPC (excitation maximum at 503 nm, emission maximum at 512 nm, Molecular Probes) as described in Esseling-Ozdoba et al. (submitted). Vesicles of various sizes were made with a mini-extruder, using a polycarbonate membrane of different pore sizes: 30 nm (45 nm vesicles), 50 nm (60 nm vesicles), 80 nm (75 nm vesicles) and 400 nm (150 nm vesicles). The size of the vesicles after preparation was measured with dynamic light scattering.

Polystyrene beads of 40 nm, carboxylated-modified FluoroSpheres (Fluorescent Microspheres) were purchased from Molecular Probes (F10720, The Netherlands). We used yellow-green beads with an excitation maximum at 505 nm and an emission maximum at 515 nm and red beads with an excitation maximum at 580 nm and an emission maximum at 605 nm. The solution contained 5% (v/v) of beads (1,4 x 10^{15} beads per ml). For microinjection, polystyrene beads were diluted 1:500 in microinjection buffer (5 mM HEPES, 0.1 mM KCl, pH 7.0). With a scanning electron microscope (SEM) and dynamic light scattering (DLS), we observed that the beads did not cluster in microinjection buffer. Because the beads solution contained small numbers of larger beads (95 nm, 2-5%), the solution was sonicated (2 x 30 min.) and centrifuged at 25.000 x g for another 30 min. before microinjections to remove the large beads that could block the needle during microinjection. After centrifugation, the supernatant was sonicated for 30 min. in order to have beads well dispersed in the solution. Beside this, we added 1% of

BSA (Albumin fraction V, Merck, Germany) to the bead solution to prevent clustering of the beads and possible needle blockage during microinjection. BSA in this concentration did not disturb cell plate formation.

Small polystyrene beads were purchased from Micromod Partikeltechnologie GmbH (Micromer – GreenF, Germany). These beads were also carboxylate-modified. The solution contained 5.5 x 10^{15} beads per ml, without any preservatives. Although they were described by the manufacturer as beads of 15 nm, most of the beads (95%, SEM data) in the solution appeared to have a size of 20 nm. For this reason we call these beads 20 nm polystyrene beads. For microinjection, polystyrene beads were diluted 1: 100 in microinjection buffer. The solution used for microinjection contained 5.5 x 10^{13} beads per ml. Before the beads were injected into the cells they were sonicated (2 x 30 min.) and 1% BSA was added to prevent clustering of the beads during microinjection.

For co-injection experiments, vesicles or polystyrene beads were mixed with fluorescent dextran (0.5 mg/ml, Alexa 568-dextran, 10 kD, Molecular Probes, Invitrogen BV, The Netherlands or Eugene, Oreg., U.S.A.). For co-injection experiments with dextran yellow-green beads were used.

Until microinjection experiments, vesicles and polystyrene beads were stored on ice.

Coating of polystyrene beads with DOPG membrane

Negatively charged (carboxylated) polystyrene beads were first coated with the positively charged surfactant cetyl trimethyl ammonium bromide (CTAB), in concentration of 100 µM, and then with the negatively charged DOPG in concentration of 400 µM. CTAB was dissolved in microinjection buffer as 1 mM stock. DOPG vesicles of 200 nm were prepared (by sonication) in microinjection buffer, with DOPG concentration of 4 mM. The coating of polystyrene beads was done by mixing the beads with CTAB and DOPG and sonicating for 10 min with a bath sonicator (Laboratory Supplies, Hicksville, USA). The quality of the coating was checked with dynamic light scattering (see supplemental data).

Microinjection

The microinjection experiments were conducted according to the detailed description of the process and equipment published by Vos et al. (1999) and for vesicles described in Esseling-Ozdoba et al. (submitted to “The Plant Cell”).

Microscopy, imaging and data analysis

Microinjections were performed on inverted microscopes. Images were collected with a MRC600 confocal laser-scanning microscope (Bio-Rad, Hemel Hempstead, UK) coupled to a Nikon Labophot microscope (Kawasaki, Japan), or with a Cell Map IC Bio-Rad (MicroScience Division, Hemel Hampstead, UK) confocal laser-scanning microscope, coupled to a Nikon Eclipse TE 2000-S microscope or with a LSM 5 Pascal confocal laser-scanning microscope, coupled to a Zeiss Axiovert 200 microscope. For imaging vesicles or beads co-injected with dextran (Bodipy/yellow-green beads/Alexa-568 dextran dual scanning), we used excitation/emission combinations of 488 nm/ 520-540 (Cell Map IC), or 488 nm/ BP 505-550 with the HFT 488 primary and NFT 545 secondary dichroic mirrors (LSM 5 Pascal) for Bodipy, and 532 nm/ 560 LP (Cell Map IC) or 543 nm/ LP 560 with the HFT 543 primary dichroic mirror (LSM 5 Pascal) for Alexa-568 dextran. For imaging of yellow-green or red beads with the MRC600, neutral density filters were set to obtain 1% transmission intensity from the laser beam, using the 488 nm wave length for yellow-green beads with DM 488 and BA 522; and the 568 nm wave length for red fluorescence of beads with DM 560 long pass BA 585. Images were obtained with 1.4 NA 60X and 1.4 NA 63X oil immersion objectives, collected by Kalman averaging of 2-3 full scans (MRC600, Cell Map IC) or with scan speed 7 (LSM 5 Pascal). Images were taken in 2 or 3 min. intervals. This choice of intervals allowed observation of the developing cell plate for a long period of time without disturbing the cell plate formation process. Images were acquired and processed with software programs including Comos (MRC600), LaserSharp 2000 (Cell Map IC), LSM 5 Pascal (version 3.5 SP1.1, Carl Zeiss), Confocal Assistant 4.02 (Todd Clark Brelje) and Adobe Photoshop 5.0 and 8.0 (Adobe Systems, Mountain View, CA).

Analysis of fluorescence of vesicles, polystyrene beads and dextran was done with Adobe Photoshop, Image J (version 1.32j, National Institute of Health, USA) and Origin (version 7.5 SR5, OriginLab Corporation, Northampton, USA). For this, rectangles of 10 x 50 pixels were cut out from the images taken on different time points, using Adobe Photoshop. The size of each rectangular section was reduced to 1 x 50 pixels in order to average the fluorescence and avoid fluorescence fluctuations. Every image was saved as a text file with Image J and fluorescence data were plotted over time in Origin.

ACKNOWLEDGEMENTS

AMCE thanks the FOM Institute for Atomic and Molecular Physics (AMOLF), Amsterdam, for financial support for this project. We thank Marileen Dogterom (AMOLF) for useful discussions.

SUPPLEMENTAL DATA

Structural resemblance between the outsides of coated CTAB/DOPG polystyrene beads and DOPG vesicles

In order to obtain objects that have surface properties like vesicles from the outside, but that are not compressible, we coated negatively charged polystyrene beads (Molecular Probes) with a positively charged surfactant, cetyl trimethyl ammonium bromide (CTAB), and a negatively charged lipid, 1,2-Dioleoyl-sn-Glycero-3-[Phospho-rac-(1-glycerol)] (DOPG).

The idea is that the positively charged head group of CTAB masks the negatively charged carboxyl groups at the surface of the polystyrene beads, while the hydrophobic tail of the surfactant is in contact with the hydrophobic polystyrene surface. This results in a decrease of the electrostatic repulsion between the beads, leading to a loss of the colloidal stability. When all carboxyl groups are screened, adsorption of more CTAB or DOPG is entirely driven by hydrophobic interaction, resulting in the formation of a surfactant/lipid monolayer on the outside of the beads. It is expected that in this monolayer the tails of the surfactant and lipid molecules are oriented towards the bead and the hydrophilic heads are directed outwards to the aqueous solution. Therefore, the outside of this monolayer would closely resemble the outside of a DOPG vesicle. These assumptions were checked by dynamic light scattering experiments (DLS) and by self-consistent field (SCF) model calculations of which the results are given here.

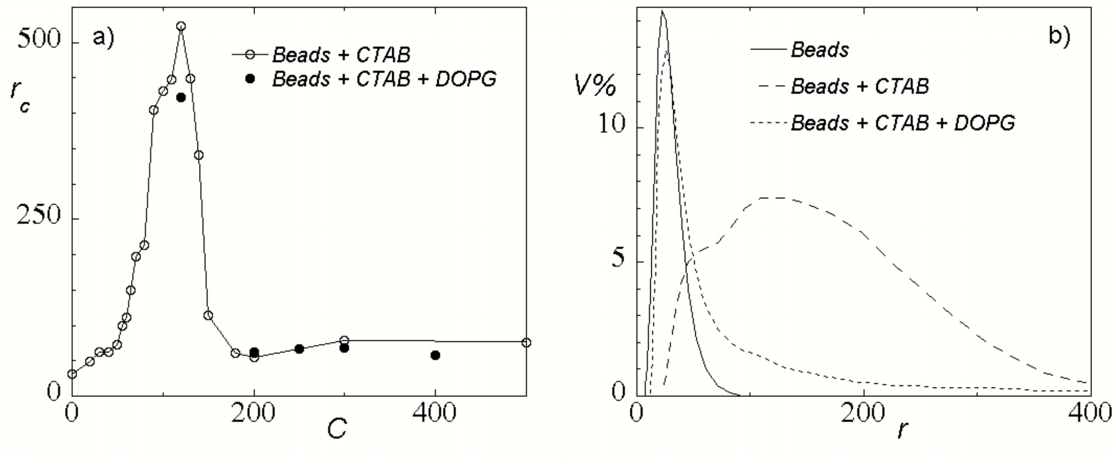

Figure S1. a) The mean radius r of particles and/or aggregates determined by cumulant fitting of dynamic light scattering results as a function of the CTAB concentration in μM (open circles), and of the CTAB + DOPG concentration in μM (closed circles) where C_{CTAB} = 100 μM and C_{DOPG} = C - C_{CTAB}. b) The size distribution of the beads (continuous line), the beads in a 100 μM CTAB solution (long dashed line) and in a solution of 100 μM CTAB and 400 μM DOPG (short dashed line). In all cases the solution is a 5 mM Hepes, 0.1 mM KCl buffer of pH = 7. The concentration of the beads is approximately 1.4x10^{12} ml^{-1} in all cases and the mean radius of the beads *r* = 20 nm.

In figure S1 DLS results for polystyrene bead dispersions with varying concentrations of CTAB and DOPG are shown. The aqueous solution was a 5 mM Hepes, 0.1 mM KCl buffer of pH 7 (the microinjection buffer) with $1.4\text{x}10^{12}$ polystyrene beads per ml. The average size r_c of the beads (or aggregates of the beads) shown in figure S1a was retrieved by cumulant fitting, while the size distribution in r, which is plotted in figure 1b, was obtained by contin fitting.

Figure S1a shows that when CTAB > 50 µM (open circles) the cumulant size r_c starts to increase, which is, as argued above, due to aggregation of the beads as a consequence of decreasing electrostatic repulsion. When $C_{\mathrm{CTAB}} \approx 100$ µM the electrostatic repulsion has reached a minimum. Adding more CTAB (open circles) or adding DOPG (closed circles) to this 100 µM CTAB dispersion results in a decrease of r_c. This improvement of the colloidal stability is caused by the adsorption of additional surfactant or DOPG molecules to the CTAB-coated polystyrene beads, eventually resulting in the formation of a densely packed monolayer, where the hydrophilic groups are directed to the aqueous solution.

In figure S1b the size distributions determined by contin fitting are shown for three different systems. For the uncoated polystyrene beads (continuous line) a rather narrow size distribution was found with a maximum at $r \approx 20$ nm, which agrees well with the bead size as provided by the manufacturer. In the presence of 100 µM CTAB (long dashed line) the size distribution becomes rather broad and the average aggregate size is increased, showing that the beads have formed aggregates. When besides 100 µM CTAB also 400 µM DOPG was added to the buffer solution (short dashed line), the average size returned to approximately its original value and the size distribution became narrow again. These results confirm the idea of the formation of a densely packed lipid/surfactant monolayer on the outside of the CTAB-coated polystyrene bead.

To gain more insight into the molecular organization of the adsorbed layer, we performed a number of calculations using a molecularly realistic self-consistent field (SCF) model. We will explain briefly how the model works, and refer to the literature for full details (Evers et al, 1990; Meijer et al, 1999; Kik et al, 2005).

The SCF method is based on the reduction of the many-molecule problem (i.e., each molecule in a system has interactions with all other molecules) to the problem of one molecule in the field of mean force of all the others. In general this field depends on the distributions and conformations of all molecules and their interactions. In the model used here the molecules are divided in segments ('united atoms', for example a CH_2 or CH_3 group forms a segment C) and these segments are placed on a lattice (one segment per lattice site). The segment-type dependent potential fields depend on the way in which the segments are distributed over the lattice. These potentials have contributions due to the short-range interactions between the segments, the electrostatic interactions and a contribution linked to packing constraints. If a surface is present in the system, the segment-specific interactions with this surface are also included in the potential fields.

The equilibrium state of a system is obtained by determining the distribution corresponding to the minimal mean-field free energy in an iterative way. We routinely find this distribution with a very high accuracy by a numerical algorithm.

In the calculations discussed below, we consider the structure of a free lipid bilayer and the adsorbed CTAB/DOPG layer on the polystyrene beads in one direction only, namely the direction perpendicular to the layers. This enables us to reduce the problem to a one-dimensional one (using a one-dimensional lattice), which saves a lot of calculation time. It implies that lateral structural fluctuations in the layers are averaged out.

The polystyrene surface is taken to be hydrophobic and 10% of this surface is covered with carboxyl groups, which are partly uncharged and partly negatively charged, depending on the pH of the solution. In the calculations the pKa of the COOH groups was taken to be 4.5 and a pH value of 7 was used.

There are three molecular species in the system that consist of just one segment, namely water (W), of which a small part occurs as a positive species ($H3O^+$) or a negative one (hydroxyl) depending on the pH of the solution and the local electrostatic potential. In addition there are two small salt ions, a positively charged ion (K) and a negatively charged ion (S). The surfactant CTAB is modeled as a molecule consisting of 19 segments, X_3C_{16}. The hydrophilic head group segments X each carry a charge of 1/3 and the tail is composed of 16 hydrophobic segments (united atoms, C). The negatively charged lipid $N_3C_3P_3(C_{18})_2$, which represents DOPG, consists of two hydrophobic tails, each having 18 C segments connected through a side-chain to a head group that consists of 9 united atoms, i.e., 3 negatively charged hydrophilic segments (P), each having a partial charge of –1/3, three hydrophobic segments (C) and three uncharged hydrophilic segments (N).

The short-range interactions between the segments are accounted for by so-called Flory-Huggins nearest-neighbor interaction parameters. These parameters have been chosen in such a way that the critical micellization concentration (CMC) values of CTAB and DOPG in the model closely agree with experimental data. The electrostatic potential depends on the local charge density and follows from the solution of the Poisson equation.

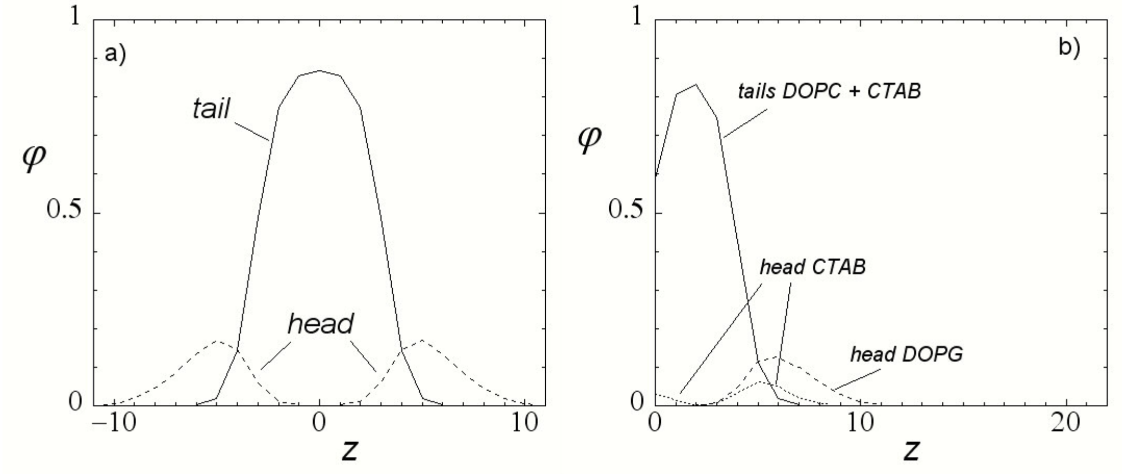

Figure S2. a) The volume fraction (φ) profile of a tensionless bilayer consisting of DOPG lipids. The *z*-axis is given in lattice layers *l*. The ionic strength φ_z= 1.0x10^{-4} (corresponding to ca 5 mM). b) The volume fraction profile of DOPG and CTAB in the presence of a polystyrene surface. The polystyrene surface is located at $z = 0$.

Using SCF calculations we first determined the CTAB concentration for which the colloidal stability of the polystyrene beads is minimal, i.e., the CTAB concentration at which the electrostatic potential of the surfactant-covered surface shows a minimum (results not shown). This CTAB concentration (volume fraction 1.0x10^{-4}, corresponding to about 250 μM) was used in further calculations, in which different amounts of DOPG were present in the system.

In figure S2 the structures of a tensionless DOPG bilayer (a) and an adsorbed layer consisting of both CTAB and DOPG (b) are shown in terms of volume fractions of head group and tail segments across the layers. The horizontal axes in figure S2 give the spatial coordinate *z* in lattice layers across the bilayer (a) or perpendicular to the polystyrene surface (b). As expected, the structure of the lipid bilayer is such that the hydrophobic tails form the core of the bilayer, and are screened at the periphery of the bilayer from the aqueous environment by the hydrophilic head groups. The volume fraction of the tail segments in the hydrophobic interior of the bilayer is approximately 0.9. The tails remain in the region given by $- 6\, l < z < 6\, l$, with *l* the thickness of a lattice layer. In figure S2b the hydrophobic surface is positioned at $z = 0$. The volume fractions of the CTAB and DOPG tails are added in order to compare the hydrophobic part of the adsorbed layer with the hydrophobic interior of the pure DOPG bilayer. From figure S2 it follows that the outer part of the adsorbed CTAB/DOPG layer is very similar to that of a pure DOPG bilayer. The volume fraction of the tail segments in the hydrophobic part of the adsorbed layer is only slightly lower than in the DOPG bilayer. (It is noted here that near the polystyrene surface the volume fraction of the tail segments is suppressed somewhat as a consequence of the presence of the carboxyl surface groups and the positively charged surfactant head groups that screen these surface groups.) The head group region of the lipid bilayer of course consists entirely of DOPG head segments, whereas in the case of the adsorbed surfactant/lipid layer a minor part of the head groups stems from CTAB. As a consequence, the electrostatic potential at the outside of the adsorbed layer is somewhat smaller than, but still very comparable to the electrostatic potential at the outside of the DOPG bilayers (not shown). That the difference in electric potential is only small is also due to the fact that already in the head group region of the DOPG bilayer a significant fraction of the negative charge is compensated by the presence of positively charged salt ions.

In conclusion, the DLS results and the SCF calculations show that the outer part of an adsorbed CTAB/DOPG layer on the negatively charged polystyrene beads corresponds quite well to the outside of a DOPG vesicle. The calculations show that the cationic surfactant molecules, needed for the adhesion of the DOPG layer on the negatively charged beads, are mostly hidden underneath the lipid layer and relatively few of the surfactants are visible on the outside of the adsorbed layer. Reducing the surfactant/lipid ratio may diminish this effect, albeit that a minimum amount of surfactants is needed to neutralize the carboxyl groups on the polystyrene surface.

References to supplemental data

Evers, O.A., Scheutjens, J.M.H.M., Fleer, G.J. (1990). Statistical thermodynamics of block copolymer adsorption. 1. Formulation of the model and results for the adsorbed layer structure. Macromolecules **23**, 5221-5232.

Meijer, L.A., Leermakers, F.A.M., and Lyklema, J. (1999). Self-consistent-field modeling of complex molecules with united atom detail in inhomogeneous systems. Cyclic and branched foreign molecules in imyristoylphosphatidylcholine membranes. J. Chem. Phys. **110**, 6560-6579.

Kik, R.A., Leermakers, F.A.M., and Kleijn, J.M. (2005). Molecular modeling of lipid bilayers and the effect of protein-like inclusions. Phys. Chem. Chem. Phys. 7, 1996-2005.

REFERENCES

Adams, R.J., and Pollard, T.D. (1989). Binding of myosin I to membrane lipids. Nature **340**, 565-568.

Austin, J.R., Seguí-Simarro, J.M. and Staehelin, L.A. (2005). Quantitative analysis of changes in spatial distribution and plus-end geometry of microtubules involved in plant- cell cytokinesis. J. Cell Sci. **118**, 3895-3903.

Baskin, T.I. and Cande, W.Z. (1990). The structure and function of the mitotic spindle in flowering plants. Annu. Rev. Plant Physiol. Plant Mol. Biol. **41**, 277-315.

Beckerle M.C. (1984). Microinjected polystyrene beads exhibit saltatory motion in tissue culture cells. J. Cell Biol. **98**, 2126-2132.

Chaen S., Inoue J., Sugi H. (1995). The force-velocity relationship of the ATP-dependent actin-myosin sliding causing cytoplasmic streaming in algal cells, studied using centrifuge microscope. J. Exp. Biol. **198**, 1021-1027.

Cleary, A.L., Gunning, B.E.S., Wasteneys, G.O., and Hepler, P.K. (1992). Microtubule and F-actin dynamics at the division site in living *Tradescantia* stamen hair cells. J. Cell Sci. **103**, 977-988.

Dogterom, M., and Yurke, B. (1997). Measurement of the force – velocity relation for growing microtubules. Science **278**, 856-860.

Esseling-Ozdoba, A., Vos, J.W., van Lammeren, A.A.M., and Emons, A.M.C. (2007) Synthetic lipid (DOPG) vesicles accumulate in the cell plate region but do not fuse. Submitted to Plant Cell.

Esseling-Ozdoba, A., Houtman, D., van Lammeren, A. A.M., Eiser, E., and Emons, A. M.C. (2007). Hydrodynamic flow in cytoplasm of plant cells. Submitted to Journal of Microscopy.

Hepler, P.K. and Jackson, W.T. (1968). Microtubules and early stages of cell-plate formation in the endosperm of *Haemanthus katherinae* Baker. J. Cell Biol. 38, 437-446.

Hepler, P.K., Cleary, A.L., Gunning, B.E.S., Wadsworth, P., Wasteneys, G.O. and Zhang, D.H. (1993). Cytoskeletal dynamics in living plant cells. Cell Biol. Int. **17**, 127-142.

Houtman, D., Pagonabarraga, I., Lowe, C.P., Esseling-Ozdoba, A., Emons A.M.C. and Eiser, E. (2007) Hydrodynamic flow caused by active transport along cytoskeletal elements. *EPL*, **78**, 18001p1-p5.

Janson, M.E., and Dogterom, M. (2004). A bending mode analysis for growing microtubules: evidence for a velocity - dependent rigidity. Biophys. J. **87**, 2723-2736.

Jürgens, G. (2005). Cytokinesis in higher plants. Annu. Rev. Plant Biol. **56**, 281-299.

Kakimoto, T. and Shibaoka, H. (1988). Actin filaments and microtubules in the preprophase band and phragmoplast of tobacco cells. Protoplasma **140**,151-156.

Ketelaar, T., de Ruijter, N.C.A., and Emons, A.M.C. (2003). Unstable F-actin specifies the area and microtubule direction of cell expansion in Arabidopsis root hairs. Plant Cell **15**, 285-292.

Koster, G., van Duijn, M., Hofs, B., and Dogterom, M. (2003). Membrane tube formation from giant vesicles by dynamic association of motor proteins. Proc. Natl. Acad. Sci. USA **26**, 15583-15588.

Kovar, D.R., and Pollard, T.D. (2004). Insertional assembly of actin filament barbed ends in association with formins produces piconewton forces. Proc. Natl. Acad. Sci. USA **101**, 14725-14730.

Mineyuki, Y. (1999). The preprophase band of microtubules: its function as a cytokinetic apparatus in higher plants. Int. Rev. Cyt. **187**, 1-49.

Miller, D.D., de Ruijter, N.C.A., Bisseling, T., and Emons, A.M.C. (1999). The role of actin in root hair morphogenesis: studies with lipochito-oligosaccharide as a growth stimulator and cytochalasin as an actin perturbing drug. Plant J. **17**, 141-154.

Molchan, T. M., Valster, A.H. and Hepler, P.K. (2002). Actomyosin promotes cell plate alignment and late lateral expansion in *Tradescantia* stamen hair cells. Planta **214**, 683-693.

Nebenführ, A., Frohlick, J.A., and Staehelin, L.A. (2000). Redistribution of Golgi stacks and other organelles during mitosis and cytokinesis in plant cells. Plant Physiol. **124**, 135-151.

Otegui, M.S., Mastronarde, D.N., Kang, B.-H., Bendarek, S.Y., and Staehelin, L.A. (2001). Three-dimensional analysis of syncytial-type cell plates during endosperm cellularization visualized by high resolution electron tomography. Plant Cell **13**, 2033-2051.

Samuels, A.L., Giddings, Jr., T.H., and Staehelin, L.A. (1995). Cytokinesis in tobacco BY-2 and root tip cells: a new model of cell plate formation in higher plants. J. Cell Biol. **130**, 1345-1357.

Sano, T., Higaki, T., Oda, Y., Hayashi, T., and Hasezawa, S. (2005). Appearance of actin microfilament "twin peaks" in mitosis and their function in cell plate formation, as visualized in tobacco BY-2 cells expressing GFP-fimbrin. Plant J. **44**, 595–605.

Seguí-Simarro, J.M., Austin, J.R. II, White, E.A., and Staehelin, L.A. (2004). Electron tomographic analysis of somatic cell plate formation in meristematic cells of Arabidopsis preserved by high-pressure freezing. Plant Cell **16**, 836-856.

Sieberer, B., and Emons, A.M.C. (2000). Cytoarchitecture and pattern of cytoplasmic streaming in developing root hairs of *Medicago truncatula* and during deformation by Nod factors. Protoplasma, **214**, 118-127.

Sieberer, B., Timmers, A.C.J., Lhuissier, F.G.P., and Emons, A.M.C. (2002). Endoplasmic microtubules configure the subapical cytoplasm and are required for fast growth of *Medicago truncatula* root hairs. Plant Physiol. **130**, 977-988.

Smith, L.G. (2002). Plant cytokinesis: motoring to the finish. Curr. Biol. **12**, R206-R209.

Staehelin, A. L. and Hepler, P.K. (1996). Cytokinesis in higher plants. Cell **84**, 821-824.

Thijsen, M.H., van Went, J.L. and van Aelst, A.C. (1998). Heptane and isooctane as embedding fluids for high-pressure freezing of *Petunia* ovules followed by freeze-substitution. J. Microsc. **192**, 228-235.

Valster, A.H., and Hepler, P.K. (1997) Caffeine inhibition of cytokinesis: effect on the phragmoplast cytoskeleton in living *Tradescantia* stamen hair cells. Protoplasma **196**:155–166.

Valster, A.H., Pierson, E.S., Valenta, R., Hepler, P.K. and Emons, A.M.C. (1997). Probing the plant actin cytoskeleton during cytokinesis and interphase by profilin microinjection. Plant Cell **9**, 1815-1824.

Vos, J.W, Valster, A.H, and Hepler, P.K. (1999). Methods for studying cell division in higher plants. In Methods in Cell Biology, C.L. Rieder, ed (San Diego, CA: Academic Press) **61**, 413-437.

Wick, S.M. (1991). Spatial aspects of cytokinesis in plant cells. Curr. Opin. Cell Biol. **3**, 253-260.

Zhang, D., Wadsworth, P. and Hepler, P.K. (1990). Microtubule dynamics in living dividing cells: confocal imaging of microinjected fluorescent brain tubulin. Proc. Natl. Acad. Sci. USA **87**, 8820-8824.

Zhang, D., Wadsworth, P. and Hepler, P.K. (1993). Dynamics of microfilaments are similar, but distinct from microtubules during cytokinesis in living, dividing plant cells. Cell Motil. Cytoskel. **24**, 151-155.

Chapter 4

Hydrodynamic Flow Caused by Active Transport along Cytoskeletal Elements

Dion Houtman[1], Ignacio Pagonabarraga[2], Christopher P. Lowe[1], Agnieszka Esseling-Ozdoba[3], Anne Mie C. Emons[3] and Erika Eiser[1]

[1] Van 't Hoff institute for molecular sciences (HIMS), Universiteit van Amsterdam, Nieuwe Achtergracht 166, 1018 WV Amsterdam (The Netherlands)

[2] Departament de Física Fonamental, Universitat de Barcelona, Carrer Martí i Franqués 1, 08028-Barcelona (Spain)

[3] Wageningen University, Laboratory of Plant Cell Biology, Arboretumlaan 4, 6703 BD, Wageningen (The Netherlands)

Published in EPL (2007), 78, 1800p1-p5.

Abstract

We develop a simple lattice model to describe the hydrodynamic influence of active mass transport along bio-filaments on freely diffusing mass in the cell. To quantify the overall mass transport we include Brownian motion, excluded volume interactions, active transport along the filaments, and hydrodynamic interactions. The model shows that the hydrodynamic forces induced by molecular motors attached to the filaments give rise to a non-negligible flux close to the filament. This additional flux appears to have two effects. Depending on the degree of filament occupation it can exert a sufficiently large influence on unbound motors and cargo to modify their transport and also regulate the flux of motors bound to the filament. We expect such a mechanism is important in situations found in plant cells, where directional transport spans the entire cell. In particular, our model can explain bulk cytoplasmic streaming observed in plant cells.

INTRODUCTION

Molecular motors play a crucial role in the organization of cells and mass transport inside cells. Therefore, they are widely studied by biologists and more recently also by physicists. Although there are many different motors, each fulfilling a specific task, they all are proteins that generate motion by converting chemical energy, derived from hydrolysis of ATP, into mechanical work. [1,2] In this work we focus exclusively on processive molecular motors that, when attached to a transport filament, e.g. actin in plant cells, can bind to organelles or vesicles, and pull these along the filaments. Transport provided by molecular motors in this way is called “active transport”. Thus, bio-filaments can be viewed as intercellular highways.

Intensive experimental work on various molecular motors has revealed the chemical and mechanical processes that an individual molecular motor undergoes in order to move along a filament. But for the understanding of the overall motion of motors and their cargo in cells, additional factors need considering. In particular the viscous interaction with the surrounding medium and steric hindrance constitute two relevant mechanisms. A third important process is thermal fluctuations because due to the motors’ small size all unbound organelles in the cell behave like colloids, hence their motion is dominated by Brownian motion and is not ballistic. However, contrary to thermal motion, which does not produce directed motion, when a motor protein binds to a filament it will start moving on average with a directed motion. The polarity of the filament determines the direction of the motion for each type of motor.

The origin of the asymmetric motion of a motor on a filament is captured by simplified models, such as the Brownian ratchet model. [3,4] When a finite fraction of the motors move along a filament, one also needs to account for their interactions. To that end, it proves useful to disregard the details of how the filament-motor interaction generates a net displacement and describes it as an asymmetric simple exclusion process (ASEP). [7] These models can be coupled to a Langmuir-type adsorption kinetics [5] to account for the interaction between motors on the filament and in the surrounding suspension. Such approaches have helped to elucidate the basic principles underlying cooperative motion of molecular motors and have been applied to analyze the relevance of strong confinement [7] and boundary [8], which constitutes important factors in highly crowded cells.

The interactions of the motors with the surrounding fluid can also have a deep influence in the collective behavior of molecular motors, although it has not been addressed. Forces exerted by bio-filaments are usually in the range of picoNewtons [1], while the drag force exerted by water on a nanometer-size particle moving at 1 *μm/s* is of the order of 10-5 *pN*. Thus the hydrodynamic drag exerted on isolated molecules is negligible, and it is small for organelles.

Despite this fact, we will show that these forces induce a qualitative change in the state of motion of suspended particles close to biofilaments, because the hydrodynamic forces generated when many active motors are present add up. As a result, moving bound motors can exert sufficient hydrodynamic force to give unbound motors in the vicinity a ”free ride”. Besides the question of size, the relevance of hydrodynamic interactions together with excluded volume and crowding effects will also depend on the specific situation of interest. Collective hydrodynamic effects may be expected to play a minor role inside the complex three-dimensional cytoskeletal network of animal cells. In this case the motion is only locally directed, on long (cell like) length scales it is not. But in some situations with well defined symmetry and boundaries, such as in neurons or plant cells, hydrodynamics may be relevant. In particular, for cytoplasmic streaming in plant cells collective hydrodynamic effects could explain the rapid transport of organelles. [10–13] Here unidirectional active transport takes place trough cytoplasmic strands. Fig. 1 shows a stamen hair cell of *Tradescantia virginiana* (spiderwort) where such strands are clearly visible, generating directional motion inside the cell. Microscopic observations have elucidated non-negligible flow in the cytoplasm caused by the movement of organelles.[14]

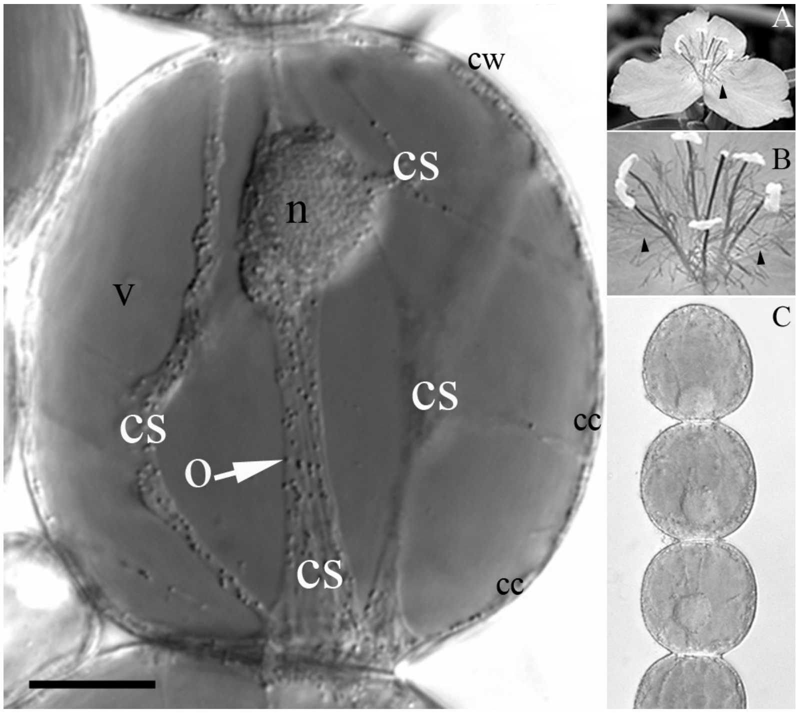

Figure1. *Tradescantia virginiana* (spiderwort) stamen hair cell. The cytoplasmic strands (CS) contain organelles (O) (white arrow); n - nucleus, v - vacuole, cc - cortical cytoplasm, cw - cell wall.

Bar = 20 µm. Inserts: A. Flower of *T. virginiana*, B. Magnification of stamens, arrowheads indicate stamen hairs, C. Single stamen hair.

MODEL

In order to analyze the effects of the surrounding fluid on the transport of bound and suspended motors, we have developed a lattice model that combines an asymmetric Brownian motion along the filament with position-dependent mobilities to include the effect of the interactions mediated by the surrounding fluid. We consider a lattice occupied by N motor-organelle complexes. These complexes are chosen to be equal to each other in size, and have the same processivity and velocity. Biofilaments are added as linear segments connecting lattice sites, see Fig. 2. The excluded volume of the motors is allowed for by forbidding two particles from occupying the same node simultaneously. Suspended motors diffuse freely, while bound motors perform an ASEP motion coupled with a Langmuir-type adsorption/desorption kinetics.

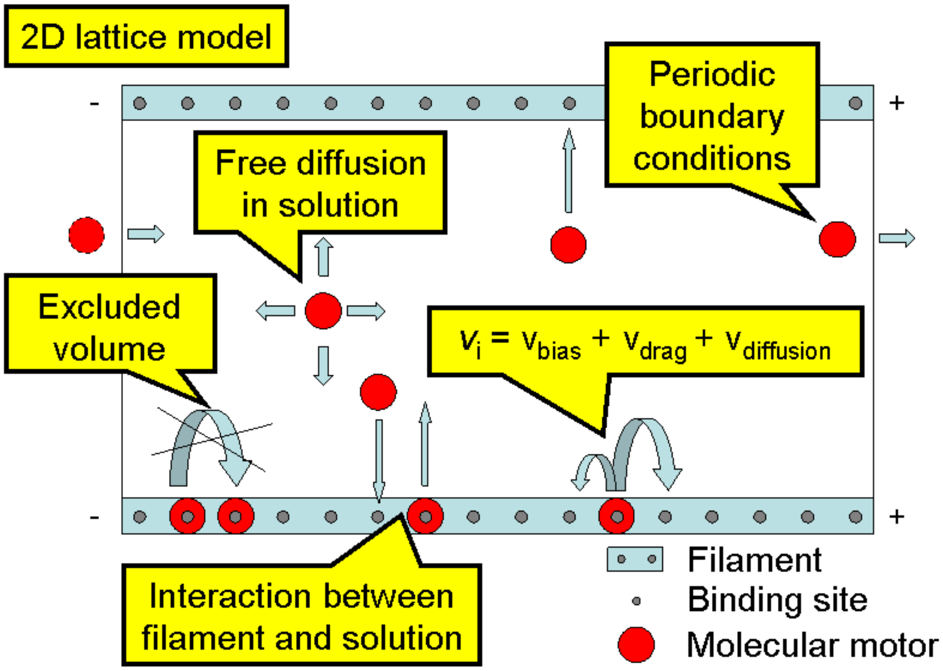
2D lattice model
Periodic boundary conditions
Free diffusion in solution
Excluded volume
$v_i = v_{bias} + v_{drag} + v_{diffusion}$
Interaction between filament and solution
-
+
-
+
Filament
Binding site
Molecular motor

Figure 2. Schematical view of model. Shown is a 2D lattice consisting of cytoplasm embedded between two filaments. The possible moves of the molecular motors are shown.

The model assumes the cytosol is Newtonian, which, to a first approximation, is reasonable for small motor/cargo velocities.

To include the hydrodynamic coupling between motors one must take into account that, due to the motors' small size and velocity, any fluid flow they induce will be at low Reynolds numbers [15]. As a result, the general fluid flow equation (the *Navier-Stokes* equations) simplifies to the linear *Stokes equation*,

$$\eta_s \nabla^2 \mathbf{V} - \nabla P = \sum_k \mathbf{F}_k \delta(\mathbf{r} - \mathbf{r}_k) \qquad (1)$$

Here η_s is the viscosity of the su, ∇p the pressure difference, δ is a delta function, r_k is the position of the k-th particle and V the fluid velocity. The flow is generated by the force F_k that particle k exerts on the fluid. This force is the sum of the effective force produced by the filament on the motor, F_0, and the net force coming from motor-motor interactions. The fluid flow induces a drag on all the motors. As a result, the velocity of motor *i* can generally be expressed as

$$\mathbf{V}_\mathrm{i} = \mu_\mathrm{ii} \cdot \mathbf{F}_\mathrm{i} + \sum_{\mathrm{j}\neq\mathrm{i}} \mu_\mathrm{ij} \cdot \mathbf{F}_\mathrm{i} + \mathbf{V}_\mathrm{i}^\mathrm{R} = \mathbf{V}_0 + \mathbf{V}_\mathrm{i,d} + \mathbf{V}_\mathrm{i,r} \tag{2}$$

where *j* sums over all motors subject to a force, $\mathbf{V}_\mathrm{i} = \mu_\mathrm{ii} \cdot \mathbf{F}_\mathrm{i} = \mathbf{V}_0$ is the single motor velocity produced by the force F_0 exerted by the filament (and it is hence non zero only for bound motors), $V_{i,r}$ is the thermal velocity and $V_{i,d}$ corresponds to the hydrodynamic coupling.

Due to the linearity of eq.(1), the last contribution is determined by the mobility matrix μ_{ij} Which in the Oseen approximation reads [16]

$$\mu_\mathrm{ij} = \frac{3}{4}\mu_\mathrm{ii} \frac{A}{r_\mathrm{ij}} \left[\hat{\mathbf{I}} + \hat{\mathbf{r}}_\mathrm{ij}\hat{\mathbf{r}}_\mathrm{ij}\right] \quad \text{for} \quad i \neq j \tag{3}$$

where A is the hydrodynamic radius of the particles, $\mu_\mathrm{ii} = 1/6\pi\eta_\mathrm{s} A$ the self mobility, $\mathbf{r}_\mathrm{ij} = \mathbf{r}_\mathrm{i} - \mathbf{r}_\mathrm{j}$, the distance between two motors and $\hat{\mathbf{r}}_\mathrm{ij} = \mathbf{r}_\mathrm{ij}/r_\mathrm{ij}$ is a unit vector.

Eq. (2) gives the dynamic equation which determines the motion of the motors. Since they move on the nodes on a lattice, we have implemented a lattice variant of the *Ermak* and *McCammon* method [17], taking into account that hydrodynamic interactions also introduce correlation in the motors' diffusion. In order to account for the hydrodynamic coupling it is necessary to estimate the interparticle forces associated with excluded volume; we do it on the basis of the velocity change of the motor.

Finally, the biofilament processivity is accounted for by allowing the motors to detach from the filament with a certain probability κ_u**.** Motors in solution close to the filament, in turn, can also attach to the filament with probability κ_b**.** Motor interchange between the filament and the embedding solution determines the ratio between the solution and filament volume fractions, ϕ_s and ϕ_μ respectively. Assuming uniform concentrations along the filament and in the solution a mass flux balance predicts the steady state relationship between solution concentration and filament occupation, $\phi_\mu^{-1} = 1 + \kappa_\mathrm{u}(1-\phi_\mathrm{s})/\kappa_\mathrm{b}\,\phi_\mathrm{s}$. We have taken values of κ_u and κ_b to ensure the required filament and solution concentrations.

For the sake of simplicity, we neglect the effects that an additional solid substrate could have on the hydrodynamic interactions between suspended and attached motors; we leave such generalizations and refinement of the analysis to subsequent work. Consequently,

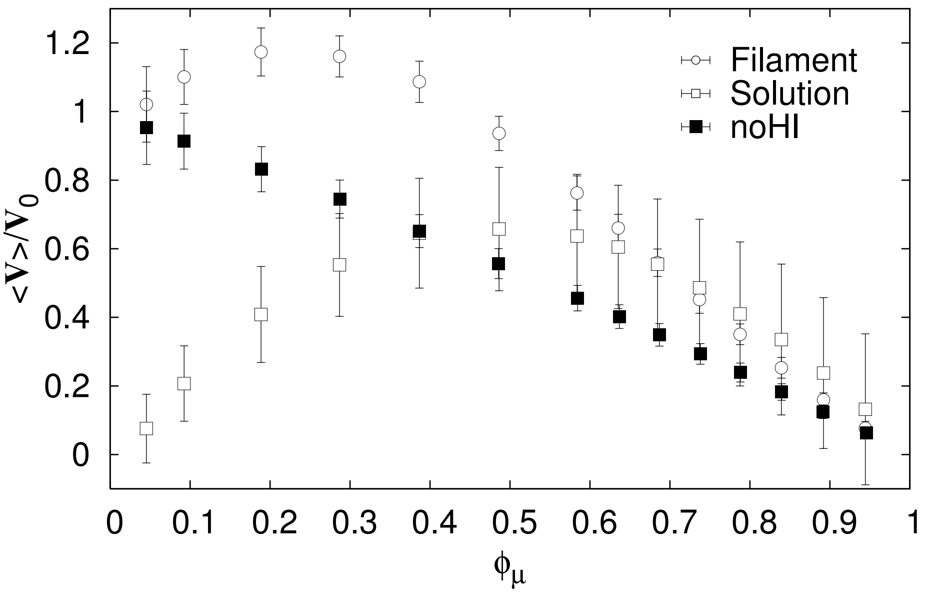

Figure 3. The normalized velocity profile for different degrees of filament occupation ϕ_μ. The open circles refer to the filament, the open squares to the solution, the filled squares show data without hydrodynamic interactions.

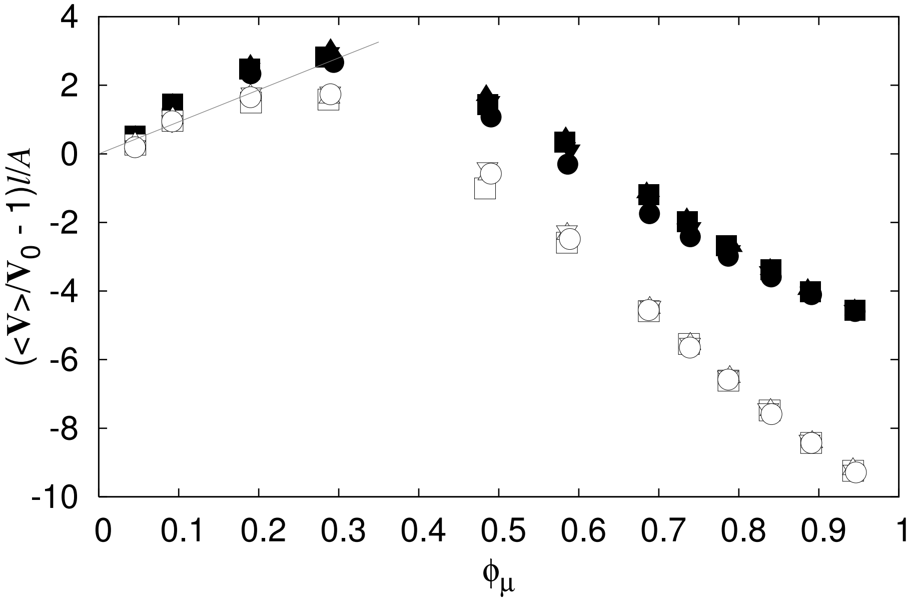

Figure 4. Bound motor velocity for different filament occupation ϕ_μ. $< V >$ is the motor velocity, V_0 the single motor velocity, *A* the hydrodynamic radius and *l* the lattice spacing. The line shows the theoretical expected increase in velocity due to HI (see text). *A* and V_0 are varied: Filled symbols *A*=0.1, Open symbols *A*=0.2; Squares V_0=0.2, Triangles V_0=0.4, Inverted triangles V_0=0.6, Circles V_0=0.8

our goal in this chapter is to look at the qualitative differences that the presence of the solvent has on the dynamics of attached and suspended motors compared to the predictions of previous analysis that concentrated exclusively on transport in the absence of solvent.

RESULTS

We have considered the simplest geometry in which particles move in the two dimensional plane confined between two filaments, although the hydrodynamic interactions correspond to those of a 3D fluid (we presume that the structure of the particles in the transverse direction can be neglected). Such an idealized geometry contains the basic dynamic couplings and facilitates the analysis. In order to analyze the interplay between activity, excluded volume and hydrodynamic forces, we fix the solution concentration to a small value, $\phi_s = 0.05$ and analyze the collective behavior of the suspension+biofilament complex at different degrees of filament's occupation. In units of the lattice spacing, l, and simulation time step, Δt, for motors of unit mass we vary the force exerted by the filament between 1/2 and 2 to control the single motor velocity, which should take values of the order (but smaller than) a lattice spacing. Simulations are run for systems size L, containing around 1000 motors and for a few thousand time steps after thermalization. In order to keep the simplified description of the hydrodynamic interactions, and making use of the linearity of the problem, we keep A smaller than 1/5. For these parameters the motor Péclet number is of order one [18]. Nevertheless, the results we will discuss should not be severely affected by this fact, since we focus on mean collective motor velocities.

In Fig. 3 we show the velocity at which motors move along a filament divided by the single motor velocity, V_0, as a function of the filament occupation, ϕ_μ. In the absence of hydrodynamic interactions (HI), the velocity decreases linearly with increasing occupation fraction due to excluded volume interactions.

When HI are considered, the drag first increases the overall bound motor velocity. At higher concentrations a second regime is achieved, where hindering due to excluded volume effects causes this velocity to decrease. Nevertheless, for all occupations the motors' velocity is larger than the corresponding one in the absence of HI. A second, qualitative, effect of the cooperativity induced by the solvent is displayed in the same figure where we show the average velocity of motors in solution. In the absence of HI particles can only display a net displacement along the filament. However, in the case with HI, there clearly exists a well defined solution velocity which increases with ϕ_μ until it reaches a maximum after which it decreases. The position of the maximum depends on the specific parameters considered. There seems to be an optimum filament occupation, which is different for both the filament $(\phi_\mu \approx 0.2)$ and the solution $(\phi_\mu \approx 0.5)$. The position of these maxima seems to be insensitive for all simulation parameters explored (data not shown). In Fig. 4, we show the increase of the motors' velocity with respect to their biased velocity. Due to the linearity of the hydrodynamic coupling, in the regime where excluded volume interactions are negligible, the profiles are linear in A. Hence, different systems collapse in a single curve as a function of filament occupation. We can then use eq. (2) to estimate the initial increase in motors' velocity. If we rewrite it as

$$\frac{(\mathbf{V}_\mathrm{i} - \mathbf{V}_0)l}{\mathbf{V}_0 A} = \frac{3}{4}\mu_\mathrm{ii}\sum \frac{l}{r_\mathrm{ij}}\left[\hat{\mathbf{I}} + \hat{\mathbf{r}}_\mathrm{ij}\hat{\mathbf{r}}_\mathrm{ij}\right] \quad \text{for} \quad i \neq j \tag{4}$$

and approximate the right hand side assuming a continuous and uniform distribution of motors, we get $\frac{(\mathbf{V}_\mathrm{i} - \mathbf{V}_0)l}{\mathbf{V}_0 A} = \frac{3}{2} l \phi_\mu \ln \frac{L}{2A}$, which agrees quantitatively with the simulation results. For total filament occupation, ϕ_μ=1 motors cannot move along the filament, <V>=0.

In Fig. 5 we display the mean velocity of unbounded motors; these two plots show how the hydrodynamic coupling can be tuned by controlling the motors' size and biased velocity. Using a more realistic choice for the mobility tensor for particles at small separations (Brenner [19], Rotne-Prager [16]) these data do not change (data not shown), indicating that the mechanism described is generic and comes from the algebraic correlations induced by the embedding solvent.

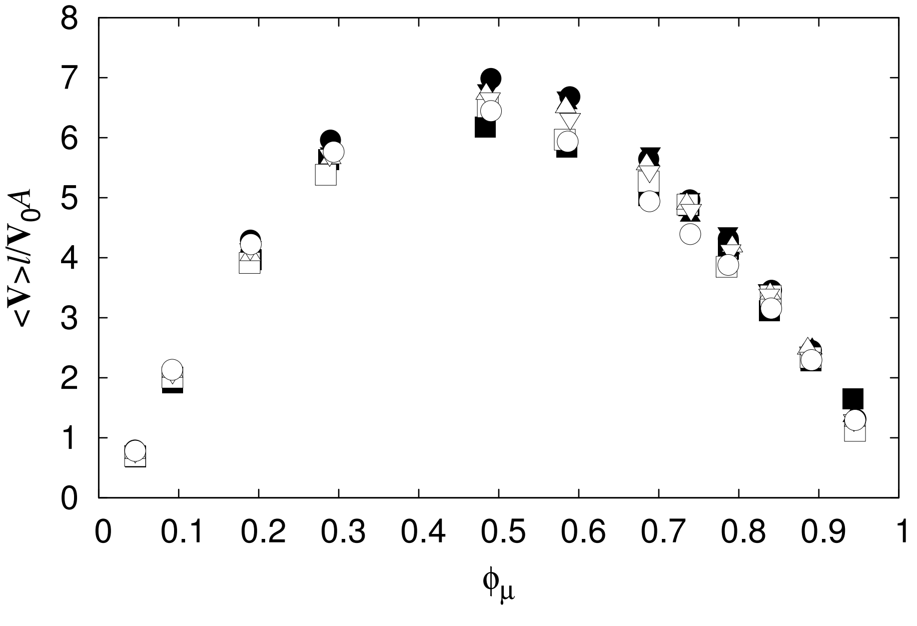

Figure 5. Mean velocity < V > in solution for different degrees of filament occupation φ_μ, hydrodynamic radius A, and single motor velocity V_0, with l being the lattice spacing. Filled symbols A=0.1, Open symbols A=0.2; Squares V_0=0.2, Triangles V_0=0.4, Inverted triangles V_0=0.6, Circles V_0=0.8.

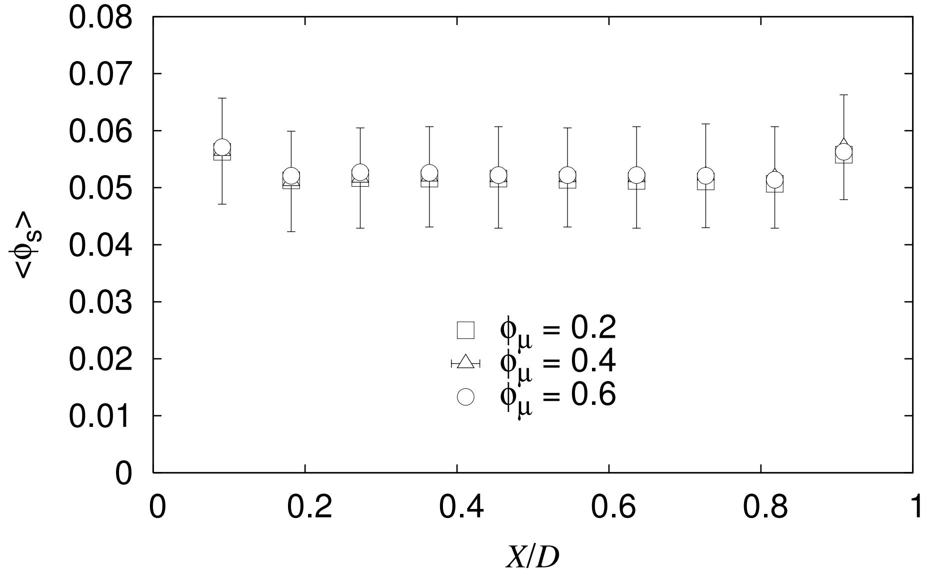

Figure 6. Concentration profiles for unbounded motors. *D* is the distance between filaments, and *X* the distance to the lower filament.

Fig. 6 shows the concentration of unbound motors across the width *D* of the system. It shows that the interactions between the attached and suspended motors induce a uniform distribution of suspended motors, independently of filament occupation. One can clearly see that the hydrodynamic interactions have a minor effect on the concentration profile between the filaments. Also the velocity profile, as displayed in Fig. 7, shows that the velocity in solution is modified only in the filaments' neighborhood.

DISCUSSION

We have shown that long range collective hydrodynamic interactions lead to a substantial increase in the effective velocity of motors attached to a filament. Moreover, their motion leads also to net transport on the nearby unbound particles. This mechanism is not captured by models that consider only the activity and steric interactions of motors attached to biofilaments. Such an additional transport mechanism may be numerically as relevant as the mass transport obtained by direct motion of attached motors.

Due to its nature, this mechanism is more relevant for larger objects (suprananoscopic), for highly viscous environments and for transport on elongated geometries. One must take into account that, as the dimensions grow, simple diffusion becomes more inefficient as compared to convection.

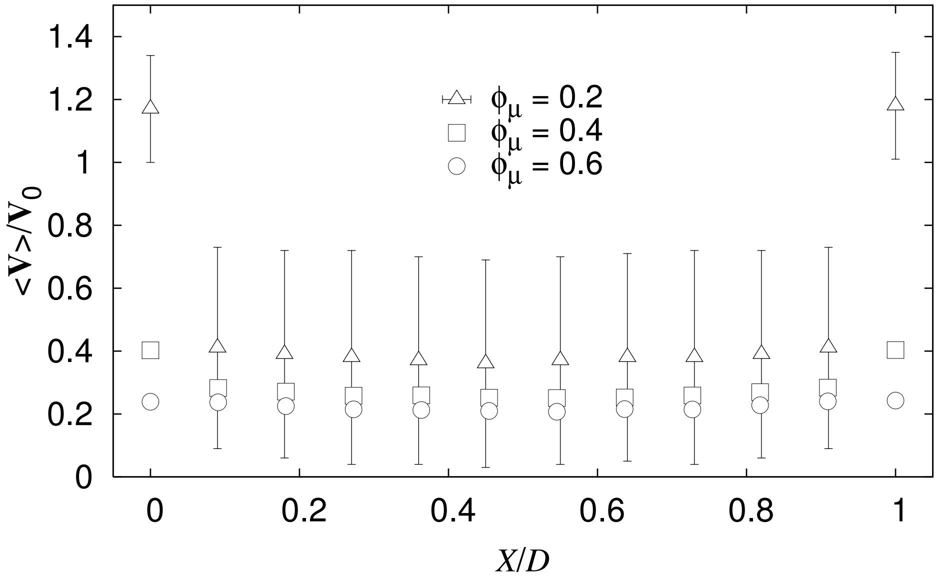

Figure 7. Velocity over the distance *D* between the filaments for a distance *X* from the lower filament for different biofilament occupation, φ_μ.

The additive hydrodynamic force, as induced by the processivity of the filament, might not be large compared with the driving force which generates the motion of the attached motors but the cumulative effect can give rise to a net significant mass transport of the system. Obviously, such a constructive mechanism will be more prominent the more ordered the environment. In this sense, such a mechanism can be envisioned to be more important in situations as found in neurons or in cytoplasmic strands in plant cells. The outcome of our simulations suggests that this mechanism is indeed a plausible explanation for how cytoplasmic streaming really takes place.

ACKNOWLEDGEMENTS

I.P. thanks DGICYT of the Spanish Government and Distinció de la Generalitat de Catalunya (Spain) for financial support. We also thank D. Frenkel for many helpful discussions.

REFERENCES

[1] Jonathan Howard, Mechanics of motor proteins and the cytoskeleton (Sinauer Associates, Sunderland) 2001

[2] Alberts B. sl et al., Molecular Biology of the Cell (Garland, New York) 2002

[3] Austumian R. D., Science, 276 (1997) 917

[4] Jülicher F., Ajdari A. and Prost J., Rev. Mod. Phys., 69 (1997) 1269

[5] Parmeggiani A., Franosch T. and Frey E., Phys. Rev. Lett., 90 (2003) 086601

[6] Nédélec F., Surrey T. and Maggs A.C., Phys. Rev. Lett., 86 (2001) 3192

[7] Lipowsky R., Klumpp S and Nieuwenhuizen T.M., Phys. Rev. Lett., 87 (2001) 108101

[8] Klumpp S. and Lipowski R., J. Stat. Phys., 113 (2003) 233

[9] Klumpp S. and Lipowski R., Europhys. Lett., 66 (2004) 90

[10] de Win A.H.N. et al., Cytometry, 29 (1997) 136

[11] Pickard W.F., Plant, Cell and Environment, 26 (2003) 1

[12] Shimmen T. and Yokota E., Current Opinion in Cell Biology, 16 (2004) 68

[13] Sieberer B. and Emons A.M.C., Protoplasma, 214 (2000) 118

[14] Esseling-Ozdoba A., Houtman D., Pagonabarraga I., Lowe C.P., Eiser E., Emons **A.E.C., submitted to Journal of Microscopy.**

[15] For organelles of a typical size *l* ~ 1μm moving in water at a characteristic velocity *u* ~ 1μm/s have a Reynolds number, $Re = ul/\nu$, of order $Re \sim 10^{-6}$

[16] Dhont J.K.G., An introduction to Dynamics of colloids (Elsevier science B.V., Amsterdam) 1996, p. 241-243, 250-253

[17] Ermak D.L. and McCammon J.A., J. Chem. Phys, 69 (1978) 1352

[18] For organelles of typical size *l* ~ 1μm that move along a bio filament with a velocity *u* ~ 1μm/s and assuming a diffusion coefficient of 10^{-12} m^2 /s we find a peclet number of order $Pe \sim 1$

[19] Brenner M.P., Physics of fluids, 11 (1999) 754

Chapter 5

Hydrodynamic Flow in the Cytoplasm of Plant Cells

Agnieszka Esseling-Ozdoba[1,*], Dion Houtman[2], André A.M. van Lammeren[1], Erika Eiser[2] and Anne Mie C. Emons[1,3]

[1] Laboratory of Plant Cell Biology, Department of Plant Sciences, Wageningen University, Arboretumlaan 4, 6703 BD Wageningen, The Netherlands

[2] van't Hoff Institute for Molecular Sciences (HIMS), Universiteit van Amsterdam, Nieuwe Achtergracht 166, 1018 WV Amsterdam, The Netherlands

Submitted to Journal of Microscopy

Abstract

Plant cells show myosin-driven organelle movement, called cytoplasmic streaming. Soluble molecules, such as metabolites do not move with motor proteins but by diffusion. However, is all of this streaming active motor-driven organelle transport? Our recent simulation study (Houtman et al., 2007) shows that active transport of organelles gives rise to a drag in the cytosol, setting up a hydrodynamic flow, which contributes to a fast distribution of proteins and nutrients in plant cells. Here, we show experimentally that actively transported organelles produce hydrodynamic flow that significantly contributes to the movement of the molecules in the cytosol. We use FRAP (Fluorescence Recovery After Photobleaching), and show that in tobacco Bright Yellow 2 (BY-2) suspension cells constitutively expressing cytoplasmic GFP (green fluorescent protein), free GFP molecules move faster in cells with active transport of organelles than in cells where this transport has been inhibited with the general myosin inhibitor BDM (2,3 – butanedione monoxime). Further we show that the direction of the GFP movement in the cells with active transport is the same as that of the organelle movement and that the speed of the GFP in the cytosol is proportional to the speed of the organelle movement. In large BY-2 cells with fast cytoplasmic streaming a GFP molecule reaches the other side of the cell approximately in the same time frame (about 11 s) as in small BY-2 cells that have slow cytoplasmic streaming. With this we suggest that hydrodynamic flow is important for efficient transport of cytosolic molecules in large cells. Hydrodynamic flow might also contribute to the movement of larger structures than molecules in the cytoplasm. We show that synthetic lipid (DOPG) vesicles and "stealth" vesicles with PEG phospholipids moved in the cytoplasm.

INTRODUCTION

The cytoplasm of eukaryotic cells consists of all cell material between the nucleus and the plasma membrane and contains membrane-bound structures, organelles, which are embedded in the cytosol consisting of water, salts and organic molecules, including sugars, proteins, and many enzymes that catalyze reactions. The cytoskeleton of microtubules and actin filaments in the cytosol structures the cell by localizing and transporting the organelles bound to these tubules and filaments. The plasma membrane, enveloping the cytoplasm physically, separates the cell content from the extracellular environment, which in plant cells is the cell wall. The latter consists of cellulose microfibrils embedded in a matrix of polysaccharides, glycoproteins and phenolics. The largest organelle in the plant cell is the vacuole (Kutsuna and Hasezawa, 2002; Ruthardt et al., 2005; Higaki et al., 2006), which functions as waste managing factory and also to maintain the hydrostatic pressure in the cell. Cytoplasmic strands of cytoplasm (also called transvacuolar strands) that are bounded by the vacuolar membrane traverse the central vacuole in mature plant cells. They connect the peripheral cytoplasm to the cytoplasm that surrounds the cell nucleus (Hoffmann and Nebenführ, 2004; Ruthardt et al., 2005). Under a differential interference contrast (DIC) microscope, the rapid transport of organelles in the cytoplasmic strands can be observed. This rapid transport is called cytoplasmic streaming (e.g. pollen tubes: Iwanami 1956, root hairs: Sieberer and Emons, 2000; review: Grolig and Pierson, 2000). The organelle movement is driven by the molecular myosin motors that walk along actin filaments (Miller et al., 1995; Yokota et al., 1995; Nebenführ et al., 1999; Staiger, 2000; Shimmen and Yokota, 2004). In interphase plant cells, microtubules are not present in the cytoplasmic strands (this paper) but radiate only from the nucleus during the transitions from interphase into mitosis (Bakhuizen et al., 1985; Kutsuna and Hasezawa, 2002; Dhonukshe et al., 2005), and just after cytokinesis (Flanders et al., 1990). In cytoplasmic strands, actin filaments are mainly present in bundles (Emons, 1987; Miller et al., 1999; Grolig and Pierson, 2000, Yokota et al., 2003) and can be considered to be cellular highways, on which organelle-associated myosin motors move their cargo (Kohno and Shimmen, 1988; Miller et al., 1995; Yokota et al., 1995; Shimmen and Yokota, 2004; Romagnoli et al., 2007). The energy necessary for the movement of the myosin motors is generated by hydrolysis of ATP. In vitro, the maximum measured speed of the higher plant myosin XI is 7 μm/s (Tominaga et al., 2003). Organelle movement in different plant cells can reach various velocities (Table 1). The bulk of soluble molecules such as metabolites do not move with motor proteins in the cytoplasm. In a system in which particles, organelles here, move actively inside an aqueous environment with suspended molecules, it is expected that the actively moving objects induce a flow in the surrounding medium, dragging along other particles and molecules. For this intra-cellular movement the term hydrodynamic flow may be used. In general, the term hydrodynamic flow is used when a fluid stream exerts a drag force on any obstacle placed in its wake, and the same force arises if the obstacle moves and the fluid is stationary (Encyclopedia Britannica).

Cell type	Plant	Organelle velocity (µm/s)	References
Pollen tubes	*Nicotiana tabaccum,* Arabidopsis	~ 2	De Win et al., 1999; Derksen et al., 2002
Root hairs	*Medicago truncatula* *Equisetum hyemale*	8-14* 3.5-7*	Sieberer and Emons, 2000 Emons, 1987
Hypocotyl	Arabidopsis	4.8	Holweg, 2007
Stamen hairs	*Tradescantia virginiana*	1.4 – 5*	unpublished

* Organelle velocity dependent on the developmental stage of the cell.

Table 1. Organelle velocities in various plant cells.

A recent simulation study (Houtman et al., 2007) showed that active transport of organelles gives rise to a hydrodynamic flow in the cytosol, which may be important for the fast distribution of proteins and nutrients in large cells. Here we show for the first time that actively transported organelles produce hydrodynamic flow in plant cells, which significantly contributes to the movement of the molecules in the cytosol. We show that in the cytoplasm of tobacco BY-2 suspension cells, constitutively expressing cytoplasmic GFP, free GFP molecules move faster in cells with active organelle transport than in cells where this transport has been inhibited. Further we show that the direction of the GFP movement is the same as that of the organelle movement, and that the speed of the GFP in the cytosol is proportional to the speed of the organelle movement. We conclude that hydrodynamic flow is a faster way than diffusion in distributing molecules inside plant cells.

RESULTS

Choice of inhibitors of organelle movement

Our aim was to study whether actively moving organelles influence the movement of molecules in the cytosol. The cells of choice were tobacco BY-2 suspension cells expressing cytoplasmic GFP. In the cytoplasmic strands of those cells, actin filaments are present (Fig. 1A), but microtubules are not (Fig. 1B) showing that actin filaments are the highways for organelle movement in plant cells. Actin depolymerizing agents stop streaming while microtubule depolymerizing drugs do not influence organelle movement (data not shown). For this study we used Fluorescence Recovery After Photobleaching

(FRAP). In such experiments, a cytoplasmic area is photobleached and the time of re-appearance of the bleached fluorescence molecule is measured. FRAP was measured in 2.2 µm × 2.2 µm areas of cytoplasmic strands. Figure 2A shows the recovery of GFP fluorescence in a bleached area of a cytoplasmic strand of a young BY-2 tobacco suspension cell.

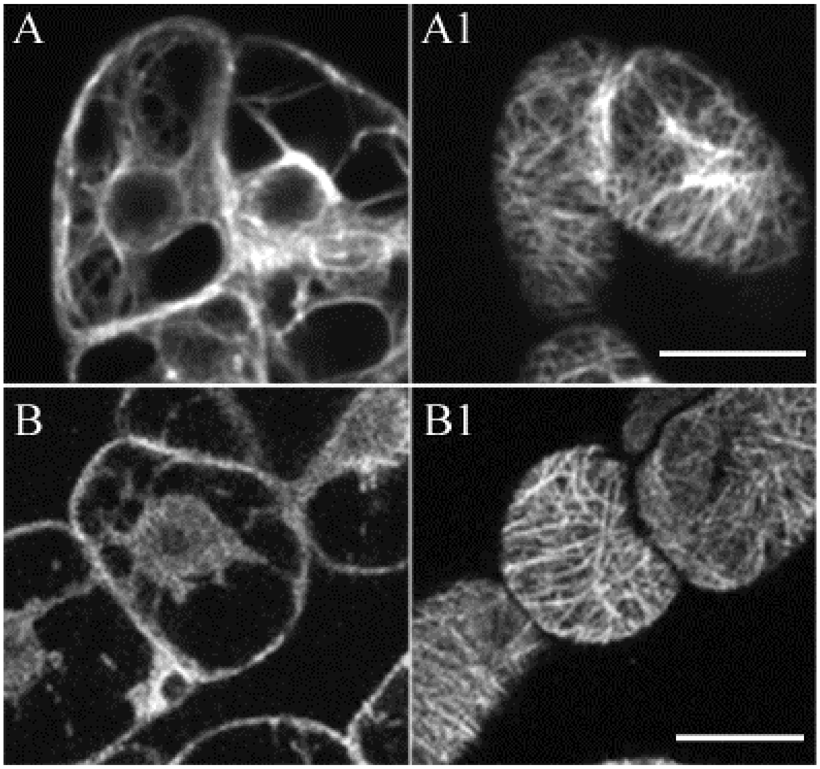

Figure 1. Confocal laser scanning microscope (CLSM) images of young tobacco BY-2 suspension cells transformed with GFP:FABD (fimbrin actin-binding domain) to visualize actin filaments (A and A1) and GFP:TUA6 (α-tubulin) (B and B1) to visualize microtubules. Actin filaments (A) but not microtubules (B) are present in the cytoplasmic strands. Both microtubules and actin filaments are present in the cell cortex seen as filamentous structures (Figures A1 and B1). The fluorescence in cytoplasmic strands in A is possibly free GFP- tubulin, bar = 20 µm.

We used 2,3 – butanedione monoxime (BDM) as an inhibitor of active organelle transport in the cytoplasm of BY-2 suspension cells expressing cytoplasmic GFP. Our purpose was to inhibit organelle movement, but not the Brownian movement of GFP.

BDM is a general myosin ATPase inhibitor (Herrmann et al., 1992; Tominaga et al., 2000; Molchan et al., 2002). BDM at a concentration of 50 mM stopped organelle transport, but recovery of GFP occurred (Fig. 2B), similarly like in the control cells (Fig. 2A). The recovery of GFP ceases in cells chemically fixed with 2% paraformaldehyde (PA) and 0.2% glutaraldehyde (GA). In those cells no GFP recovery occurred during a typical FRAP experiment (Fig. 2C).

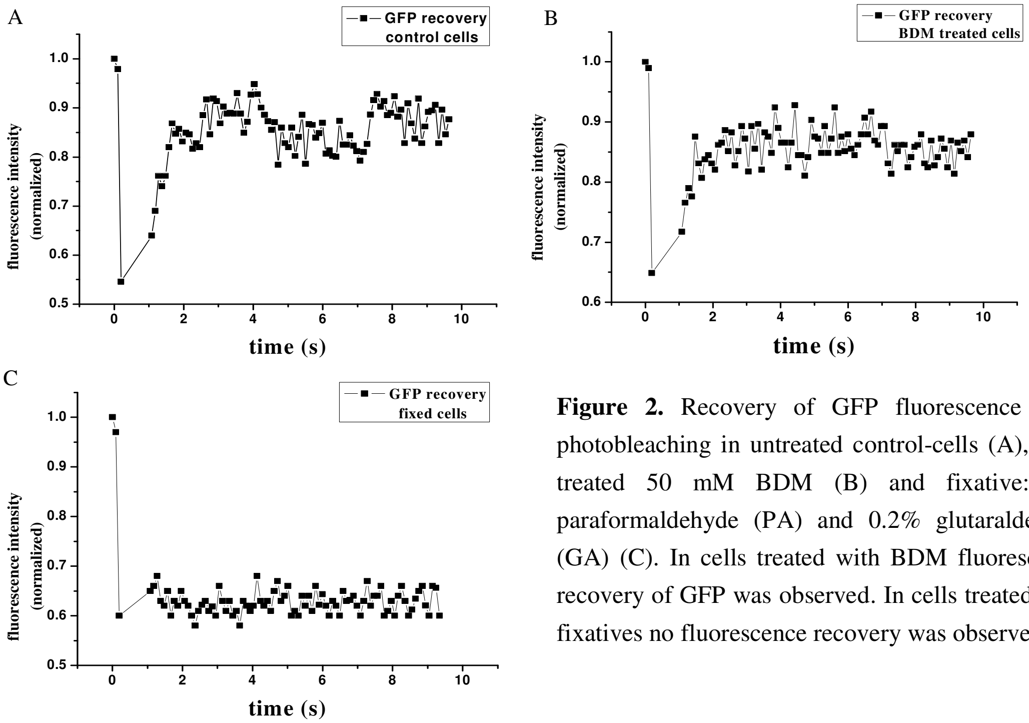

Figure 2. Recovery of GFP fluorescence after photobleaching in untreated control-cells (A), cells treated 50 mM BDM (B) and fixative: 2% paraformaldehyde (PA) and 0.2% glutaraldehyde (GA) (C). In cells treated with BDM fluorescence recovery of GFP was observed. In cells treated with fixatives no fluorescence recovery was observed.

Free GFP molecules move faster in cells with active transport than in those treated with BDM

To test whether the moving organelles induce hydrodynamic flow in the cytoplasm, we used cells with active transport and compared the GFP recovery after photobleaching in control cells with cells in which this movement is inhibited with BDM. With this, we test if hydrodynamic flow is produced by moving organelles and to what extent this contributes to the movement of molecules in the cytoplasm. If our hypothesis is correct, then the recovery of GFP molecules in the cytoplasm of control cells should be faster than in the cells in which this movement is inhibited. Instead of using young small cells that hardly have visible organelle movement (Fig. 3A) and consequently hardly any hydrodynamic flow, we used large elongated cells (Fig. 3B) from 10-day old subcultures of tobacco BY-2 suspension cells, expressing cytoplasmic GFP.

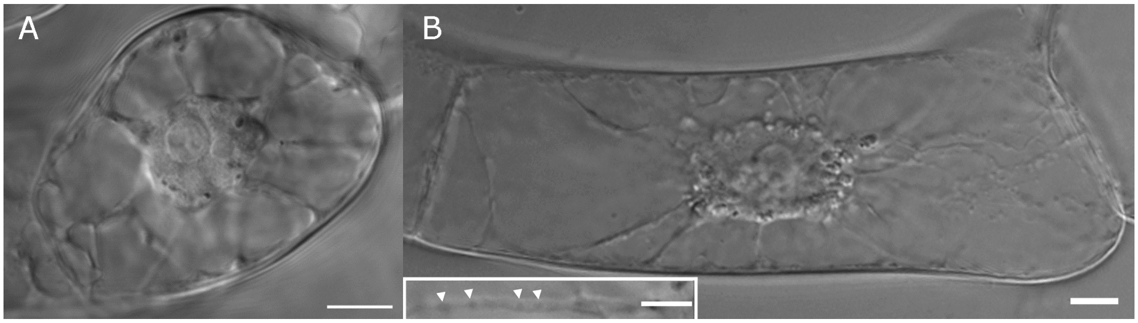

Figure 3. BY-2 cells from a suspension culture: A. Typical cell from a three to four day old culture, B. Typical cell from a 10-day old culture. The cells in a 10-day old culture show vigorous cytoplasmic streaming with easily visible moving organelles. Insert in B shows a cytoplasmic strand with organelles indicated by arrowheads. Bars in A and B correspond to 10 µm and in the insert to 5 µm.

Like in young cells from three to four day old subcultures (Fig. 1A), actin filaments but not microtubules are present in the cytoplasmic strands (Fig. 4) and are responsible for active movement of organelles, since treatment with the actin depolymerizing drug latrunculin stops cytoplasmic streaming (data not shown; van Gestel et al., 1999; Nebenführ et al., 1999; Jedd & Chua, 2002).

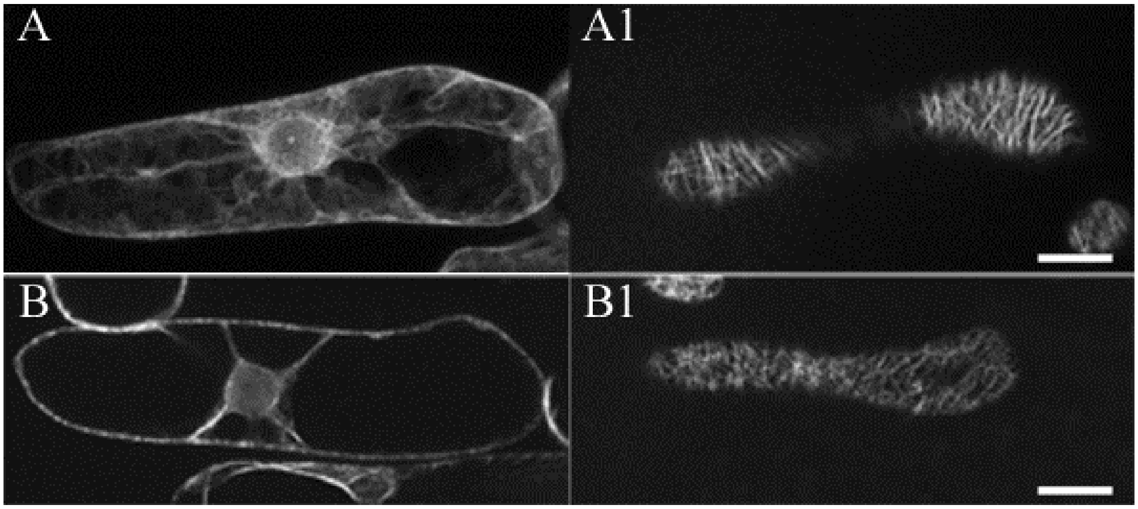

Figure 4. CLSM images of 10-day old tobacco BY-2 suspension cells labeled with GFP:FABD (fimbrin actin-binding domain) to visualize actin filaments (A) and GFP:TUA6 (α-tubulin) to visualize microtubules (B). Actin filaments (A) but not microtubules (B) are present in the cytoplasmic strands; fluorescence in the cytoplasmic strands in B is due to free GFP-tubulin. Bar = 10µm. A1 and B1 are images of cell cortex.

In comparison with young small cells, 10-day old cells have visible, vigorous cytoplasmic streaming (0.78 µm/s ± 0.17). We measured the half time of GFP recovery after photobleaching in a cytoplasmic strand region of 2.2 µm × 2.2 µm. GFP recovers faster (within 0.31 s ± 0.07) in untreated cells with active organelle transport, than in cells treated with 50 mM BDM (within 0.48 s ± 0.12) (Fig. 5). This shows that actively transported organelles contribute significantly to the movement of GFP in the cytoplasm of BY-2 cells. We conclude that organelle movement causes a hydrodynamic flow that contributes significantly to the movement of free GFP in the cytoplasm.

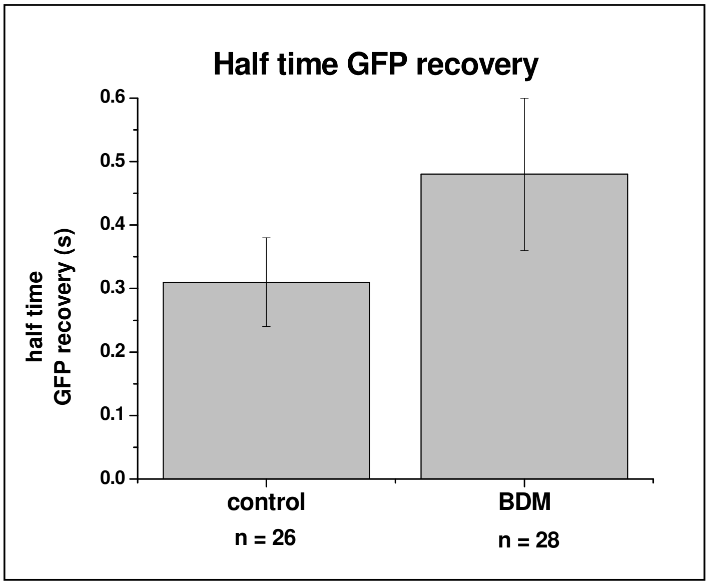

Figure 5. Recovery of cytoplasmic GFP after photobleaching in control BY-2 cells and cells treated with 50 mM BDM. GFP recovered faster in control cells with active organelle transport than in cells in which this transport was inhibited with the myosin inhibitor BDM. This shows that organelle movement causes movement of GFP in the cytoplasm. For FRAP experiments, we used large elongated cells from a 10 day-old culture. Half time of GFP recovery after photobleaching is shown in a region of 2.2 µm × 2.2 µm, data shown with SD.

Hydrodynamic flow is higher in cells in which the velocity of organelle movement is faster

If motor-driven organelle movement causes hydrodynamic flow of cytoplasmic molecules, the speed of GFP movement in the cytoplasm should positively relate to the speed of organelle movement. To show this, we measured the GFP recovery after photobleaching in cells with different velocities of organelle movement (Fig. 6). In cells in which organelles moved with an average velocity of 0.21 ± 0.02 µm/s, the recovery of GFP fluorescence took 0.73 ± 0.19 s, which was slower than in cells having faster organelle movement of 0.75 ± 0.10 µm/s. In those cells, GFP recovery was 0.14 ± 0.04 s. This shows that the fluorescence recovery of GFP increases with the increasing velocity of organelles in the cytoplasm, and confirms that organelle transport induced hydrodynamic flow occurs in plant cells.

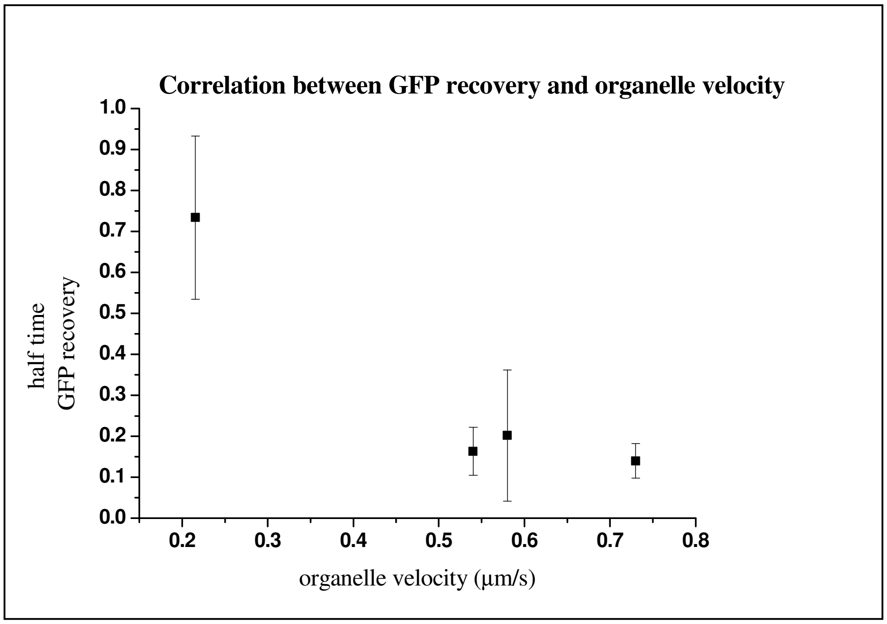

Figure 6. Correlation between GFP fluorescence recovery after photobleaching and the velocity of organelles in the cytoplasm of BY-2 suspension cells. GFP recovery after photobleaching is faster in cells with faster organelle movement. Half time of GFP recovery is shown, measured in regions of 2.2 µm × 2.2 µm, data presented from 8-10 measurements and shown with SD.

Knowing how fast GFP moves in those cells and knowing the dimensions of the cells, we calculated the time that GFP needs to traverse from the cell center to its end in a short young cell and a long mature one (divide the velocity by the traveled distance). Without speeding up the movement by organelle transport (with BDM), GFP needed 12.7 s (a short young cell) and 26.2 s (a long mature cell) to reach the cell end, and with speeding up the movement by organelle transport (without BDM), 11.8 s and 11.4 s respectively. We conclude that in large cells organelle movement is faster than in a small cells and that it is responsible for an efficient distribution of GFP molecules.

Direction of GFP movement in a cytoplasmic strand is the same as that of moving organelles

If moving organelles cause hydrodynamic flow of molecules, the direction of flow should be the same as that of the organelle transport. To check this, GFP was photobleached in a region of 2.2 µm × 2.2 µm and its fluorescence recovery was followed in time. After photobleaching we checked the direction in which organelles move in the strand. We observed that after photobleaching GFP moves in the direction of the moving organelles (N = 4) (Fig. 7). This confirms that hydrodynamic flow occurs in plant cells with moving organelles, which 'drag' molecules, in this case GFP, in their wake, as theoretically predicted (Houtman et al., 2007).

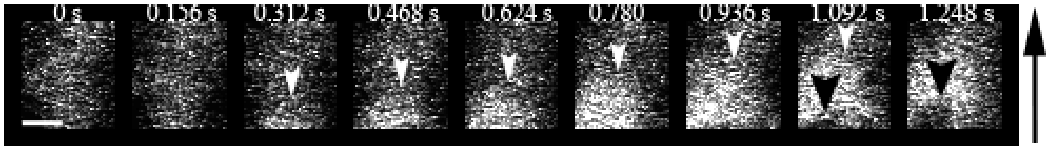

Figure 7. After photobleaching, cytoplasmic GFP (white arrowheads) moved in the same direction (black arrow) as organelles (black arrowheads). GFP is visible as fluorescent speckles and an organelle as a black spot of about 1 µm. For this experiment we used 10 days old elongated cells with an average organelle velocity of 0.78 µm/s (± 0.17); time is indicated in seconds after photobleaching; bar = 1 µm.

Synthetic lipid vesicles and "stealth" vesicles move in cytoplasmic strands

To test if hydrodynamic flow could contribute to the movement of larger structures such as vesicles, we injected synthetic lipid vesicles of size of 80 nm in diameter into *Tradescantia virginiana* stamen hair cells and observed if they moved inside the cytoplasm. The vesicles were made only of phospholipids without any proteins and their membrane contained 98% of 1,2-Dioleoyl-*sn*-Glycero-3-[Phospho-*rac*-(1-glycerol)] (DOPG) and 2% of fluorescent phosphocholine Bodipy FC12-HPC. Injected vesicles distributed in the cytoplasm of the whole cell within 10-15 min after the injection (Fig. 8A). This result would suggest that these vesicles moved by hydrodynamic flow produced by moving organelles in the cytoplasm. We could not exclude that vesicles were coated with cytoplasmic motor proteins upon the injection and moved along the actin cytoskeleton. Therefore we injected so called "stealth" vesicles to which proteins cannot be attached. "Stealth" vesicles are phospholipid vesicles with addition of PEG (polyethylene glycol) phospholipids. The presence of PEG phospholipids prevents the attachment of proteins to the surface of vesicles. "Stealth" vesicles are often used in drugs therapy to prevent the attachment of proteins and lysis of vesicles that carry the drugs (Discher and Eisenberg, 2002). The concentration of PEG phospholipids used in those studies was 5-10%. The concentrations of PEG phospholipids that we used to make stealth vesicles varied from 2% up to 30% in combination with DOPG. All injected "stealth" vesicles distributed in the cytoplasm (Fig. 8B) similar to DOPG vesicles without PEG and moved in the cytoplasm but slower (0.8 ± 0.13 µm/s) than 1-2 microns organelles (1.4 ± 0.25 µm/s, Fig. 8C). The fast distribution of "stealth" vesicles and their movement in the cytoplasm could be an indication that structures larger than molecules and possibly organelles move by hydrodynamic flow in the cytoplasm of plant cells.

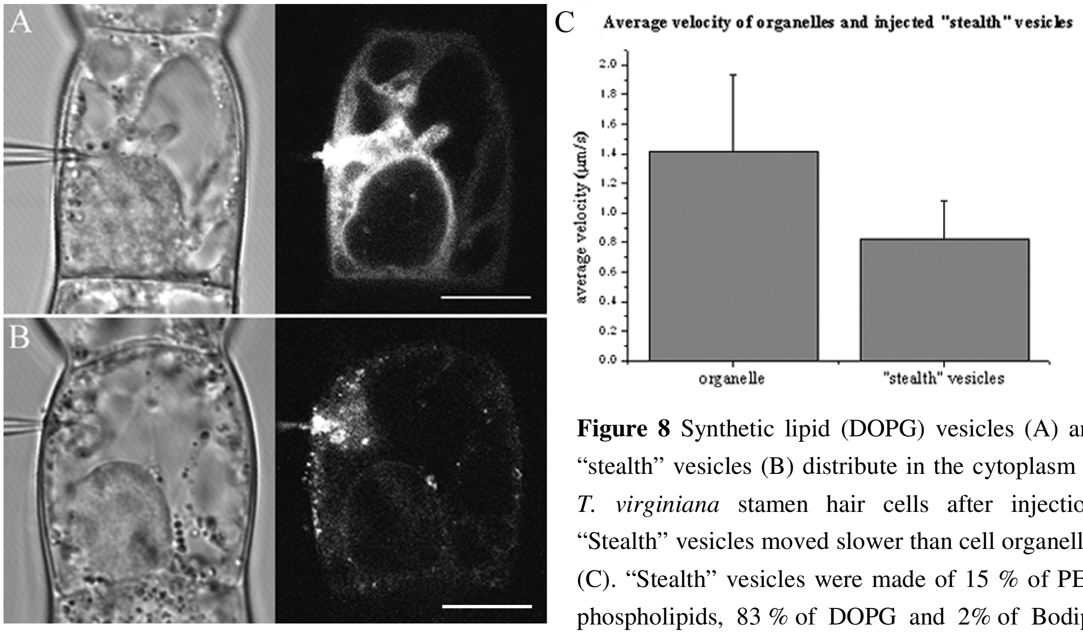

Figure 8 Synthetic lipid (DOPG) vesicles (A) and "stealth" vesicles (B) distribute in the cytoplasm of *T. virginiana* stamen hair cells after injection. "Stealth" vesicles moved slower than cell organelles (C). "Stealth" vesicles were made of 15 % of PEG phospholipids, 83 % of DOPG and 2% of Bodipy FC12-HPC. Images were taken 15 minutes after injection, bar = 10 µm.

DISCUSSION

Transport in cytoplasmic strands

A major characteristic of mature plant cells is that they have large vacuoles that expand considerably during cell elongation and together become one central vacuole that takes up most of the cell volume. The vacuole confines the cytoplasm to a thin layer in the periphery of the cell and an area around the nucleus. The cytoplasm of these two regions is connected to each other by a few thin tunnels of cytoplasm: the cytoplasmic strands, also called transvacuolar strands (Hoffmann and Nebenführ, 2004; Higaki et al., 2006). These cytoplasmic strands are essential transport routes for the distribution of organelles and metabolites (Nebenführ et al., 1999; Grolig and Pierson, 2000). The mechanism of this transport is organelle movement, caused by an ATP-driven movement of myosin motors attached to the organelles along the actin cytoskeleton (Staiger and Schliwa, 1987; Grolig and Pierson, 2000; Shimmen and Yokota, 2004). Unbound structures move via diffusion, a passive process of molecule distribution. We raised the question whether what we see as cytoplasmic streaming includes a passive component of organelle drag induced by the actively moving organelles. Our experimental work indeed is in agreement with our theoretical considerations that the active transport induces hydrodynamic flow in the cytoplasm that surrounds the organelles, speeding up the transport of otherwise only diffusing molecules.

Difference between young and mature cells in organelle transport

The velocities of cytoplasmic streaming vary between different cell types, the developmental stage of the cell, and the species. This is interesting, because these cells have similar myosins that belong to plant specific subfamilies of Myosin VIII and XI. Myosins XI are more abundantly expressed in plant cells than Myosin VIII and are co-localized with most of the organelles. This makes Myosin XI the candidate motor molecule involved in organelle transport (Lee and Liu, 2004). We observed differences in velocities of organelle movement through cytoplasmic strands between small elongating and large fully elongated cells of a tobacco BY-2 suspension culture. This phenomenon is not specific for cells from this suspension culture. Also in other fully elongated plant cells, of for instance *Tradescantia virginiana* stamen hairs, the velocity of organelle movement increases during cell elongation and is maximal in fully elongated large mature cells (own observation, unpublished). The most obvious visible difference between these cells, besides their difference in size, is the larger volume that is taken up by the vacuole in the fully elongated cells. Molecules move faster for longer distances through thinner tubes. Differences in speed of cytoplasmic streaming have been observed within different parts of one and the same cell, namely in root hairs and pollen tubes, that grow at the cell tip that contains only vesicles, which show little movement (Sieberer and Emons 2000). In the subapical cytoplasmic dense region of these growing hairs the net-speed of organelles is low up to 2 µm/s (*Equisetum hyemale*: Emons 1987, *Vicia sativa*: Miller et al., 1999, *Medicago truncatula*: Sieberer and Emons, 2000). In the shank of tip growing root hairs where the central vacuole is present, the net-speed of organelles is 8-14 µm/s (*Equisetum hyemale*: Emons 1987, *Vicia sativa*: Miller et al., 1999, *Medicago truncatula*: Sieberer and Emons, 2000). In these cells, these differences can be linked to the configuration of the actin cytoskeleton, which consists of thick bundles in the hair tube but of thin bundles in the subapex (*Equisetum hyemale*: Emons 1987, *Vicia sativa*: Miller et al. 1999, *Arabidopsis thaliana*: Ketelaar et al., 2003; *Eucalyptus globulus*: Dauphin et al. 2006). In the subapex, organelles often stop for a short time and jump for a short distance from one place to the other (Sieberer and Emons, 2000). Also the possible differences in the configuration of the actin cytoskeleton between the elongating and fully elongated BY-2 suspension cells are expected to be the underlying mechanism of the measured differences in velocities of organelle movement. If indeed the myosin type is the same in both cell structures, it cannot be the step size that determines organelle velocity, but the number of steps made per time unit.

Need for hydrodynamic flow in large cells

Molecules in the cytosol that are not attached to the cytoskeleton do not posses an active driving force for transport. They move by Brownian motion only. If a concentration gradient is produced for instance by the consumption of molecules at one side of the cell, such as the high rate of sugar use at the cell cortex to produce the cell wall, directional movement governed by Brownian motion is the result. Here we show that movement of molecules in a cell, and maybe also ribosomes, vesicles and small organelles, is faster than mere diffusion, and that the cause for this speeding up is the active transport of organelles along bundles of actin filaments, as theoretically predicted (Houtman et al., 2007). If the velocity of organelles in the cytosol of tobacco BY-2 suspension cells is three times faster, the GFP molecules move also three times faster (Fig. 6). Why would this be useful for cells? Signaling and other proteins have to find a partner to bind to for their activity, and these activities have to be carried out at the right sites in the cell. If all of these molecules had to be produced at the site where needed, this would require precise targeting of ribosomes, including the free ribosomes and polysomes not attached to the endoplasmic reticulum. Now we show that random molecule movement inside the cytoplasm, can be speeded up by myosin-driven organelle movement along the actin cytoskeleton, increasing the chance for finding a partner. In the cells that have fast cytoplasmic streaming, hydrodynamic coupling between actively transported organelles and the surrounding solvent causes molecules to spread faster, with the result that those molecules will reach their target with greater efficiency.

The mature BY-2 suspension cells that we studied have velocities of cytoplasmic streaming 10-15 times lower than for instance some of the root hairs studied, or than mature *Tradescantia* stamen hair cells. We expect that in those cells also organelles, or at least vesicles could be dragged along with the actively moved motor-driven organelles. The movement of fluorescent "stealth" vesicles injected into *T. virginiana* stamen hair cells in the cytoplasmic strands indicates that these vesicles and possibly organelles can also move by hydrodynamic flow in the cytoplasm of plant cells.

MATERIAL AND METHODS

Plant material

Tobacco Bright Yellow - 2 (BY-2) suspension cells expressing cytoplasmic GFP (stably transformed with plasmid pBin-35S-smGFP) were used for experiments. Suspension cultures were grown in standard BY-2 medium containing Murashige and Skoog macro- and microsalts, 3% sucrose, 100 mg/l myo-inositol, 200 mg/l KH_2PO_4, 1 mg/l thiamine, and 0.2 µg/l 2,4-dichlorophenoxyacetic acid (Nagata and Kumagai, 1999) and 50 mg/l kanamycin. Suspension cells were prepared in about 50 µm thick, gas- permeable micro-chambers lined on one side with BioFoil (Vivascience, Hanover, Germany) and on the other side with a 24 × 24 mm coverslip (Vos et al., 2004). The micro-chamber contained about 20 µl of cell suspensions.

T. virginiana plants were grown in a growth chamber with a 16-hrs photoperiod at 25°C and 8-hrs dark period at 18°C and 75-80% relative humidity. Stamen hairs with dividing cells in the apical region were dissected from immature flower buds with a length of approximately 5 mm.

Cell treatment with BDM

Tobacco BY-2 suspension cells expressing cytoplasmic GFP were treated with 50 mM BDM from a freshly made stock of 0.5 M in demi water. The control cells were treated with demi water in appropriate amount used for drug treatment. After treatment cells were transferred into micro-chambers and within 30 min. were used for FRAP experiments.

FRAP

FRAP experiments were preformed on confocal laser scanning microscope (CLSM) Zeiss LSM 510 Meta coupled to Zeiss Axiovert 200M inverted microscope, equipped with 63 × 1.4 NA oil immersion objective. Prebleach and postbleach images were acquired using low levels (2 – 4 %) of excitation at 488 nm. Photobleaching was performed using 3 scans with the 488 nm laser line at 100% transmission in a square region of 2.2 µm × 2.2 µm of cytoplasmic strands. The bleached region was always perpendicular to the long axis of the cytoplasmic strands and covered the entire width of the strand. Fluorescence intensity values of the bleached region in the cytoplasmic strand were measured every 0.0491 or 0.0983 s. and followed for 5 or 10 s. Fluorescence intensity values were normalized to compare the experiments of different treatments. The average time for 50 % recovery (half time of recovery, $t_{1/2}$) was determined from fitting recovery curves.

Microinjection

For microinjection experiments we immobilized *Tradescantia virginiana* stamen hairs in a thin layer of 1% low temperature gelling agarose (BDH Laboratory Supplies, UK) in culture medium (5 mM HEPES, 1 mM $MgCl_2$, and 0.1 mM $CaCl_2$, pH 7.0) and 0.025% Triton X-100 (BDH Laboratory Supplies, UK), following the procedure described by Vos et al. (1999).

Synthetic lipid (DOPG) vesicles were made of 98% of the anionic non-fluorescent phospholipid 1,2-Dioleoyl-*sn*-Glycero-3-[Phospho-*rac*-(1-glycerol)] (DOPG, Avanti Polar Lipids) and for 2% of the fluorescent phosphocholine Bodipy FC12-HPC (Molecular Probes, excitation maximum at 503 nm, emission maximum at 512 nm). Phospholipids were mixed together and dried onto a glass surface under a stream of nitrogen, followed by at least 2 hours under vacuum to remove the last traces of solvent. The dried lipid mixture was hydrated with microinjection buffer (5 mM HEPES, 0.1 mM KCl, pH 7.0) to a concentration of 0.5 mg/ml. The lipids were freeze-thawed with liquid nitrogen for five cycles to disperse them and pushed through an extruder with a polycarbonate filter with a 60 nm pore size to yield vesicles with a diameter of ~80 nm. The vesicle diameter was determined using dynamic light scattering. "Stealth" vesicles were made in a similar way, only with addition of 2, 5, 10, 20 and 30% of PEG phospholipids (1,2 – Distearoyl – *sn* – Glycero – 3 – Phosphoethanolamine – N -[Methoxy (Polyethylene glycol) - 5000] (Ammonium Salt) (Avanti Polar Lipids)).

The microinjection experiments were conducted according to Vos et al. (1999). In short, borosilicate needles with filament were back-filled with vesicle solution and mounted onto a micro-needle holder and attached into a screw type syringe (Gilmont Instruments, Barrington, Illinois) via water-filled fine polyethylene tubing. The needle holder was placed into a micro-manipulator (model N0-303, Narashige Scientific Instruments, Tokyo, Japan) mounted on an Eclipse TE-2000-S inverted microscope (Nikon, Tokyo, Japan). Images were collected with a 63x, 1.4 NA DIC lens with a Cell Map IC (BioRad, Hemel Hampstead, UK) confocal laser-scanning microscope.

ACKNOWLEDGEMENTS

AMCE thanks the FOM Institute for Atomic and Molecular Physics (AMOLF), Amsterdam, for financial support for this project. DH and EE thank C. Lowe (Universiteit van Amsterdam) and I. Pagonabarraga (Universitat de Barcelona) for useful discussions.

REFERENCES

Bakhuizen, R., van Spronsen, P.C., Sluiman-den Hertog, F.A.J., Venverloo, C.J. & Goosen-de Roo, L. (1985) Nuclear envelope radiating microtubules in plant cells during interphase mitosis transition. *Protoplasma* **128**, 43-51.

Dauphin, A., De Ruijter, N.C.A., Emons, A.M.C. & Legué, V. (2006) Actin organization during *Eucalyptus* root hair development and its response to fungal hypaphorine. *Plant Biol.* **8**, 204-211.

Derksen, J., Knuiman, B., Hoedemaekers, K., Guyon, A., Bonhomme, S. & Pierson, E.S. (2002) Growth and cellular organization of Arabidopsis pollen tubes in vitro. *Sex. Plant Reprod.* **15**, 133-139.

Dhonukshe, P., Mathur, P., Hülskamp, J.M. & Gadella Jr. T.W.J. (2005) Microtubule plus-ends reveal essential links between intracellular polarization and localized modulation of endocytosis during division-plane establishment in plant cells. *BMC Biology* **3**, 11.

Discher, D.E & Eisenberg, A. (2002) Polymer vesicles. *Science* **297**, 967-973.

Emons, A.M.C (1987) The cytoskeleton and secretory vesicles in root hairs of *Equisetum* and *Limnobium* and cytoplasmic streaming in root hairs of Equisetum. *Annals of Botany* **60**, 625-632.

Encyclopedia Britannica, http://www.britannica.com/eb/article-77496/fluid-mechanics.

Flanders, D.J., Rawlings, D.J., Shaw, P.J. & Lloyd, C.W. (1990) Re-establishment of the interphase microtubule array in vacuolated plant cells, studied by confocal microscopy and 3-D imaging. *Development* **10**, 897-904.

Van Gestel, K., Köhler, R.H. & Verbelen, J-P. (1999) Plant mitochondria move on F-actin, but their positioning in the cortical cytoplasm depends on both F-actin and microtubules. *J. Exp. Bot.* **53**, 659-667.

Grolig, S. & Pierson, E.S. (2000) Cytoplasmic streaming: from flow to track. In: Actin: a dynamic framework for multiple plant cell functions (ed. C.J. Staiger, F. Baluska, D. Volkmann and P. Barlow), pp. 165-190, Dordrecht: Kluwer Academic Publishers.

Herrmann, C., Wray, J., Travers, F. & Barman, T. (1992) Effect of 2,3-butanedione monoxime on myosin and myofibrillar ATPases. An example of an uncompetitive inhibitor. *Biochemistry* **31**, 12227–12232.

Higaki, T., Kutsuna, N., Okubo, E., Sano, T. & Hasezawa, S. (2006) Actin microfilaments regulate vacuolar structures and dynamics: dual observation of actin microfilaments and vacuolar membrane in living tobacco BY-2 cells. *Plant Cell Physiol.* **47**, 839-852.

Hoffmann, A. & Nebenführ, A. (2004) Dynamic rearrangements of transvacuolar strands in BY-2 cells imply a role of myosin in remodeling the plant actin cytoskeleton. *Protoplasma* **24,** 201-210.

Holweg, C.L. (2007) Living markers for actin block myosin-dependent motility of plant organelles and auxin. Cell Motil. Cytoskeleton **62**, 69-81.

Houtman, D., Pagonabarraga, I., Lowe, C.P., Esseling-Ozdoba, A., Emons A.M.C. & Eiser, E. (2007) Hydrodynamic flow caused by active transport along cytoskeletal elements. *EPL*, **78**, 18001p1-p5.

Iwanami, Y. (1956) Protoplasmic movement in pollen grains and tubes. Phytomorphology 6, 288-295.

Jedd, G. & Chua, N.-H. (2002) Visualization of peroxisomes in living plant cells reveals acto-myosin-dependent cytoplasmic streaming and peroxisome budding. *Plant Cell Physiol*. **43**, 384-392.

Ketelaar, T., de Ruijter, N.C.A. & Emons, A.M.C. (2003) Unstable F-actin specifies the area and microtubule direction of cell expansion in Arabidopsis root hairs. Plant Cell **15**, 285-292.

Kohno, T. & Shimmen, T. (1988) Accelerated sliding of pollen tube organelles along Characeae actin bundles regulated by Ca^{2+}. *J. Cell Biol*. **106**, 1539-1543.

Kutsuna, N., and Hasezawa, S. (2002) Dynamic organization of vacuolar and microtubule structure during cell cycle progression in synchronized tobacco BY-2 cells. *Plant Cell Physiol.* **43**, 965-973.

Lee, Y.-R.J. & Liu, B. (2004) Cytoskeletal motors in Arabidopsis. Sixty-one kinesins and seventeen myosins. *Plant Physiol*. **136**, 3877-3883.

Miller, D.D., de Ruijter, N.C.A., Bisseling, T. & Emons, A.M.C. (1999) The role of actin in root hair morphogenesis: studies with lipochito-oligosaccharide as a growth stimulator and cytochalasin as an actin perturbing drug. *Plant J*. **17**, 141-154.

Miller, D.D., Scordilis, S.P. & Hepler, P.K. (1995) Identification and localization of three classes of myosins in pollen tubes of *Lilium longiflorum* and *Nicotiana alata*. *J. Cell Sc*i. **108**, 2549-2563.

Molchan, T. M., Valster, A.H. & Hepler, P.K. (2002) Actomyosin promotes cell plate alignment and late lateral expansion in *Tradescantia* stamen hair cells. *Planta* **214**, 683-693.

Nagata, T. & Kumagai, F. (1999) Plant cell biology through the window of the highly synchronized tobacco BY-2 cell line. *Methods Cell Sci*. **21**, 123-127.

Nebenführ, A., Gallagher, L.A., Dunahay, T.G., Frohlick, J.A., Mazurkiewicz, A.M., Meehl, J.B. & Staehelin, L.A. (1999) Stop-and-go movements of plant Golgi stacks are mediated by the acto-myosin system. *Plant Physiol*. **121**,1127-1141.

Romagnoli, S., Cai, G., Faleri, C., Yokota, E., Shimmen, T. & Cresti, M. (2007) Microtubule- and actin filament-dependent motors are distributed on pollen tube mitochondria and contribute differently to their movement. *Plant Cell Physiol*., **48**, 345-361.

Ruthardt, N., Gulde, N., Spiegel, H., Fischer, R. & Emans, N. (2005) Four-dimensional imaging of cytoplasmic strand dynamics in tobacco BY-2 cells. *Protoplasma* **225**, 205–215.

Shimmen, T. & Yokota, E. (2004) Cytoplasmic streaming in plants. *Curr Opin. Cell Biol* **16**, 68–72.

Sieberer, B. & Emons, A.M.C. (2000) Cytoarchitecture and pattern of cytoplasmic streaming in root hairs of *Medicago truncatula* during development and deformation by nodulation factors. *Protoplasma* **214**, 118–127.

Staiger, C.J. & Schliwa, M. (1987) Actin localization and function in higher plants. *Protoplasma* **141**, 1–12.

Staiger, C.J. (2000) Signaling to the actin cytoskeleton in plants. *Annu. Rev. Plant Physiol. Plant Mol. Biol*. **51**, 257-288.

Tominaga, M., Kojima, H., Yokota, E., Orii, H., Nakamori, R., Katayama, E., Anson, M., Shimmen, T. & Oiwa, K. (2003) Higher plant myosin XI moves processively on actin with 35 nm steps at high velocity. *EMBO J.* **22**, 1263-1272.

Tominaga, M., Yokota, E., Sonobe, S. & Shimmen, T. (2000) Mechanism of inhibition cytoplasmic streaming by a myosin inhibitor 2,3-butanedione monoxime. *Protoplasma* **213**, 46-54.

De Win, A., Pierson, E.S. & Derkesen, J. (1999) Rational analyses of organelle trajectories in tobacco pollen tubes reveal characteristics of the actomyosin cytoskeleton. *Biophys. J.* **76**, 1648–1658.

Vos, J. W., Valster, A. H. & Hepler, P. K. (1999) Methods for studying cell division in higher plants. Mitosis and Meiosis **61**, (ed. by C. L. Rieder), pp 413-437, Academic Press, San Diego.

Vos, J.W., Dogterom, M. & Emons, A.M.C. (2004) Microtubules become more dynamic but not shorter during preprophase band formation: a possible "search-and-capture" mechanism for microtubule translocation. *Cell Motil. Cytoskel.* **57**, 246-258.

Yokota, E., McDonald, A.R., Liu, B., Shimmen, T. & Palevitz, B.A. (1995) Localization of a 170-kDa myosin heavy chain in plant cells. *Protoplasma* **185**, 178-187

Yokota, E., Vidali, L., Tominaga, M., Tahara, H., Orii, H., Morizane, Y., Hepler, P.K & Shimmen, T. (2003) Plant 115-kDa-actin-filament-bundling protein, P115-ABP, is a homologue of plant villin and is widely distributed in cells. *Plant Cell Physiol.* **44**, 957-960.

Chapter 6

General Discussion

GENERAL DISCUSSION: what has been learned?

During cytokinesis in plant cells, the cell plate is formed to create a new cell wall that separates the daughter cells. The cell plate is formed by fusion of vesicles (60-80 nm in diameter) which contain cell wall material (polysaccharides and glycoproteins) in their interior and callose/cellulose synthesizing enzymes in their membrane. The vesicles are transported through the phragmoplast, a cytoplasmic dense area containing endoplasmic reticulum and (Golgi) vesicle membranes, microtubules and actin filaments. Microtubules and actin filaments form two antiparallel arrays with their plus-ends facing the forming cell plate (Kakimoto and Shibaoka, 1988; Baskin and Cande, 1990; Wick, 1991; Cleary et al., 1992; Zhang et al., 1990, 1993; Hepler et al., 1993; Sano et al., 2005). Our aim was to elucidate which physical parameters the vesicles need to have in order to be transported through the phragmoplast and to accumulate in the area where the cell plate is being made during plant cytokinesis. We focused our research on the parameters size and stiffness. Using microinjection of fluorescent synthetic lipid vesicles and polystyrene beads, we determined that vesicle size (up to 150 nm in diameter) does not matter for their transport through the phragmoplast towards the cell plate but that the parameter vesicle stiffness co-determines transport through this specific cell structure. In this last chapter, first I discuss the importance of structure in cells, cyto-architecture, for vesicular targeting, and the benefits of the microinjection technique for such studies. Second, I will discuss our, though still indirectly obtained, results showing earlier not reported roles for the actin cytoskeleton. Since injected vesicles have to be able to arrive at the phragmoplast area, additional research was needed on the role of hydrodynamic flow in plant cells. The role of this phenomenon in cell life is the last discussion point of this chapter.

The role of cyto-architecture in targeting of vesicles: microinjection of beads as tool

Synthetic vesicles, having diameters ranging from 45 to 150 nm, and polystyrene beads, with diameters of 20 and 40 nm, reached the phragmoplast and were transported through it, but only the vesicles accumulated in a region slightly broader than the cell plate proper, while the beads hung up in the phragmoplast. Within the limits studied, 45-150 nm diameter, the size of synthetic vesicles did not matter, neither for the velocity of movement through the phragmoplast, nor for their accumulation in the cell plate region, nor for their being non-obstructive for endogenous vesicles. Once accumulated in the cell plate region, the vesicles were kept in that region, as long as the cell plate did not attach to the mother cell wall. After attachment of the cell plate, this is the moment that the plate becomes the wall that divides the daughter cells, the vesicles redistributed into the cytoplasm of two new cells. This indicates that these vesicles did not fuse with each other and the developing cell plate. The reason why they did not fuse with the endogenous vesicles and the growing cell plate is obviously their lack of SNARE proteins and other proteins required for vesicle fusion. An interesting follow-up of this work would be to incorporate specific membrane fusion related proteins into the lipid layer of the synthetic vesicles, or attach such proteins to them, for testing of the function of these proteins. The result that they did not fuse together shows that the phragmoplast environment alone, combined with the close proximity of the vesicles, is not enough for fusion of these synthetic DOPG vesicles.

Polystyrene beads measuring 20 and 40 nm in diameter, which are even smaller than the smallest injected vesicles (45 nm), entered the phragmoplast, but were not released from the phragmoplast to accumulate in the cell plate region. This physical barrier for beads was not overcome by coating of the beads with the same phospholipids of which synthetic vesicles are made. The 40 nm beads, but not the 20 nm ones, even blocked the transport of endogenous vesicles since they delayed cell plate formation. Thus, stiffness is a limiting factor for transport through the phragmoplast.

The phragmoplast, this dense network of ER membranes (Seguí-Simarro et al. 2004), microtubules, actin filaments and packed with vesicles has a very specific cyto-architecture with an obvious function. At one side of this structure all types of organelles including vesicles are present, at the other side solely vesicles occur (Nebenführ et al., 2000; Seguí-Simarro et al., 2004). The organelles are excluded from entering this cell structure, but the vesicles, 60-80 nm wide in the natural situation, can enter and are transported through it. We have not determined yet which, or whether, molecular motors are needed for this transport. The properties of enabling delivery to and transport through the phragmoplast area, in combination of consumption of vesicles at their fusion site, could even be enough to allow a constant flow of vesicles without motor activity. The phragmoplast then acts as a sieve discriminating on the basis of size together with flexibility. Our results show that the size exclusion limit would be around 20 nm, the size of the beads that enter the phragmoplast, but do not pass it, and do not hinder endogenous vesicles in their passage towards the cell plate.

Contrary to the stiff beads, the flexible vesicles having a diameter of more that 7 times, 150 nm, the diameter of the beads, 20 nm, move completely through the phragmoplast area and also endogenous vesicles are larger than the beads, 60-80 nm (Chapter 3). Although microtubules (Dogterom et al., 1997, Janson et al., 2004) and actin filaments (Kovar et al., 2004) can buckle, this does not seem to happen efficiently enough to make a complete passageway for the beads. The large DOPG and the endogenous vesicles have to be squeezed flat to move through this dense area. This could be facilitated by molecular motors moving along cytoskeletal elements (Koster et al., 2003).

Our work shows that targeting in cells is not only a process of movement and binding of molecules/structures, but that specific cell structures working as sieves are involved, which discriminate on the basis of physical parameters such as the parameter stiffness. From the technical side, it becomes clear that micro-injection of vesicles and beads cannot only be used as a tool to study movement and targeting in cells, but in addition to study cyto-architecture.

The actin cytoskeleton in cell plate formation: role in transport

Our results shed new light on the function of the actin cytoskeleton during cytokinesis, namely the transport of the vesicles through the phragmoplast, and the residing of the vesicles in the cell plate region during cell plate formation.

During growth and expansion of the cell plate, microtubules and actin filaments behave in different ways. Microtubules are present at the edges of the developing cell plate and disappear from the middle of the phragmoplast as soon as a cell plate has formed (Zhang et al., 1990, 1993; Cleary et al., 1992; Hepler et al., 1993; Granger and Cyr, 2000; Ueda at al., 2003), whereas actin filaments become shorter but remain present in the whole area throughout cell plate formation (Hepler et al., 1993; Zhang et al., 1993; own observations: chapter 2).

During late telophase, synthetic DOPG vesicles moved towards the cell plate through the whole phragmoplast area, including the central area (chapter 2) that contains only few microtubules during the second phase of cell plate formation (Seguí-Simarro et al., 2004; Austin et al., 2005), but does contain the two opposing cylinders of densely packed, short, and to a high degree non-bundled, actin filaments (Hepler et al., 1993; chapter 2). Since the vesicles still accumulate in the center of the cell plate region when the microtubules are hardly there anymore, we hypothesize that at least during the later stages of cell plate formation, also endogenous vesicles move along the actin filaments of the phragmoplast. Endogenous vesicles are seen in the proximity of fenestrae of the developing cell plate (Seguí-Simarro et al., 2004), suggesting that vesicles are still transported to the central part of cell plate during a late telophase. Whether this is active or passive movement we have not shown yet. While actin filaments of the phragmoplast facilitate transport of the vesicles, at least during the maturation phase of cell plate formation, microtubules could be the leaders of cell plate growth by (actively) transporting vesicles to the cell plate edges for their initial fusion with each other to form vesicular tubes, the first stage of cell plate formation (Seguí-Simarro et al., 2004).

The actin cytoskeleton in cell plate formation: role in keeping vesicles in place

Microinjected synthetic vesicles are kept in the cell plate region until the end of telophase but disappear from that region when the actin phragmoplast disappears. Once accumulated inside the cell plate region, the vesicles did not go back into the phragmoplast (Chapter 2). Since during the later stages of cell plate formation, the microtubules are only at the border of the growing cell plate and the actin filaments are in addition located in the center of the plate, the microtubules cannot be the cytoskeletal structures that keep the vesicles in place in the cell plate region. The actin filaments on the other hand could perform this job. However, we can only speculate about the mechanism that keeps the vesicles in the cell plate region. An obvious mechanism could be that molecular motors are directing material only towards the cell plate and not away from it. If this is the case, it can only be the actin cytoskeleton-based motors, since at the later stages of cell plate formation, microtubules have already disappeared from the central part of the phragmoplast. Alternatively, a tethering, binding protein may keep the synthetic vesicles inside the CPAM, without them fusing together or with endogenous vesicles. The fact that membrane-covered beads do not line up in the cell plate region is not in contradiction with this last hypothesis, since these beads do not seem to reach that region.

The result that the actin cytoskeleton of the phragmoplast plays a role in keeping the vesicles near the forming cell plate is supported by the fact that the vesicles disappear from the cell plate region rapidly at the same time as the disappearance of the actin filaments of the phragmoplast (Chapter 2). As soon as the growing cell plate attaches to the mother cell wall and cytokinesis is completed and the interphase cortical cytoplasm has been formed, the injected vesicles are released from the cell plate region and redistributed inside the two daughter cells. Since these accumulated vesicles stay in place in the cell plate region as long as the actin phragmoplast of unbundled actin filaments persists, we hypothesize that it is the actin cytoskeleton that keeps them there. A similar mechanism has been proposed for keeping exocytotic vesicles close to the growing tip of tip growing cells, where fine (bundles of) actin filaments deliver vesicles to the vesicle rich region in the root hair tip (Miller et al., 1999) and keep them in the tip (Ketelaar et al., 2003).

Hydrodynamic flow: why is that useful for a cell?

Plant cells show rapid organelle movement called cytoplasmic streaming, which is known to be acto-myosin based (Shimmen and Yokota, 2004). The organelles are transported by motor proteins that use energy of ATP hydrolysis and move along actin filaments. We have shown that synthetic vesicles and polystyrene beads also can move, similar to organelles (Chapter 2 and 3). Microinjected synthetic vesicles and polystyrene beads move rapidly through the cytoplasm; within 5-10 minutes after injection, they reach the opposite side of the 40-80 μm long cell. From velocity measurements, both DOPG vesicles and beads appeared to move similarly to organelles visible with DIC microscopy, but their movement was slightly slower than that of these larger organelles. This slower movement of micro-injected DOPG synthetic vesicles and polystyrene beads in transvacuolar strands of interphase cells could indicate that they move not directly, using recruited motor molecules along the actin cytoskeleton, but indirectly by hydrodynamic flow induced by active movement of endogenous organelles. Experiments in which the vesicles and beads were added to isolated plant extracts (J.W. Vos, unpublished) after which the beads were collected, the proteins released from them, and subjected to electrophoretic analysis, revealed that the surface of vesicles and beads was coated with proteins from cytoplasmic extracts (data not shown). We have not yet analyzed whether motor molecules are among these proteins, nor isolated them for motility assays.

In a system, in which organelles move actively inside a cytosol, it is expected that the actively moving particles induce a flow in the surrounding medium, dragging along other particles and molecules. This type of intra-cellular movement is called hydrodynamic flow. Movement in cells via hydrodynamic flow cannot be neglected as we have shown theoretically (chapter 4) and experimentally (chapter 5). Hydrodynamic flow in cells is movement of molecules/particles driven by active transport of molecules/particles/organelles by motor proteins moving along the cytoskeleton, in the case of interphase plant cells, the actin filament bundles in transvacuolar strands. Theoretically, these forces are sufficient to cause hydrodynamic flow (Houtman et al., 2007) as in other organisms studied (Pickard, 1974). We have shown experimentally that, indeed, cytoplasmic GFP is being moved in this way, as in other organisms studied (movement of water in *Elodea canadensis*, Vorob'ev et al., 2004). GFP movement in the cytoplasm of tobacco BY-2 suspension cells is positively correlated with the velocity of organelle movement and is in the same direction.

Movement of molecules via hydrodynamic flow might be important for efficient distribution of metabolites throughout the cytoplasm of large cells, where diffusion alone is expected not be enough for their distribution. Without this movement, all proteins would have to be made at the site where they function, which would involve a complete orchestration of all ribosome/polysome transport and targeting to specific cell areas. With hydrodynamic flow of cell molecules, directed movement is required for proteins inside membranes but not for the less specific cytoplasmic molecules, which then move through the cell and are captured by their partners at the location where they function.

Our work on hydrodynamic flow and motility inside cells shows that much still has to be learned about living cells, for which, next to molecular genetics, and biochemistry, cell biology studies of physical aspects are needed to understand life.

REFERENCES

Austin, J.R., Seguí-Simarro, J.M. and Staehelin, L.A. (2005). Quantitative analysis of changes in spatial distribution and plus-end geometry of microtubules involved in plant- cell cytokinesis. J. Cell Sci. **118**, 3895-3903.

Baskin, T.I. and Cande, W.Z. (1990). The structure and function of the mitotic spindle in flowering plants. Annu. Rev. Plant Physiol. Plant Mol. Biol. **41**, 277-315.

Cleary, A.L., Gunning, B.E.S., Wasteneys, G.O., and Hepler, P.K. (1992). Microtubule and F-actin dynamics at the division site in living *Tradescantia* stamen hair cells. J. Cell Sci. **103**, 977-988.

Esseling-Ozdoba, A., Houtman, D., van Lammeren, A. A. M., Eiser, E. and Emons A.M.C. (2007)**.** Hydrodynamic flow in cytoplasm of plant cells. Submitted to Journal of Microscopy.

Esseling-Ozdoba, A., Kik, R., van Lammeren, A.A.M., Kleijn, M.J., and Emons, A.M.C. (2007). Flexibility contra stiffness: the phragmoplast exit as a physical barrier for polystyrene beads but not for synthetic membranous vesicles. Submitted to Journal of Cell Science.

Esseling-Ozdoba, A., Vos, J.W., van Lammeren, A.A.M., and Emons, A.M.C. (2007). Synthetic lipid (DOPG) vesicles accumulate in the cell plate region but do not fuse. Submitted to Plant Cell.

Granger, C.L. and Cyr, R.J. (2000). Expression of GFP-MAP4 reporter gene in a stably transformed tobacco cell line reveals dynamics of microtubule reorganization. Planta **210**: 502-509.

Hepler, P.K., Cleary, A.L., Gunning, B.E.S., Wadsworth, P., Wasteneys, G.O. and Zhang, D.H. (1993). Cytoskeletal dynamics in living plant cells. Cell Biol. Int. **17**, 127-142.

Houtman, D., Pagonabarraga, I., Lowe, C.P., Esseling-Ozdoba, A., Emons A.M.C. and Eiser, E. (2007). Hydrodynamic flow caused by active transport along cytoskeletal elements. *EPL*, **78**, 18001p1-p5.

Kakimoto, T. and Shibaoka, H. (1988). Actin filaments and microtubules in the preprophase band and phragmoplast of tobacco cells. Protoplasma **140**, 151-156.

Ketelaar, T., de Ruijter, N.C.A., and Emons, A.M.C. (2003). Unstable F-actin specifies the area and microtubule direction of cell expansion in Arabidopsis root hairs. Plant Cell **15**, 285-292.

Koster, G., van Duijn, M., Hofs, B., and Dogterom, M. (2003). Membrane tube formation from giant vesicles by dynamic association of motor proteins. Proc. Natl. Acad. Sci. USA **26**, 15583-15588.

Miller, D.D., de Ruijter, N.C.A., Bisseling, T., and Emons, A.M.C. (1999). The role of actin in root hair morphogenesis: studies with lipochito-oligosaccharide as a growth stimulator and cytochalasin as an actin perturbing drug. Plant J. **17**, 141-154.

Nebenführ, A., Frohlick, J.A., and Staehelin, L.A. (2000). Redistribution of Golgi stacks and other organelles during mitosis and cytokinesis in plant cells. Plant Physiol. **124**, 135-151.

Pickard W.F. (1974). Hydrodynamic Aspects of Protoplasmic Streaming in *Chara braunii*. Protoplasma **82**, 321-339.

Sano, T., Higaki, T., Oda, Y., Hayashi, T., and Hasezawa, S. (2005). Appearance of actin microfilament “twin peaks” in mitosis and their function in cell plate formation, as visualized in tobacco BY-2 cells expressing GFP-fimbrin. Plant J. **44**, 595–605.

Seguí-Simarro, J.M., Austin, J.R. II, White, E.A., and Staehelin, L.A. (2004). Electron tomographic analysis of somatic cell plate formation in meristematic cells of Arabidopsis preserved by high-pressure freezing. Plant Cell **16**, 836-856.

Shimmen, T. and Yokota, E. (2004) Cytoplasmic streaming in plants. Curr. Opin Cell Biol. **16,** 68-72.

Ueda, K., Sakaguchi, S., Kumagai, F., Hasezawa, S., Quader, H. and Kristen, U. (2003) Development and disintegration of phragmoplasts in living cultured cells of a GFP:TUA6 transgenic Arabidopsis thaliana plant. Protoplasma **220**: 111-118.

Wick, S.M. (1991). Spatial aspects of cytokinesis in plant cells. Curr. Opin. Cell Biol. **3**, 253-260.

Zhang, D., Wadsworth, P. and Hepler, P.K. (1990). Microtubule dynamics in living dividing cells: confocal imaging of microinjected fluorescent brain tubulin. Proc. Natl. Acad. Sci. USA **87**, 8820-8824.

Vorob'ev, V.N., Anisimov, A.V., and Dautova, N.R. (2004). Contribution of the actomyosin motor to the temperature-dependent translational diffusion of water by cytoplasmic streaming in *Elodea canadensis* cells. Protoplasma 224, 195-199.

Zhang, D., Wadsworth, P. and Hepler, P.K. (1993). Dynamics of microfilaments are similar, but distinct from microtubules during cytokinesis in living, dividing plant cells. Cell Motil. Cytoskel. **24**, 151-155.

SAMENVATTING

In dit proefschrift beschrijf ik de conclusies van studies aan hydrodynamische vloeiing in het cytoplasma van plantencellen en aan de fysische parameters die blaasjes nodig hebben om door de fragmoplast getransporteerd te worden en om te accumuleren in de regio waar de celplaat gemaakt wordt gedurende celdeling in planten.

In hoofdstuk 2 beschrijf ik de resultaten die behaald zijn met het microinjecteren van fluorescente synthetische blaasjes, gemaakt van het lipide 1,2-Dioleoyl-*sn*-Glycero-3-[Phospho-*rac*-(1-glycerol)] (DOPG), in interfase en delende *Tradescantia virginiana* meeldraadhaarcellen. In interfase cellen bewogen synthetische DOPG blaasjes van 60 nm door het cytoplasma, vergelijkbaar met endogene organellen. In delende cellen bewogen de DOPG blaasjes naar – en door de fragmoplast en accumuleerden in de celplaatregio, samen met endogene blaasjes, maar fuseerden niet met de zich ontwikkelende celplaat. Met behulp van deze synthetische blaasjes hebben we ontdekt dat het actine cytoskelet een functie heeft in het transport van blaasjes naar de celplaat, een nieuwe rol voor dit celskelet in celplaatvorming.

In hoofdstuk 3 beschrijven we dat niet de grootte, maar de stijfheid van de blaasjes een belangrijke limiterende parameter is voor het transport naar de celplaat. Polystyreen bolletjes van 20 en 40 nm in diameter, die zelfs kleiner zijn dan de kleinste geinjecteerde blaasjes (45 nm), kwamen de fragmoplast binnen, maar werden niet losgelaten uit de fragmoplast om te accumuleren in de celplaatregio. Coating van deze bolletjes met dezelfde fosfolipiden als waar de synthetische blaasjes van gemaakt zijn, zorgde er ook niet voor dat deze fysieke barrière genomen kon worden. Bovendien blokkeerden de bolletjes van 40 nm – niet die van 20 nm – het transport van endogene blaasjes, omdat ze de celplaatvorming vertraagden.

Hydrodynamische vloeiing in cellen is een passieve vorm van beweging van moleculen/deeltjes, aangedreven door actief transport van andere moleculen/deeltjes/organellen die door motor eiwitten bewegen langs het celskelet. In interfase plantencellen zijn gebundelde filamenten van het actine celskelet het transportsysteem.

In hoofdstuk 4 en 5 van dit proefschrift hebben we dit fenomeen bestudeerd. In hoofdstuk 4 beschrijven we een simpel raster model om hydrodynamische invloed van actief massa-transport (b.v. organeltransport) langs bio-filamenten (het celskelet) op een vrijelijk diffunderende massa (cytosolmoleculen) in de cel, te laten zien. In dit hoofdstuk laten we theoretisch zien dat hydrodynamische krachten, geinduceerd door de beweging van moleculaire motor-oganel complexen langs filamenten, een niet-verwaarloosbare flux veroorzaken dicht bij het filament. Het blijkt dat deze flux twee effecten heeft. Afhankelijk van de bezettingsgraad van het filament kan het een voldoende grote invloed uitoefenen op niet-gebonden moleculaire motor-organel complexen, zodanig dat hun transport beinvloedt wordt en het kan ook de flux reguleren van filament-gebonden motor-organel complexen.

In hoofdstuk 5 laten we zien dat bewegende organellen een hydrodynamische vloeiing produceren, die bijdraagt aan de beweging van moleculen in de cytosol. Met ‘Fluorescence

Recovery After Photobleaching' (FRAP) laten we zien dat moleculen van het zogenaamde 'Green Fluorescent Protein' (GFP) sneller bewegen in cellen met actief organeltransport dan in cellen waarin dit transport is geremd, dat de richting van GFP-beweging is hetzelfde als die van organellen en dat de snelheid van organellen de snelheid van GFP beinvloedt.

Hoofdstuk 6 is een algemene discussie en geeft een visie over de mogelijkheden van – en inzichten die verkregen kunnen worden met microinjectie van een verschillend assortiment aan synthetische blaasjes en bolletjes.

SUMMARY

In this thesis, I report conclusions from studies on hydrodynamic flow in the cytoplasm of plant cells and on the physical parameters vesicles require to be transported through the phragmoplast and to accumulate in the area where the cell plate is being made during plant cytokinesis.

In chapter 2, I describe the results obtained after microinjection of fluorescent synthetic lipid vesicles made of 1,2-Dioleoyl-*sn*-Glycero-3-[Phospho-*rac*-(1-glycerol)] (DOPG) into interphase and dividing *Tradescantia virginiana* stamen hair cells. In interphase cells, synthetic DOPG vesicles of 60 nm moved through the cytoplasm, similarly to endogenous organelles. In cells at cytokinesis, DOPG vesicles moved to and through the whole phragmoplast and accumulated in the cell plate region together with endogenous vesicles, but did not fuse with the developing cell plate. Using these vesicles, we uncovered that the actin cytoskeleton functions in transport of vesicles to the cell plate, a new role for this cytoskeleton in cell plate formation.

In chapter 3 we describe that the size of vesicles is not important for their transport towards the cell plate but that stiffness is a limiting parameter. Polystyrene beads measuring 20 and 40 nm in diameter, which are even smaller than the smallest injected vesicles (45 nm) entered the phragmoplast, but were not released from the phragmoplast to accumulate in the cell plate region. This physical barrier for beads was not overcome by coating of the beads with the same phospholipids of which synthetic vesicles are made. The 40 nm beads, but not the 20 nm ones blocked the transport of endogenous vesicles since they delayed cell plate formation.

Hydrodynamic flow in cells is passive movement of molecules/particles, but driven by active transport of other molecules/particles/organelles by motor proteins moving along the cytoskeleton. In interphase plant cells, the cytoskeleton of actin filament bundles is the transport system.

In chapter 4 and 5 of this thesis we study this phenomenon. In chapter 4 we describe a simple lattice model to show the hydrodynamic influence of active mass transport (i.e. organelle transport) along bio-filaments (the cytoskeleton) on a freely diffusing mass (the molecules of the cytosol) in the cell. In this chapter we show that, theoretically, the hydrodynamic forces induced by the movement of molecular motor-organelle complexes attached to the filaments give rise to a non-negligible flux close to the filament. This flux appears to have two effects. Depending on the degree of filament occupation it can exert a sufficiently large influence on unbound molecular motor-organelle complexes to modify their transport and also regulate the flux of motor-organelle complexes bound to the filament.

In chapter 5 we show that moving organelles produce hydrodynamic flow, which is contributing to the movement of molecules in the cytosol. With Fluorescence Recovery After Photobleaching (FRAP), we show that GFP molecules move faster in cells with active transport of organelles than in cells where this transport has been inhibited, that the direction of GFP movement is the same as that of organelle movement, and that the speed of organelle movement influences the speed of GFP movement.

Chapter 6 is a general discussion and gives an outlook of the possibilities and insights to be obtained with microinjection of a variety of synthetic vesicles and beads.

DANKWOORD

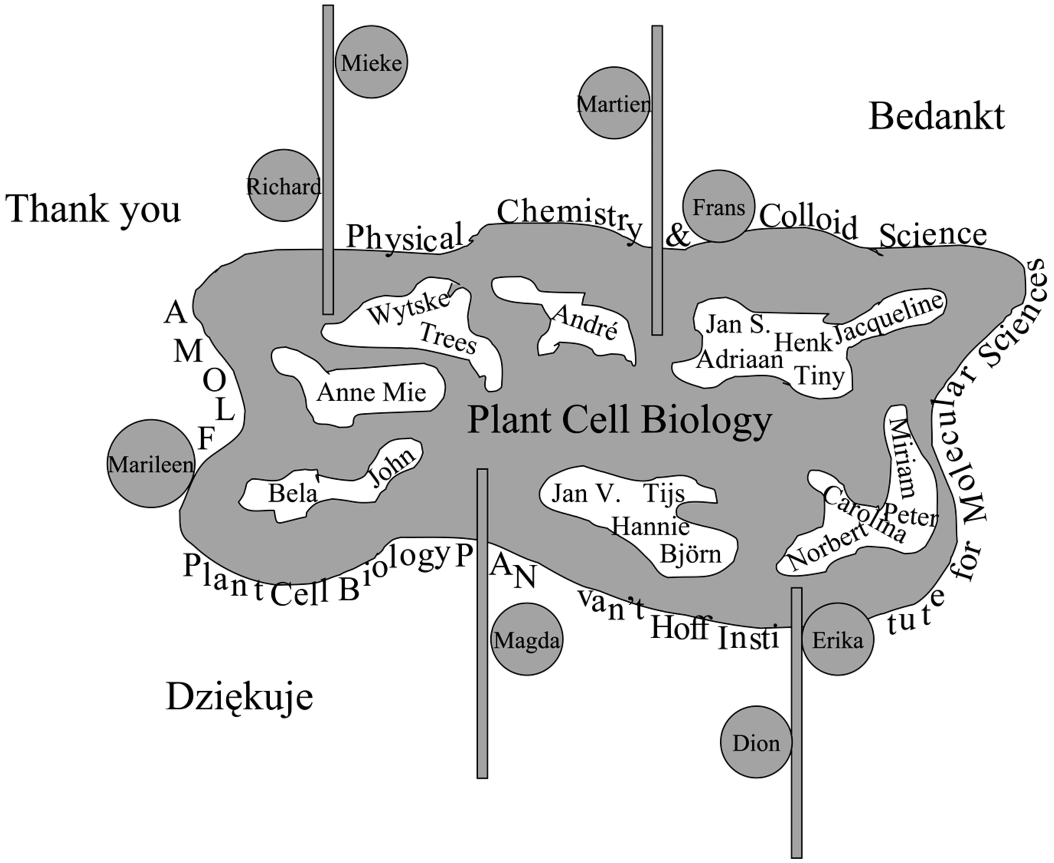
Thank you
Bedankt
Dziękuje
Mieke
Martien
Richard
Frans
Physical Chemistry & Colloid Science
AMOLF
Marileen
Wytske
Trees
André
Jan S.
Adriaan
Henk
Jacqueline
Tiny
Anne Mie
Plant Cell Biology
Bela
John
Jan V.
Tijs
Hannie
Björn
Miriam
Peter
Carolina
Norbert
Van 't Hoff Institute for Molecular Sciences
Plant Cell Biology
PAN
Magda
Erika
Dion

Agnieszka

CURRICULUM VITAE

I was born on the 21st December 1972, in Dwikozy, in Poland. At the University Maria Curie-Skłodowska (UMCS), in Lublin, Poland I studied biotechnology. In 1996, I graduated cum laude after which I started working as a research assistant at the Laboratory of Plant Anatomy and Cytology (UMCS) in Lublin, in the group of Prof.dr.hab. Józef Bednara. In 2000, I came to the Netherlands for a six months IAC fellowship at the Laboratory of Plant Cell Biology, Wageningen University. Here, I was working in the group of Dr. André van Lammeren. From 2002 until 2006 I was working as a PhD-student at the same laboratory in Wageningen on the project that resulted in this thesis under supervision of Prof. Dr. Anne Mie Emons. In March 2007 I started as a postdoc at the Department of Tumor Immunology, Nijmegen Center for Molecular Life Sciences, Radboud University, in Nijmegen, in the group of Prof. Dr. Carl Figdor.

Education Statement of the Graduate School
Experimental Plant Sciences

The Graduate School EXPERIMENTAL PLANT SCIENCES

Issued to: **Agnieszka Esseling-Ozdoba**
Date: **9 October 2007**
Group: **Laboratory of Plant Cell Biology, Wageningen University**

1) Start-up phase	*date*
▶ **First presentation of your project**	
Cell plate formation: Research plan.	Apr 15, 2002
▶ **Writing or rewriting a project proposal**	
▶ **Writing a review or book chapter**	
▶ **MSc courses**	
▶ **Laboratory use of isotopes**	
Subtotal Start-up Phase	*1.5 credits**

2) Scientific Exposure	*date*
▶ **EPS PhD student days**	
EPS PhD student day, Utrecht University	Mar 27, 2002
EPS PhD student day, Vrije Universiteit Amsterdam	Jun 03, 2004
EPS PhD student day, Radboud University Nijmegen	Jun 02, 2005
▶ **EPS theme symposia**	
EPS Theme 1 symposium 'Developmental Biology of Plants', 2002, Wageningen	Feb 18, 2002
EPS Theme 1 symposium 'Developmental Biology of Plants', 2003, Leiden	Feb 06, 2003
EPS Theme 1 symposium 'Developmental Biology of Plants', 2004, Wageningen	Feb 17, 2004
EPS Theme 1 symposium 'Developmental Biology of Plants', 2005, Wageningen	Apr, 26, 2005
▶ **NWO Lunteren days and other National Platforms**	
ALW meeting, Plant Sciences, 2002, Lunteren	Apr 15 & 16, 2002
ALW/FOM/VvBBMT-meeting on molecular and cellular biophysics, 2002, Lunteren	Oct, 2002
ALW meeting, Plant Sciences, Lunteren, 2003	Apr 07 & 08, 2003
ALW/FOM/VvBBMT-meeting on molecular and cellular biophysics, 2003, Lunteren	Sep 29 & 30, 2003
ALW meeting, Plant Sciences, Lunteren, 2004	Apr 05 & 06, 2003
ALW/FOM/VvBBMT-meeting on molecular and cellular biophysics, 2004, Lunteren	Sep 2004
ALW meeting, Plant Sciences, Lunteren, 2005	Apr 04 & 05, 2003
ALW/FOM/VvBBMT-meeting on molecular and cellular biophysics, 2005, Lunteren	Oct 10 & 11 2005
ALW meeting, Plant Sciences, Lunteren, 2006	Apr 03 & 04, 2003
ALW/FOM/VvBBMT-meeting on molecular and cellular biophysics, 2006, Lunteren	Oct 09 & 10, 2006
▶ **Seminars (series), workshops and symposia**	
Flying Seminars (5x)	2002-2006
Second Dutch Workshop on Molecular Systems Biology	Jan 20 & 21, 2004
WU Seminar Series: Mathematics and Plant Biology (6x)	Jan-Dec, 2005
NVvM Meeting 2005, Papendal	Nov 28 & 29, 2005
Capita selecta 'Physics and physical chemistry of cellular processes (6x)	Nov-Dec, 2005
Seminar plus	
▶ **International symposia and congresses**	
▶ 17th European Cytoskeleton Forum, Nyon, Switzerland	Aug 31-Sept 04, 2002
	Apr 12-17, 2003
European Cytoskletal Forum, Luxembourg	Aug 27-31, 2005
Gordon Research Conference on Plant and Fungal Cytoskeleton	Aug 20-25, 2006
▶ **Presentations**	
Theme symposium 1, 2002 - oral presentation	Feb 18, 2002
Cell Biophysics Meeting, AMC, Amsterdam	May 28, 2005
ALW meeting, Plant Sciences, Lunteren - oral presenation	Apr 03-04, 2003
NVvM Meeting, Papendal - oral presentation	Nov 28-29, 2005
Poster presentations (5x)	2002-2006
▶ **IAB interview**	Jun 03, 2005
▶ **Excursions**	
Subtotal Scientific Exposure	*24.3 credits**

3) In-Depth Studies	*date*
▶ **EPS courses or other PhD courses**	
EMBO course on Plant Cell Biology	Jun 16-26, 2002
Molecular Systems Biology Course	Jan 18-19, 2004
Mathematics in Biology	Feb 19-24, 2006
▶ **Journal club**	
Member of literature discussion group	2002-2006
▶ **Individual research training**	
Subtotal In-Depth Studies	*8.1 credits**

4) Personal development	*date*
▶ **Skill training courses**	
Techniques for Writing and Presenting a Scientific Paper	Nov 15-18, 2005
Organisation of PhD students day, course or conference	
▶ **Membership of Board, Committee or PhD council**	
Subtotal Personal Development	*1.2 credits**

TOTAL NUMBER OF CREDIT POINTS*	**35.1**

Herewith the Graduate School declares that the PhD candidate has complied with the educational requirements set by the Educational Committee of EPS which comprises of a minimum total of 30 credits

** A credit represents a normative study load of 28 hours of study*

LIST OF PUBLICATIONS

Szwacka, M., Piworun, E., **Ozdoba, A.**, Szeląg, T., Urbańczyk-Wochniak, E. (2002): Spatial and temporal expression of the sweet protein (thaumatin II) gene in transgenic cucumber plants. In Vitro Cell Dev. Biol. 38: P-1037.

Houtman, D., Pagonabarraga, I., Lowe, C.P., **Esseling-Ozdoba, A.**, Emons A.M.C. & Eiser, E. (2007): Hydrodynamic flow caused by active transport along cytoskeletal elements. *EPL*, 78, 18001p1-p5.

van Gisbergen P. A. C., **Esseling-Ozdoba, A.** & Vos J.W. (2007): Microinjecting FM4-64 validates it as a marker of the endocytic pathway in plants. Journal of Microscopy, accepted.

Esseling-Ozdoba, A., Houtman, D., van Lammeren, A.A.M., Eiser, E. & Emons, A.M.C. (2007): Hydrodynamic flow in the cytoplasm of plant cells. Submitted to Journal of Microscopy.

Esseling-Ozdoba, A., Vos, J.W., van Lammeren, A.A.M. & Emons, A.M.C. (2007): Synthetic lipid (DOPG) vesicles accumulate in the cell plate region but do not fuse. Submitted to The Plant Cell.

Esseling-Ozdoba, A., Kik, R., Kleijn, M., van Lammeren, A.A.M. & Emons, A.M.C. (2007): Flexibility contra stiffness: the phragmoplast exit as a physical barrier for polystyrene beads but not for synthetic membranous vesicles. Submitted to Journal of Cell Science.